RESEARCH ON DISPLAY SCANNING, SAMPLING, AND RECONSTRUCTION USING SEPARATE MAIN AND SECONDARY TRACKING TASKS

by R. W. Allen, W. F. Clement, and H. R. Jex

Prepared by
SYSTEMS TECHNOLOGY, INC.
Hawthorne, Calif.
for Ames Research Center

NATIONAL AERONAUTICS AND SPACE ADMINISTRATION • WASHINGTON, D. C. • JULY 1970

NASA CR-1569

RESEARCH ON DISPLAY SCANNING, SAMPLING, AND RECONSTRUCTION USING SEPARATE MAIN AND SECONDARY TRACKING TASKS

By R. W. Allen, W. F. Clement, and H. R. Jex

Issued by Originator as Technical Report No. 170-2

Prepared under Contract No. NAS 2-3746 by
SYSTEMS TECHNOLOGY, INC.
Hawthorne, Calif.

for Ames Research Center

NATIONAL AERONAUTICS AND SPACE ADMINISTRATION

For sale by the Clearinghouse for Federal Scientific and Technical Information
Springfield, Virginia 22151 – CFSTI price $3.00

ABSTRACT

Theoretical models and corroborative experimental data are presented on the human operator's scanning behavior and tracking performance while simultaneously controlling two closed-loop tasks using separate displays. These results form a basis for estimating and correlating human performance and scanning workload in multidisplay piloting tasks.

A novel experimental technique is used to force the subjects (skilled instrument-rated pilots) to scan two displays in a manner that is realistic yet controllable by the experimenter. This is done via a "subcritical" side task (stabilizing a slightly unstable first-order plant), such that the time-away-from-the-side-task (i.e., available for the main task) is limited by the time-constant of the divergence. The scanning statistics reveal an average minimum dwell time of about 0.4 sec, and skewed sampling interval histograms which are fitted by a Pearson Type III distribution function. The scanning frequency is forced to vary over a wide range (from 0.5 to 2.0 per second) yet the sampling frequency fluctuations during a run remain within 20 to 30 percent of the mean value. In order to preclude parafoveal cues, eye-movement signals are used to blank the nonfixated display in certain cases, and some performance decrements occur. A new "scan frequency parameter", S, is derived to correlate the combined effects of sampling frequency and finite dwell time.

It is shown that the pilot's average scanning, sampling and reconstruction behavior can be accurately modeled by an adjustable quasi-linear describing function, plus an injected "scanning remnant" (observation noise) having wideband properties. Two likely mental processes for reconstruction of an estimated signal from the finite-dwell, almost-periodic samples are analyzed: a "switched gain" model and a "reconstruction-hold" model. The experimental data from this experiment (where no operator equalization was required) favor the former. A theoretical model for the sampling remnant is given, which has the form of first-order-filtered noise; it depends on the displayed signal variance, sampling frequency, fixation dwell time and sampling frequency variations. The experimental remnant data fit this model well, and thereby provide good correlations between theoretical and experimental tracking performance measures.

CONTENTS

FIGURES

TABLES

SYMBOLS

c	Pilot output
e	System error
i	Input forcing function
K_h	Scanning describing function attenuation
m	System output
n_c	Pilot output remnant
n_s	Display scanning remnant
R	Reconstruction rate weighting fraction
S	Sampling frequency parameter (Eq. 7)
T_d	Display dwell time
T_I	Pilot lag time constant
T_L	Pilot lead time constant
T_N	Pilot neuromuscular lag time constant
T_o	Lower bound on sampling interval
T_s	Display sampling interval
T_Δ	Side task dwell time
T_λ	Side task divergence time constant = λ^{-1}
$Y_c(j\omega)$	Controlled element describing function
$Y_H(j\omega)$	Describing function of scanning, sampling and reconstruction processes
$Y_p(j\omega)$	Overall pilot describing function
δ	Sampling variability parameter, T_o/T_s
Δ_s	Theoretical sampling coherence factor (Eq. 6)
η	Scanning dwell fraction, T_d/T_s
η_e	Effective dwell fraction (Eq. 17)

λ	Unstable root of side task
$\overline{\rho_c^2}$	Ratio of input correlated to total mean-square control stick motion
$\overline{\rho_e^2}$	Ratio of input correlated to total mean-square error power
τ_e	Pilot time delay
τ_s	Incremental time delay due to sampling and reconstruction
Φ_{ee}	Power spectrum of error signal
Φ_{ii}	Power spectrum of input signal
Φ_{nn_e}	Remnant power spectrum injected at error signal
Φ_{nn_s}	Sampling remnant power spectrum
ω_c	Crossover frequency
ω_i	Input bandwidth
Ω	Ratio of crossover frequency for continuous parafoveal relative to continuous foveal tracking (Eq. 17)

SECTION I

INTRODUCTION

A. SCOPE

The research described in this report is part of a larger effort to develop a systems analysis theory of displays for manual control of vehicles (Refs. 1, 2, and 3). The analytical procedures require calculation of the closed-loop dynamic response of pilot/vehicle control systems. The theory for single axis systems with compensatory displays is fairly well developed (Ref. 4). However, in a multi-axis aircraft control situation (e.g., IFR flight), a pilot is often required to scan an array of instruments, and the changes in dynamic response caused by the scanning process and sequential sampling of displayed information are not yet well enough understood to permit quantitative predictions of display requirements.

The scanning process is influenced by a variety of factors, including the importance and content of the various components of displayed information and the instrument panel layout. Clement, et al, (Ref. 5) have reviewed the literature and advanced some factors known to affect scanning behavior. Scanning of an instrument panel causes the displayed information on any one instrument to be sampled* rather than continuously perceived by foveal† viewing, as in single axis control. Clement (Ref. 6) has theoretically estimated some implications of display sampling, and Levison and Elkind (Ref. 7) have measured some effects of two-display sampling and proposed a model which includes the effect of parallel display perception via parafoveal† vision.

---

*Sampling is used herein, in a general context, including the finite fixation dwell times (during which portions of the sample are perceived), as well as aperiodic sampling, etc.

†The viewing regions defined herein include: foveal — the high acuity region within roughly 3 deg off the visual axis; parafoveal — the decreasing acuity region from 3 to about 40 deg off-axis; and peripheral — the remaining region out to the limits of moving-object detectability.

Research into display utilization behavior and the factors that govern the scanning process is difficult, because it requires complex simulations, sophisticated measurements under realistic conditions, and comprehensive experimental designs. Because of the dearth of data on scanning and the existence of a preliminary analytical model for it, emphasis in this study was placed on investigation of the scanning and sampling problem.

The **purpose** of the present study was to accomplish the following goals in a well-controlled laboratory experiment:

- Measure the effect of scanning and sampling on pilots' performance and dynamic response
- Identify the signal "reconstruction" process adopted by pilots when sampling the displayed information
- Test some recently developed theoretical models (Ref. 6) designed to predict the effects of sampling on performance and dynamic response.

The spirit of the research reported here was more like that of a preliminary examination of a complex landscape, rather than a definitive study of small areas in previously charted territory. We were looking for large, practical effects in our measures that would lend some validity and empirical constants for the theoretical models.

B. PLAN OF THIS REPORT

Section II reviews some previous scanning and sampling research relevant to manual control displays, and summarizes some newly developed analytical models for sampling and reconstruction effects.

Section III describes the experimental program, including the design, setup, training, and data analysis procedures.

Section IV presents the basic data, in the form of overall scanning and performance measures, detailed scanning statistics, describing function measurements, and power spectra of errors and remnant. Typical time traces are shown to illustrate the modes of scanning induced by the experimental techniques.

Section V shows the good correlation between these data and the theory of Section II, and discusses some of the complex performance and adaptation interactions which can be untangled by the analytical model.

Section VI briefly summarizes the main conclusions and recommendations.

SECTION II

EMPIRICAL AND THEORETICAL BACKGROUND

In this section we first review the basic concepts of scanning during multiloop control tasks and give an overview of our model for the scanning, sampling and perceptual reconstruction process. After a review of some past work relevant to this model, the detailed analytical models are presented. These are accompanied by results of some numerical computations, which show the penalties in tracking performance resulting from scanning, and suggest an experimental design to validate the model.

A. BASIC CONCEPTS AND MODEL

1. Scanning During Multiloop Control Tasks

We are concerned with the class of pilot/vehicle situations characterized by a closed-loop pilcted multiloop regulation or tracking task, having more than one display, and requiring manipulation of one or more control sticks. The pilot's selection of preferred display feedbacks from the presented array has been found to be governed by a set of "Multiloop Feedback Selection Rules" which have been evolved previously and verified experimentally for integrated displays (see Refs. 1, 2, 4, 8, and 9). In any case, past work (to be reviewed later herein) shows that: (1) a fairly stable scanning and sampling strategy evolves for a given task and instrument array, and (2) the control motions are much more continuous than the discrete sampling would seem to imply on a pure stimulus-response sequence. Furthermore, most of the information used in aircraft maneuvering is of an analog nature, displayed as the motion of a moving pointer or scale.

These facts indicate that a form of sampled data feedback theory is appropriate to model this process. In this formulation, the display feedbacks ultimately selected would be affected not only by vehicle and task criteria but also by penalties from the required scanning and sampling operations.

The display scanning model should also be compatible with the existing multiloop pilot models for integrated displays, and must be

simple enough to permit practical computations and efficient data reduction. Finally, it should yield verifiable predictions.

Before proceeding let us clarify some terms that are used frequently herein:

> **Scanning** is defined here as the process of selecting and fixating each instrument in an array of, or specific portions of, a complex display field. For the manual control tasks a "scanning traffic pattern" is evolved, causing a given instrument to be sampled frequently. However, not all instruments are sampled at the same frequency.
>
> **Sampling** covers the perceptual acts of: focusing on a display; interpreting this as an appropriate command or error signal; and perceiving its displacement, rate (or direction), and, possibly, acceleration during a sequence of fixations. In the present context, the sampling does not have to be impulsive or periodic.
>
> **Reconstruction** covers the process of extrapolating a hypothetical continuous signal using the series of samples available from each display, plus parafoveal (nonfixated) information which may be perceived between samples. Reconstruction provides the mental signal upon which the subsequent pilot equalization operations are assumed to operate.

2. Description of the Model

The development of a display scanning and sampling model for multiloop manual control tasks is reported in Ref. 2. Basically, it treats the complex processes involved in scanning, selecting, sampling, and reconstructing internal signals from an array of dials as an added "perceptual" functional block in a quasi-linear description of the pilot. Figure 1a shows the assumed basic model and Fig. 1b its simplified equivalent. The latter represents the simplest form that can be measured from inputs and outputs external to the human operator.

Let us review the key elements in the basic model before proceeding with its background. The human display control behavior is represented by a series of functional blocks, loosely labeled "Perceptual", "Adaptive", and "Neuromuscular" in Fig. 1a. The signals shown connecting the blocks are practically unmeasurable (being located in the central nervous system), and, in fact, the functions may overlap. It is useful to consider the

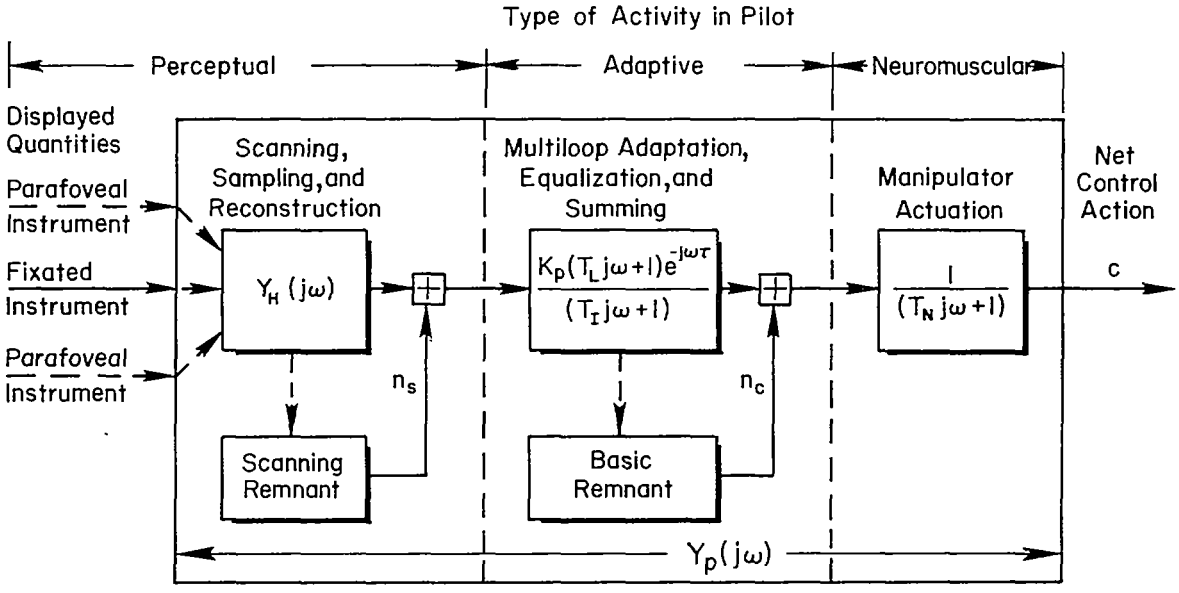

a) Assumed Basic Model (Sequential Scanning)

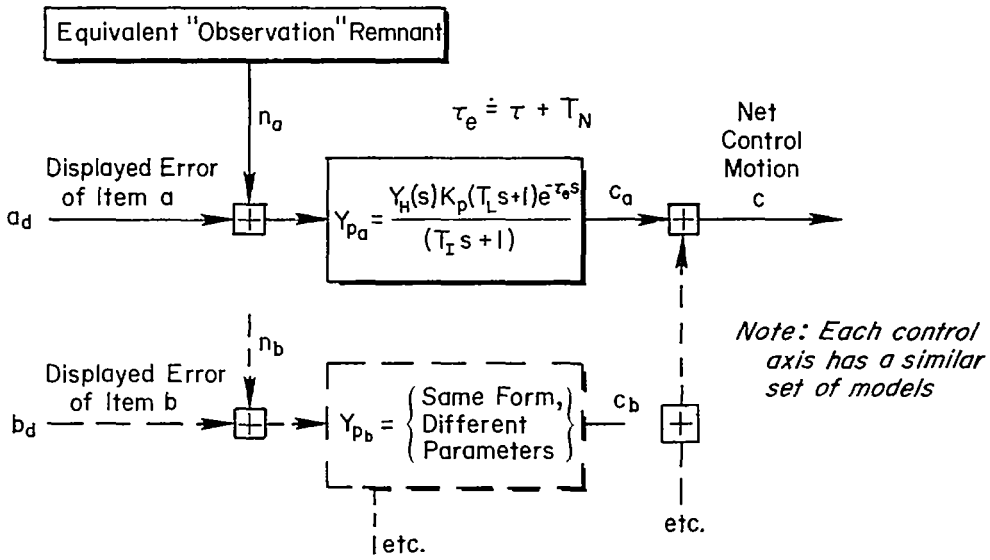

b) Equivalent Simplified Model (Parallel, continuous)

Figure 1. Assumed Form of Pilot Models

perceptual block as an additional serial element, and to define the scanning and sampling effects as the ratio between behavior under continuous, full-foveal tracking and the actual sampled tracking, in each of the multiple loops. We will not dwell further on the adaptive block (feedback selection, equalization, summing, etc.) or neuromuscular block (manipulator interfacing and actuation) which have been well documented in recent years (e.g., Refs. 4, 10, 11).

At this stage the conceptual model is still quite general, and any of several mathematical or physical models could be used to describe the above processes. Before selecting a particular set of forms and assumptions, it is necessary to review the relevant background material, which follows.

B. REVIEW OF PREVIOUS RESEARCH ON DISPLAY SCANNING, SAMPLING AND RECONSTRUCTION

1. Intermittent Human Response

Early in the investigation of human tracking in single-axis tasks, there were speculations as to the possible intermittent nature of human operator response. Most of this work was an outgrowth of early concepts of psychological refactory period, and the observation of oscillatory components in the error and control signals. The works of Craik, North, Hayes, and Ward are notable examples (Refs. 12–15). It is now known that most of the oscillatory components observed in single-axis tracking are due to remnant-excited peaks of the lightly damped closed-loop system; nevertheless, the analytic models and insights provided by this early work are useful in the present scanning context.

Sampled-data operator models were extended by LeMay and Wescott (Ref. 16), and they have been brought to a high degree of algorithmic sophistication by G. Bekey and his colleagues (e.g., Refs. 17 and 18).

2. Instrument Scanning In Flight

Following the work of ophthalmologists prior to World War II, McGehee, Fitts, Jones, Senders, and others investigated the natural scanning patterns of pilots during flight in order to more efficiently train pilots

and lay out instrument panels for blind-flight conditions (Refs. 19–30). Most of these ad hoc data were collected by laborious manual data reduction of eye-camera movie films, but unfortunately, the instrument readings were not simultaneously recorded, so there is no way of correlating the displayed signals with the fixations. Nevertheless, these data (especially the monumental work of Milton, Fitts, et al, in Refs. 19-25) clearly reveal the essential features of natural instrument scanning, validated over hundreds of flights, dozens of pilots, and numerous display and task conditions.

The main scanning properties revealed in IFR flight were: (1) the pilot's scanning was not perfectly periodic, but a given instrument was sampled at a definite average interval, T_s, the interval differing for each instrument and dependent on the flight task, (2) the dwell time, T_d, spent on each instrument varied around a specific mean value, this value being remarkably stable among pilots and flight conditions (mean dwell times varied from 0.2 to over 1.0 seconds, with more complex, higher-bandwidth displays requiring more fixation time), and (3) over typical mission-phase intervals of two to four minutes time, the scan patterns appeared roughly randomized among the instruments, and the dwell times and scan intervals (on a given instrument among several) were quasi-randomly distributed and statistically independent. A reexamination of these data has been made by using the present multiloop pilot/vehicle theory as a guide (Refs. 2 and 5), and a definite hierarchy of scanning frequency and dwell times was found, ranging from: high-frequency, short dwells for inner-loop displays (attitudes and path rates); to low-frequency, long dwells for outer-loop instruments (low bandwidth commands).

Some further detailed conclusions drawn in Refs. 2 and 5 from this in-flight research are summarized below.

a. **Dwell Time (Fixation Duration); T_d**

- Results of a reexamination (Ref. 5) of the data from four sources spanning 20 years of flight history in three distinctly different types of aircraft (Refs. 19-30) all suggest that average dwell time on the class of conventional, separated instruments studied may be a physiological characteristic of the pilot population.

- For cruising flight maneuvers, one coarsely quantized mean duration of fixations, 0.5 sec, appears to be a sufficient summary of results for all flight instruments in all maneuvers.

- A second coarsely quantized mean duration of fixations, 1 sec, is termed a "group-monitor" dwell time, since it represents an average for a group of engine instrument signals.

- Results in landing approaches support more finely quantized mean values of dwell time, as follows:

Duration (sec)	Displayed Signal
0.8	Glide-slope/localizer deviation combined on cross-pointer in approach and tightly controlled "outer-loop" signals.
0.6	Primary "inner-loop" signals such as pitch and roll attitude combined in artificial horizon, heading, and airspeed.
0.4	Loosely-controlled "outer-loop" and monitored signals, such as pressure altitude, vertical speed, turn rate, lateral acceleration and, sometimes, airspeed.

- A threshold or refractory interval for dwell time seems to exist at 0.2 to 0.25 sec. The sampling interval must be at least twice this value.

- There is some evidence in the numbers themselves that the more finely quantized mean levels of dwell time are approximately integral multiples of this mean refractory interval.

b. Sampling Frequency (Fixation Frequency); $f_s = 1/T_s$

- Fixation Frequency versus Signal Bandwidth. The simple theory that fixation frequency should be slightly more than twice the bandwidth of the displayed signal is insufficient. The pilot usually fixates on a given instrument much more frequently than required by the lower bound of the sampling theorem. A fixation frequency three to four times the estimated bandwidth of the displayed signal appears in the case of the principal flight instruments. The higher ratios usually occur for "inner-loop" signals and lower ratios for "outer-loop" signals.

- Fixation Frequency versus Maneuvers. In particular maneuvers, the pilot will fixate even more frequently on instruments displaying signals required by instructions to be

nulled and unique to the maneuver. He will fixate less frequently on instruments displaying inessential information. He will also fixate more frequently on instruments whose readings he expects to be disturbed ("vigilant determinism"). However, except for the turn-rate/lateral-acceleration ("turn-and-bank") instrument during nonturning flight and engine group, fixation frequency very rarely falls below the lower bound required by the sampling theorem.

- Fixation Frequency versus Display Arrangement. Instruments with inessential or no information may be fixated if they are centrally located near or between displays which require attention. In this regard, there is probably an immense transfer of training effect from earlier displays and/or doctrines. Thus the display arrangement chosen may influence the fixation frequencies which might have governed the choice in the first place.

- Fixation Frequency versus Correlated Displayed Signals. There is informational redundancy and correlation among the instruments in an aircraft because of the intrinsic dynamic coupling among the several degrees of freedom. However, the partial redundancy of information is seldom, if ever, used to decrease the fixation frequency on a particular display. The problem of instrument correlation was also investigated by Senders, Ref. 33. Although a rather coarse threshold exceedance criterion was used, it was found that correlation did not significantly increase or decrease fixation frequency between the pair of correlated instruments, relative to fixation frequencies on the same instruments with uncorrelated signals.

- Other factors which will influence the scanning rate are the "urgency" of a particular signal for the task, the demands of other control axes or noncontrol tasks and the duration of each sample. If magnitude, rate, and higher derivatives can be detected during each fixation, then the signal can be predicted for longer periods between fixations.

A grand model to account for all such factors is not yet available.

There has been practically no systematic in-flight research recently except for a few ad hoc investigations, e.g., instrument scanning during takeoffs and landings in a jet transport (Ref. 29) and some integrated versus separated instrument scan patterns on an X-15 panel (Ref. 30). Scan and display data under realistic conditions, using modern instruments and data processing, is urgently needed.

3. Display Monitoring

A parallel interest to closed-loop control displays is the open-loop monitoring of an array of dials to perceive exceedance of tolerances or specified values. This condition is common to engine or radar instrument monitoring, where effects of manual control are not displayed. Senders has led several of these investigations, starting with early investigations of intermittently lit dials (Ref. 31). He was among the first to assert (Ref. 27) that the minimum frequency with which a given instrument in an array should be scanned would be related to the bandwidth of its signal, basing his predictions on Shannon's sampling theory, then in its infancy. His experiments with open-loop monitored displays (Ref. 32) showed that naturally scanned sampling rates were proportional to bandwidth for four different input bandwidths presented simultaneously on separate dials. For these monitoring tasks (detection exceedance, not reconstruction, was the criteria) the dwell times were in the range of 0.3 to 0.5 sec, somewhat below the longer values of 0.6 to 0.8 sec measured by Fitts, et al, under flight (tracking) conditions (Refs. 19–24).

More recently, Senders and his colleagues have added the concepts of statistical decision and queuing theory to provide an explanation for the multiloop scanning process (Refs. 32, 33, 34). This is one natural formulation of the questions of how particular scan patterns evolve, and how to describe the scan-to-scan behavior. Numerical simulation results in Ref. 33 show, for example, that narrowband signals with disparate center frequencies should give rise to strongly patterned scanning, while wider band signals with a greater uncertainty factor result in much more random scanning. However, this theory does not yet include the essential closed-loop feedback effects on the nature of the signal, and thus it cannot predict the scanning parameters or closed-loop performance.

4. Single Channel Tracking with Sampled Presentations

A number of investigations of tracking with intermittently illuminated or presented displays (as distinct from natural operator-induced scanning) have been performed. We term this "forced sampling."

Battig, et al, (Ref. 35) studied interrupted illuminated displays at sampling rates between 0.4 and 16.1 Hz. As the frequency of target intermittence increased to 1 Hz there was an abrupt fourfold improvement in tracking proficiency (measured by cumulative time on target), thence a slight further improvement in proficiency as a linear function of frequency until the fusion frequency of 15 Hz was reached.

Katz and Spragg (Ref. 36) studied tracking error with sinusoidal and irregular forcing functions. Frequencies of intermittent display illumination were between 0.5 and 4 Hz. Mean-tracking error decreased nearly fourfold with the logarithm of frequency between 0.5 and 2 Hz. Further increase in frequency to continuous illumination resulted in additionally halving mean error.

Platzer and Krendel (Ref. 37) report tracking error (but not describing function) results in which first derivative perception was forcibly excluded from a sampled display by employing a zero-order intersample hold. The controlled element was K/s^2. Much larger average errors and frequent losses of control were observed when the first derivative was absent as compared with the same cases where it could be derived visually by the operator.

Senders (Ref. 31) also shows degradation in performance directly related to decreased sampling frequency.

Bennett (Ref. 38) established the importance of operator control of output sampling rate as a determinant of tracking performance, as measured by target recovery time from two discrete disturbances. Mean recovery time was inversely proportional to approximately the square root of output sampling frequency. For step disturbed targets, a sampling rate of about 9 Hz yielded recovery times equivalent to those for continuous tracking. For targets disturbed by a ramp, a sampling rate of about 5 Hz yielded recovery times equivalent to those for continuous tracking.

Experimental work by Vossius and Wezel (Refs. 39, 40) with single channel forced periodic visual sampling has produced manual tracking results in conformity with the Nyquist Sampling Theorem (Refs. 41, 42)

which is the antecedent of the Generalized Sampling Theorem (Ref. 43).* The Nyquist theorem expresses a lower bound for sampling frequency (in terms of signal bandwidth) when no signal derivatives are sampled for use in reconstruction. Wezel employed sample duration intervals in the range 4 to 40 milliseconds, whereas, where some form of signal reconstruction is probable, pilots' average fixation dwell times observed by McGhee, Fitts, et al, are in the range 500 to 800 milliseconds and seldom less than 400 milliseconds, even for "monitoring" a signal. If the operator employs increasing dwell time for derivative recognition, as Poulton's and Senders' results suggest (Refs. 31 and 44), Wezel would have excluded derivative recognition in his experiment by his short sample exposure times; therefore, he was probably justified in seeking confirmation of the simple Nyquist theorem instead of its subsequent generalization which requires simultaneous rate samples.

The failure to recognize that simultaneous sampling of magnitude and derivative information could theoretically reduce the required sampling frequency, misled a number of earlier investigators of forced sampling into overlooking the effects of longer presentation dwell times.

5. Perception of Signals During a Fixated Sample

In an ingenious experiment, Poulton (Ref. 44) had operators fixate on repetitive samples of a moving quasi-random signal through an aperture in a rotating plate, which permitted control of both sampling rate and (presentation) dwell times. The operators reported whether they could subjectively detect sign, magnitude, direction, rate, and acceleration of the signal, as the dwell times were varied. Figure 2 reproduces the results, which clearly show a hierarchy of required on-times, ranked in the above order. Subjective perception of magnitude alone could be achieved with very short on-times, on the order of 0.01 sec (making use of the retinal afterimage). But rate detection typically required 0.1 sec,

*The Generalized Sampling Theorem states that: given a signal having bandwidth of f_i (Hz), then sampling its magnitude plus N time derivatives at each sample requires Sampling Rate $\geq 2f_i/(1+N)$ for accurate reproduction of the signal (see Ref. 43). Practical considerations raise the factor of 2 to 4 or more.

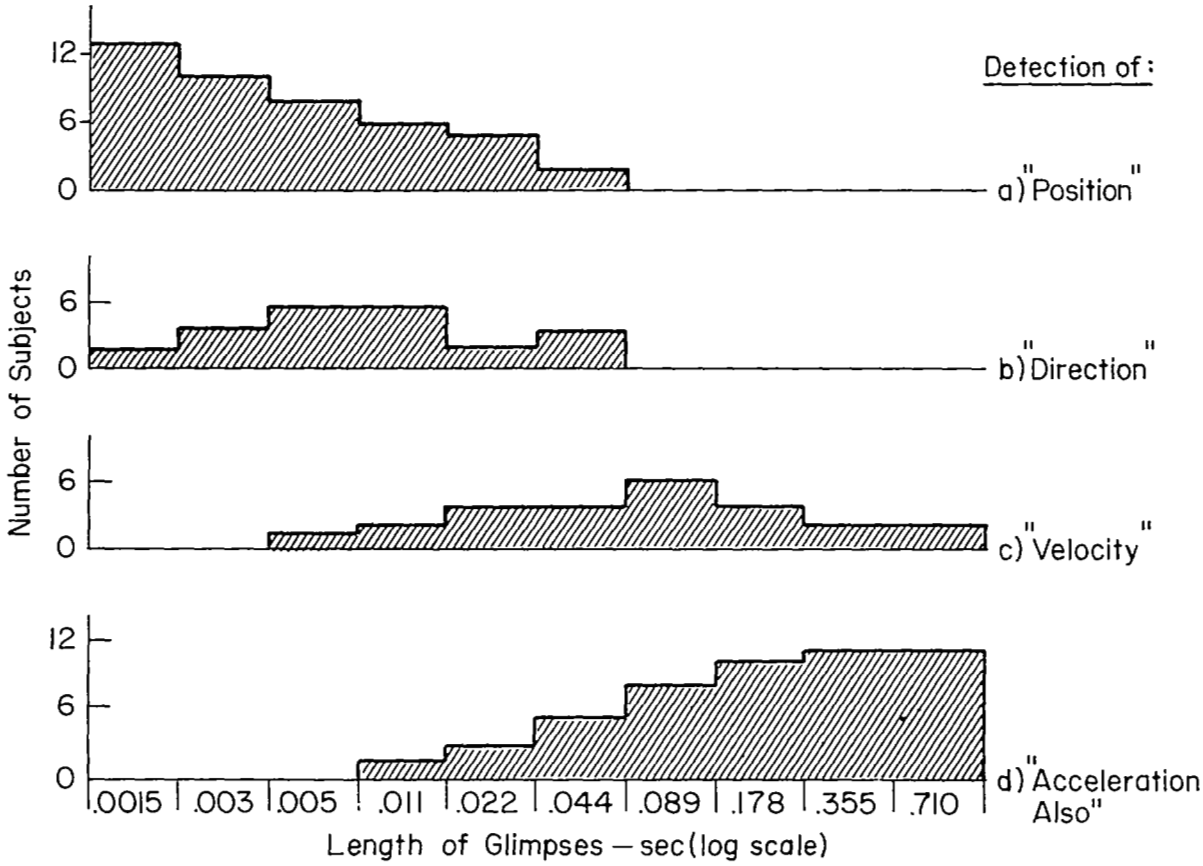

Adapted from Poulton (Ref. 44)

A complex (3 sinusiod) course and 1.0 sec blackouts were used between glimpses to detect:

a) Position of pointer

b) Direction of movement, but not speed

c) Speed, but not acceleration

d) Acceleration as well as speed

Subjects merely reported the perceivable cues and direction

Figure 2. Speed Cues Reported for Dwell Times of Various Length (from Poulton, Ref. 44)

while acceleration detection typically required 0.5 sec of presentation time. Sampling frequency had only secondary effects on these values at the slower frequencies typical of aircraft display sampling.

McColgin (Ref. 57) measured parafoveal motion perception thresholds among ten airline pilots for the pointer on a standard 3-inch aircraft altimeter viewed at 38 inch range. The absolute threshold isograms on perimetric charts for both rotary and linear motion were foveal-concentric bisymmetrical ellipses with major horizontal axis approximately twice the vertical axis. Except near the limits of the peripheral field, the absolute thresholds increased linearly with field angle; from 2 to 8 rev/min for rotary motion, and from 3.5 to 26 in./min for linear motion. Vertical motion thresholds were 10 to 20 percent lower at comparable peripheral field angles than were horizontal motion thresholds in areas adjacent to the horizontal axis. There was also more variability in threshold among subjects with increasing peripheral angle.

6. Natural Scanning and Sampling of Separated Tracking Displays

Although a number of separated tracking displays have been investigated over the years, most have not recorded the eye fixations, so that much valuable material background has been lost. Among the first were Fitts and Simon (Ref. 45) who investigated a two-axis pursuit tracking task wherein cumulative time-on-target performance decreased with increasing display separation. No describing functions were obtained, but the authors recognized the significance of parafoveal and peripheral perception in motivating scanning and control output.

Levison and Elkind (Ref. 7) found reduced gain, increasing remnant, and increasing time delay while tracking a compensatory display using parafoveal viewing. Remnant power nearly doubled and effective time delay increased from 0.11 to 0.3 sec, both linearly with field angle for one-axis parafoveal tracking. Wierwille and Gagne (Ref. 46) also found more describing function variability for separated displays than for an integrated two-axis display. Obviously, remnant increases under scanning conditions.

The research on simple two-axis displays with simple controlled elements of the form K/s and K/s^2 is continuing and is providing important data. However, there has been no serious attempt to control the scanning behavior under natural conditions, to validate a model for scanning, sampling and reconstruction. There is a need for a simple two-axis case where the second axis is made to substitute for a multi-axis set of displays, while sampling effects on the main task are investigated. Also there is great need for more eye movement data under more realistic multiloop control situations both in simulators and in flight.

C. PRESENT THEORY

1. Assumptions

Because of our interest in the overall closed-loop performance of display-pilot-vehicle systems, we need a form of analytical model compatible with feedback analysis. After much investigation (much of it based on the background information just reviewed), we have made the following assumptions and choices of model form, and have accepted certain limitations in consequence:

- The basic analytical models are extensions of the quasi-linear descriptions presently used for nonscanned multiloop cases (i.e., adjustable, random-input describing functions, plus a remnant for the noncoherent effects). Although the fine-grain scanning and sampling processes are difficult to model this way, the resulting pilot output is sufficiently continuous so that describing functions can still account for the major closed-loop effects.

- It is assumed that the pilot's learning process has stabilized so that scanning behavior is stable (in the statistical sense). Sampling of a given display is assumed to be "almost periodic," with appreciable statistical fluctuations which randomize the data. The model then treats the average properties of this scanning during typical task intervals. Although sampling effects on loop closures and scanning statistics are well represented this way, it is not possible to account for the particular order in which the displays are scanned. This assumption should improve as the number of instruments and control axes increases, thereby tending to randomize the scanning.

- The detailed high frequency effects of the scanning, sampling, and reconstruction are circulated around the closed-loop system, giving rise to a broadband "sampling" remnant. This is modeled as an injected noise at the pilot's input (i.e., "observation noise"). The sampling remnant is a function of the scanning, sampling, and reconstruction processes, and may strongly affect the loop closures, choice of equalization, and closed-loop performance. This is in contrast to the continuous case, where a basic remnant is always present but only rarely influences the loop closures strongly.

- The resulting model for scanning, sampling, and reconstruction comprises:

  1) a quasi-linear, random-input "perceptual describing function", denoted as $Y_{p_h}(j\omega)$ which multiplies the human operator's continuous describing function, and

  2) a broadband sampling remnant, n_s, which adds to the basic remnant, and is described as a spectrum Φ_{nn_s} of wideband observation noise injected at the pilot's perceptual input.

Details of these sampling and reconstruction models will be presented next.

2. Concepts

We will start with a tutorial introduction to the basic concepts, in order to show which properties of measured signals will tell us most about the type and degree of signal sampling and reconstruction.

The prior in-flight and laboratory research reviewed previously has shown that the sampling of one instrument in a given array, has a definite average frequency and corresponding mean sampling interval, T_s. Although there is appreciable variation around this mean sampling interval, it is instructive to approximate this aperiodic sampling by almost-periodic sampling followed by suitable signal reconstruction. Figures 3 and 4 illustrate some of the essential effects of sampling and reconstruction on the resulting describing function and remnant contributions.

Let us consider impulsive sampling first as illustrated in Fig. 3. This mathematically tractable case closely models the situation when the dwell time, T_d, is very short compared with the sampling interval, T_s. As shown in Fig. 3 (b and c), the position, and possibly some fraction, R, of the rate, are simultaneously sampled.

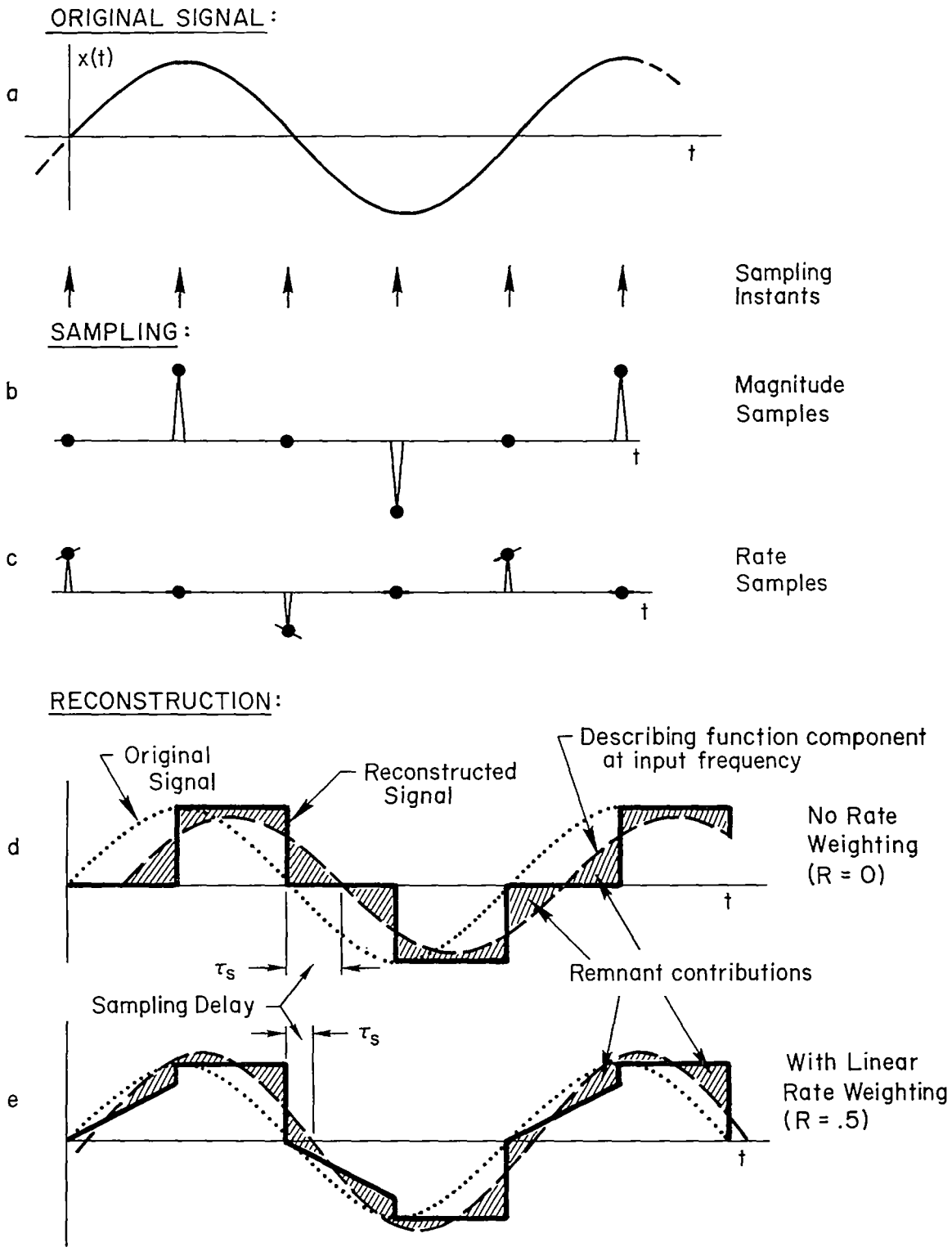

Figure 3. Basic Features of Linear Reconstruction Following Impulsive Samples of Position and Rate

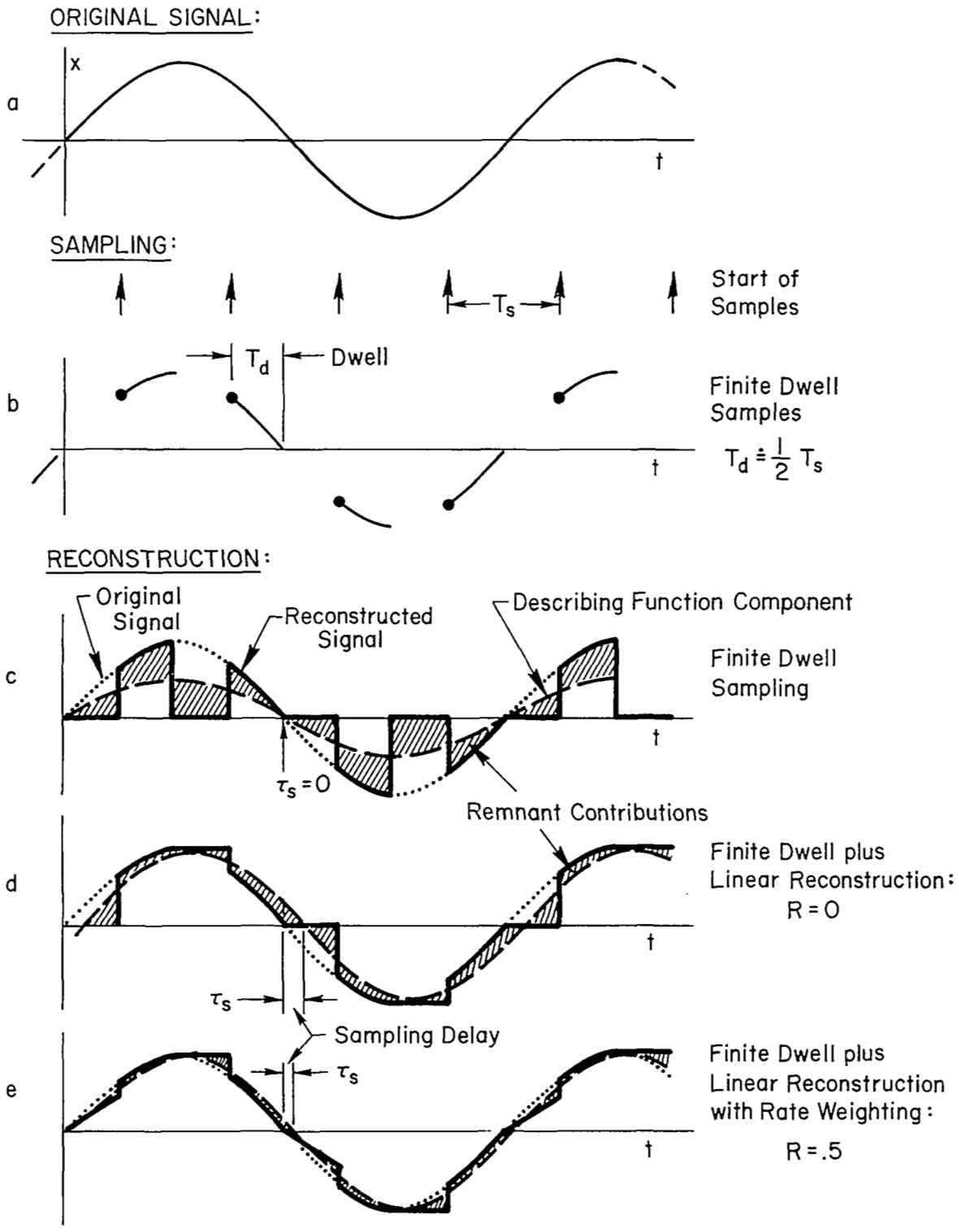

Figure 4. Basic Features of Finite Dwell Sampling and Reconstruction

To illustrate the reconstruction of a signal approximating the original, let us consider simple, linear reconstruction which consists of a series of straight-line extrapolations of the sampled position plus a fraction, R, of the slope. These are shown in lines d and e for R = 0 and R = 0.5, respectively. This jagged reconstruction is modeled by a describing function output plus a remnant component. For the sinusoidal signal shown, the describing function is the fundamental Fourier component of the waveform shown by the dashed lines. This waveform contains the same "area" as the original signal, and it is phase delayed such that the mean-squared error between the fundamental waveform and the reconstructed signal is at a minimum. Comparing the dashed line with the dotted line representing the original signal, it can be seen that the reconstruction **describing function will show a small attenuation and appreciable time delay** compared with the original signal. This effect is true in general when a zero-order hold is used. The jagged remnant contribution, shown as the shaded difference between the dashed and solid curves, will result in a fairly broadband noise addition with most of its power at higher frequencies. Considering the fact that actual sampling is not perfectly periodic, it can be shown that the sampling and reconstruction remnant spectrum will be fairly broadband when averaged over an appreciable run length (Ref. 52).

The sampled rate information can be used to improve the reconstruction, as shown in line e for R = 0.5 (extrapolated slope equals 0.5, the true tangent). Considering the same features as before, note that: the describing function magnitude is slightly higher than the input, the effective sampling delay has been reduced to half of its value for R = 0, and the remnant contribution is somewhat less.

These figures illustrate a situation where the sampling frequency is approximately four times the input frequency. It can readily be appreciated from lines d and e of Fig. 3 that the remnant contribution would grow considerably, if the sampling frequency were reduced, i.e., T_S increased. An analytical model for this is given later.

Finite dwell sampling can appreciably help the sampling and reconstruction process. Some of the essential features are shown in Fig. 4

where the same ratio of sampling to signal frequency, and a dwell fraction, $T_d/T_s = 0.5$, is illustrated. If no active reconstruction process is used in the intersample interval, the effective signal reconstruction is illustrated on line c of Fig. 4. This is representative of a perceptual model which includes only switching from one display to another without any active reconstruction in the interval between dwells. We call this Simple Finite Dwell Sampling. The describing function is attenuated by the dwell-fraction (T_d/T_s). There is no reconstruction delay, but there is a very large remnant contribution. In fact, it is obvious from the shaded area of Fig. 4c that the average amplitude of sampling remnant will be proportional to the rms signal level.

Using a combination of finite dwell and linear reconstruction, as shown in lines d and e of Fig. 4, considerably reduces the remnant at the expense of a small time delay due to the reconstruction process. By comparing the last two lines in Figs. 3 and 4 one can see that the use of modest dwell fractions and rate-weighting can result in excellent signal reconstruction, even with this simple linear reconstruction process.

Other reconstruction schemes are possible (Refs. 47-49). By choosing a weighting function for each sample other than a mere "hold" or linear extrapolation, a better fitting reconstruction can often result. Figure 5 illustrates these concepts. At the top of Fig. 5 is shown triangular weighting of impulsive position samples, wherein the height of an overlapping series of triangles is summed to give the reconstructed signal. The resulting straight-line approximation is a reasonable representation for high sampling rates. However, since one does not know the value of a sample until it has been taken, this scheme cannot be applied "on-line" without a penalty of a one-sampling-interval delay.

Nearly perfect signal reconstruction can be achieved through the use of "cardinal reconstruction", which is illustrated in the bottom half of Fig. 5 (Refs. 6 and 49). The term "cardinal" refers to use of only the minimum essential samples to reconstruct the signal. Line b of Fig. 5 shows the complete cardinal weighting function which extends from minus- to plus-infinity around each sample. The resulting sum of these weighting functions, as shown on the right, is a nearly perfect representation of

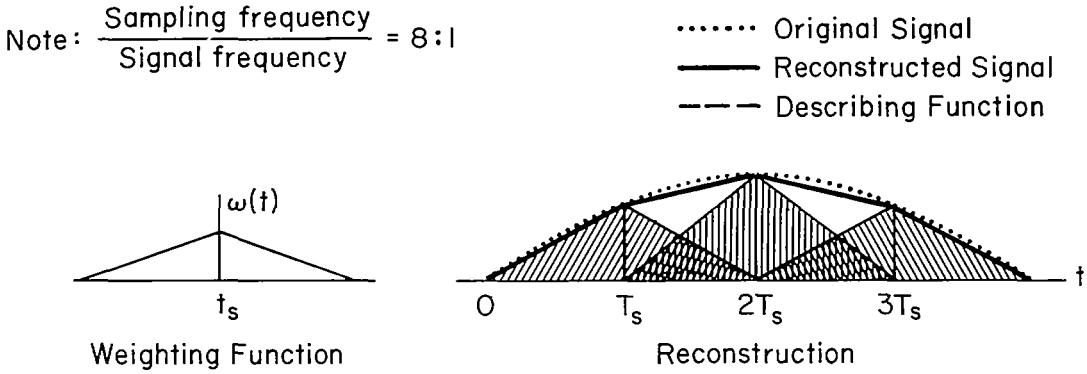

a. Triangular Weighting on Position Samples

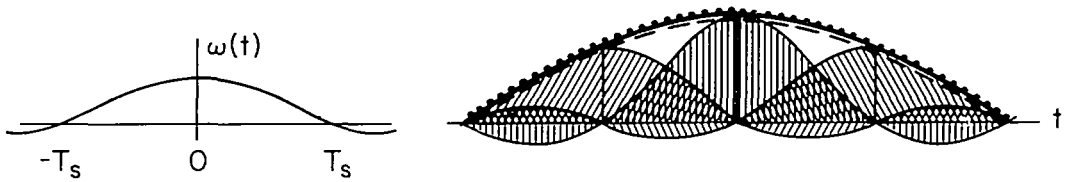

b. Complete Cardinal Weighting on Position Samples

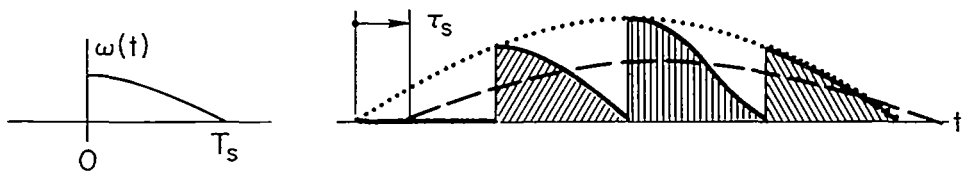

c. Truncated Cardinal Weighting on Position Samples

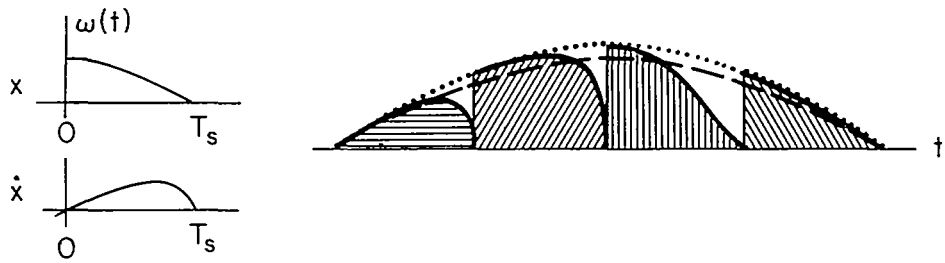

d. Truncated Cardinal Weighting on Position and Rate Samples

Figure 5. Triangular, Cardinal, and Truncated Cardinal Reconstruction from Impulsive Samples

the signal, and very low sampling rates can be used to achieve good reproduction. However, again, one does not know the impulses in advance to properly weight the leading edge of the successive weighting functions. Line c shows a realistically "truncated cardinal weighting function" on position samples only. Here, only the portion within one sampling interval is used. The resulting waveform is actually not as good as the simple linear reconstruction shown previously. However, if rate samples are weighted with position samples, each using appropriately derived cardinal weighting functions as shown in line d, a fairly good reconstruction can be obtained. A comparison between the last two lines of Figs. 3 and 5 (allowing for the higher sampling rate depicted in Fig. 5) will show that truncated cardinal reconstruction will, in general, have a higher attenuation factor than linear reconstruction; a little less effective time delay (because the bulk of the weighting function is at the beginning of the sampling interval); and either more or less remnant contribution, depending on whether or not rate weighting is used.

Mathematical derivation and adaptation of the truncated cardinal weighting to the displayed signal reconstruction, is given in Refs. 6, 49, and 52, and will not be repeated here. The analyses substantiate the points shown by the foregoing illustrations. The foregoing discussion should form an adequate heuristic basis to accept the resulting analytical models which will be presented next.

3. Mathematical Models (Describing Function)

In general, the describing function relating the reconstructed signal to the original signal will be a function of the type of sampling, and its frequency, dwell time, and reconstruction weighting scheme. Two empirical observations make possible some simplification. The first is that the scanning frequency is usually appreciably greater than the bandwidth of the signal to be reconstructed. The second is that the randomization of the sampling intervals renders the sampling describing function "fuzzy" at high frequencies, thereby justifying a simpler approximation, valid mainly at the lower frequencies of interest. It has been found that the following simple form for the operator's perceptual describing function

applies to all of the detailed mathematical models derived in Refs. 6 and 49, and to the experimental data in Ref. 7 as well. This model consists merely of an attenuation factor, K_h, and an equivalent sampling-and-reconstruction time delay, τ_s:

$$Y_H(j\omega) \doteq K_h e^{-j\omega\tau_s} \quad \text{for} \quad \omega << \omega_s \left(\text{or } \frac{2\pi}{T_s}\right) \qquad (1)$$

Reconstructed Signal / Displayed Signal — Attenuation — Sampling-and-Reconstruction Delay

The values of K_h and τ_s depend on the scanning interval, T_s, the dwell fraction, $\eta = T_d/T_s$, the rate weighting, R, and the type of reconstruction weighting function. The attenuation factor and delays are given in Table I.

TABLE I

SUMMARY OF RECONSTRUCTION DESCRIBING FUNCTION PARAMETERS

(At frequencies much less than the sampling frequency)

TYPE OF RECONSTRUCTION	GAIN, K_h	DELAY, τ_s
Simple Finite Dwell Sampling	η	0
Gain-Switched, Finite Dwell (K_1 during T_d; K_2 otherwise)	$\eta K_1 + (1-\eta)K_2$	0
Finite Dwell with Linear Reconstruction	$\doteq 1.0$	$0.50(1-\eta)(1-R)T_s$
Finite Dwell with Truncated Cardinal Reconstruction	$\eta + \frac{\sqrt{3}}{\pi}\sin\frac{\pi}{\sqrt{3}}(1-\eta)$ $\doteq 0.54$ as $\eta \to 0$ $\doteq 1.0$ as $\eta \to 1$	$\left\{\begin{matrix}4/3\pi \\ 0.425\end{matrix}\right\}(1-\eta)(1-R)T_s$

Note: T_s = Sampling period; T_d = Dwell time

$\eta = T_d/T_s$ = Dwell fraction; R = Rate weighting

The expressions in Table I verify the points made in the previous sections in connection with Figs. 3 through 5, notably that dwell time and rate weighting tend to reduce the effective time delay and that truncated cardinal reconstruction is quite similar to the linear reconstruction.

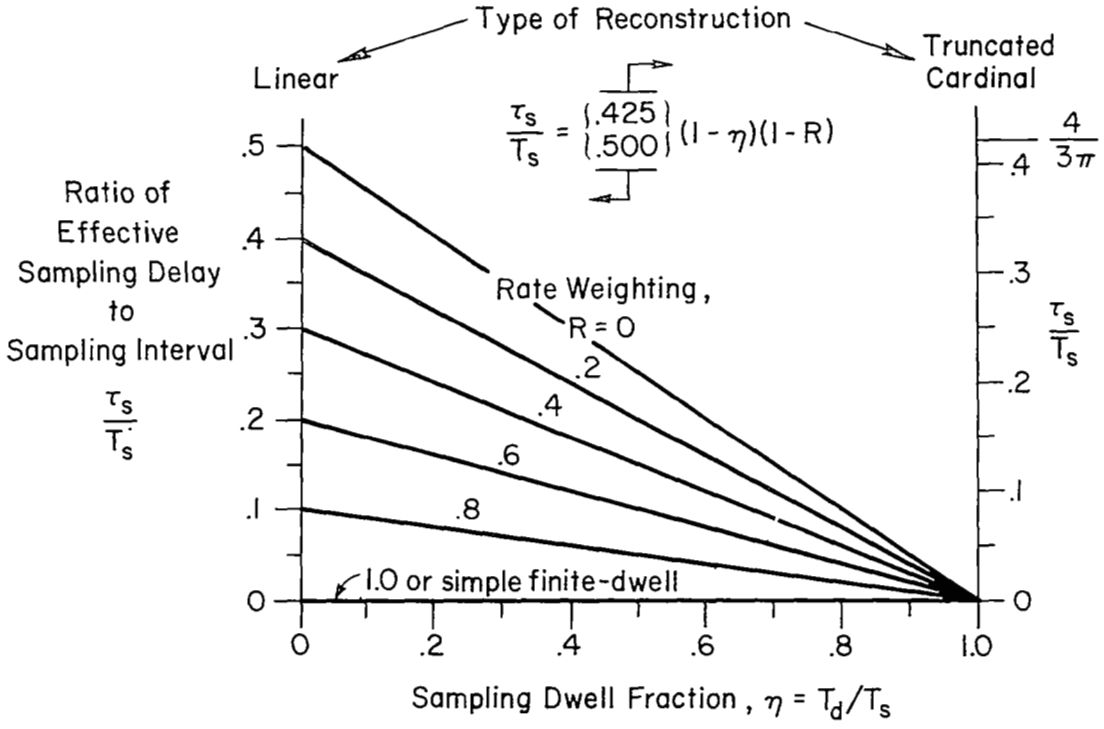

Figure 6. Effects of Reconstruction on Sampling Delay

Typical delays are plotted on Fig. 6. Perceptually, increased R requires increased dwell time, and both contribute similar terms to reducing the effective reconstruction delay. Consequently, modest values of each can eliminate most of the reconstruction delay and remnant.

4. Sampling Remnant Model

As discussed in the previous subsection on concepts, the sampling and reconstruction process results in the generation of considerable remnant power in addition to the fundamental describing function. We have also noted that the lack of perfect sampling periodicity smears out any sampling-harmonic peaks in the remnant spectrum. These observations lead to a simple model for sampling remnant. The basic model has already been presented in Fig. 1, and this is simplified for closed-loop analysis to a modified crossover model, as shown in Sketch A. Here, the attenuation of Y_H has been absorbed into the crossover gain, ω_c, and the sampling remnant is modeled by an injected sampling noise, n_s, having a spectrum, Φ_{nn_s}. The key assumptions are that the sampling interval is quasi-random and is uncorrelated

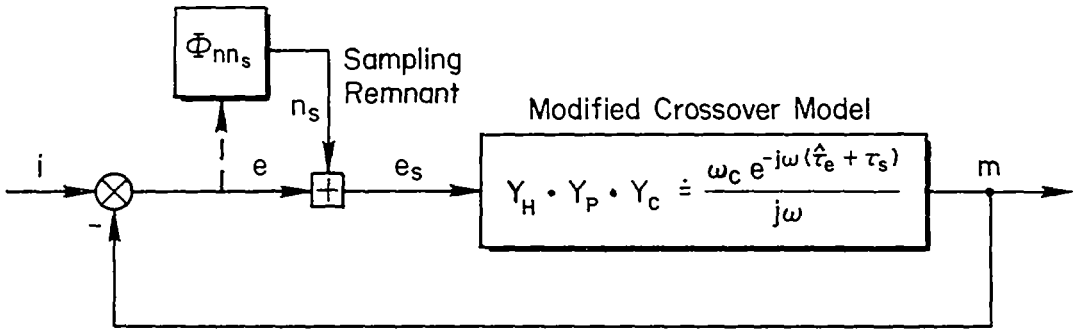

Sketch A. Model for Sampling Remnant Computation

with the displayed signal level. One might suspect that a larger error signal would be sampled more frequently, but the meager evidence available does not offer any clear indication. It is obvious that the feedback signal of the vehicle motion will contain low frequency sampling effects, and these in turn will affect the sampling remnant on subsequent passes around the loop. This phenomenon can lead to catastrophic sampling errors under certain conditions, as will be shown below.

Bergen (Ref. 51) has analyzed the output power spectral density of an impulsive modulator whose sampling interval varies randomly (in a Poisson sense) about some mean value, $\overline{T}_s$. The total output spectrum turns out to be equivalent to that of a continuous signal path (unity describing function) with additive white noise (remnant), whose power spectral density is proportional to the product of $\overline{T}_s$ and the mean-square value of the signal x(t) into the sampler. Thus, the remnant power spectrum* for random impulsive sampling is:

$$\Phi_{nn_s}(\omega) \doteq \frac{\overline{T}_s \overline{e^2}}{\pi} \quad ; \quad (\text{error units})^2/\text{rad/sec} \qquad (2)$$

*While Bergen used two-sided integrals and power/Hz in his derivations, we shall use one-sided definitions and power/rad/sec for consistency with other remnant investigators:

$$\overline{x^2} \equiv \int_0^\infty \Phi_{xx}(\omega) d\omega$$

where the units of Φ_{xx} are units^2/rad/sec.

Based on Bergen's approach and previous work on finite-dwell periodic sampling (Refs. 47 and 50), Clement has recently developed a theoretical model for quasi-random sampling with a constant average dwell time, T_d (Ref. 52). The sampling intervals have a lower bound, T_o, which constrains their variability about $\overline{T}_s$ to less than the purely random case as $T_o \rightarrow \overline{T}_s$. For a wide range of interval distributions, all represented by one of the Pearson Type III modified gamma functions, a remarkably similar expression to Eq. 2 results [here, $x(t) = e(t)$] for quasi-random finite-dwell sampling remnant at frequencies well below the average sampling frequency:

$$\Phi_{nn_s}(\omega)\Big|_{\omega << \omega_s} \doteq \frac{\overline{T}_s \overline{e^2}(1-\eta)(1-\delta)}{\pi\left[1+\left(\frac{\omega T_d}{2}\right)^2\right]} \quad ; \quad \frac{(\text{error units})^2}{\text{rad/sec}} \tag{3}$$

$$\text{where:} \quad \delta = T_o/\overline{T}_s < 1 \quad , \quad 0 > \eta = T_d/T_s < 1$$

Thus the low-frequency scanning remnant level is reduced by both increased dwell time (via $1-\eta$) and by increased δ (which constrains the sampling interval variability in proportion to $1-\delta$).

The closed-loop net error spectrum Φ_{ee} is composed of one part Φ_{ee_i} (linearly correlated with the input via the describing function) and another part Φ_{ee_n} (due to the uncorrelated sampling remnant injection), each shaped by a closed-loop describing function, (e/i) or (e/n_s), respectively.

$$\Phi_{ee}(\omega) = \overbrace{\left|\frac{e}{i}(j\omega)\right|^2 \Phi_{ii}(\omega)}^{\Phi_{ee_i}} + \overbrace{\left|\frac{e}{n_s}(j\omega)\right|^2 \Phi_{nn_s}(\omega)}^{\Phi_{ee_n}} \tag{4}$$

Integration gives the mean-square error:

$$\overline{e^2} = \underbrace{\int_0^\infty \left|\frac{e}{i}(j\omega)\right|^2 \Phi_{ii}(\omega)\,d\omega}_{\overline{e_i^2}} + \underbrace{\frac{\overline{T}_s \overline{e^2}(1-\eta)(1-\delta)}{\pi} \int_0^\infty \left|\frac{e}{n_s}(j\omega)\right|^2 \frac{d\omega}{\left[1+(\omega T_d/2)^2\right]}}_{\overline{e_s^2}} \tag{5}$$

The appearance of $\overline{e^2}$ on both sides of the equation results in the final expression:

$$\overline{e^2} = \overline{e_i^2}\underbrace{\left\{\frac{1}{1-\frac{\overline{T}_s(1-\eta)(1-\delta)}{\pi}\int_0^\infty \left|\frac{e}{n_s}(j\omega)\right|^2 \left[1+(\omega T_d/2)^2\right]^{-1} d\omega}\right\}}_{\text{Denominator} \equiv \Delta_s} \tag{6}$$

Here, the transfer function $|e/n_s|(j\omega)$ is equal to the closed-loop transfer function $|m/i|(j\omega)$.

The factor in curly brackets is greater than 1.0 and can become infinite if the denominator sum (denoted by Δ_s) goes to zero. This shows that the average closed-loop error induced by sampling remnant can increase without bound when $\Delta_s \rightarrow 0$, even though the loop structure is dynamically stable! This effect is called "instability in the mean-squared error sense," and it is governed by an equation similar to the determinant of closed-loop dynamic stability. Notice that Δ_s is independent of the input spectrum.

Another interpretation of this effect is to note that the ratio of input-correlated-to-total-power in the error is just the average error power coherence, $\overline{\rho_e^2} = \overline{e_i^2}/\overline{e^2} = \Delta_s$. Thus, error coherence Δ_s is a good figure of merit for the detrimental effects of sampling.

Using the modified crossover model to calculate $|e/n_s|(j\omega)$, values for Δ_s have been computed in Ref. 52 for a range of dwell-fractions, sampling intervals, and loop gains; all normalized with respect to the <u>total</u> effective time delay: $\tau_e = \hat{\tau}_e + \tau_s$. Three graphs are shown in Fig. 7, illustrating the effects of dwell fraction, sampling frequency, and variability on the sampling coherence. Also given on the right is the multiplier, $1/\Delta_s$, between (total) sampled and unsampled mean-square errors. For the finite-dwell sampling assumed here, it is apparent that the sampled error can exceed by severalfold the continuous value unless large dwell fractions and sampling frequencies are employed. Figure 7c also shows that decreasing sampling variability rapidly improves $\overline{\rho_e^2}$.

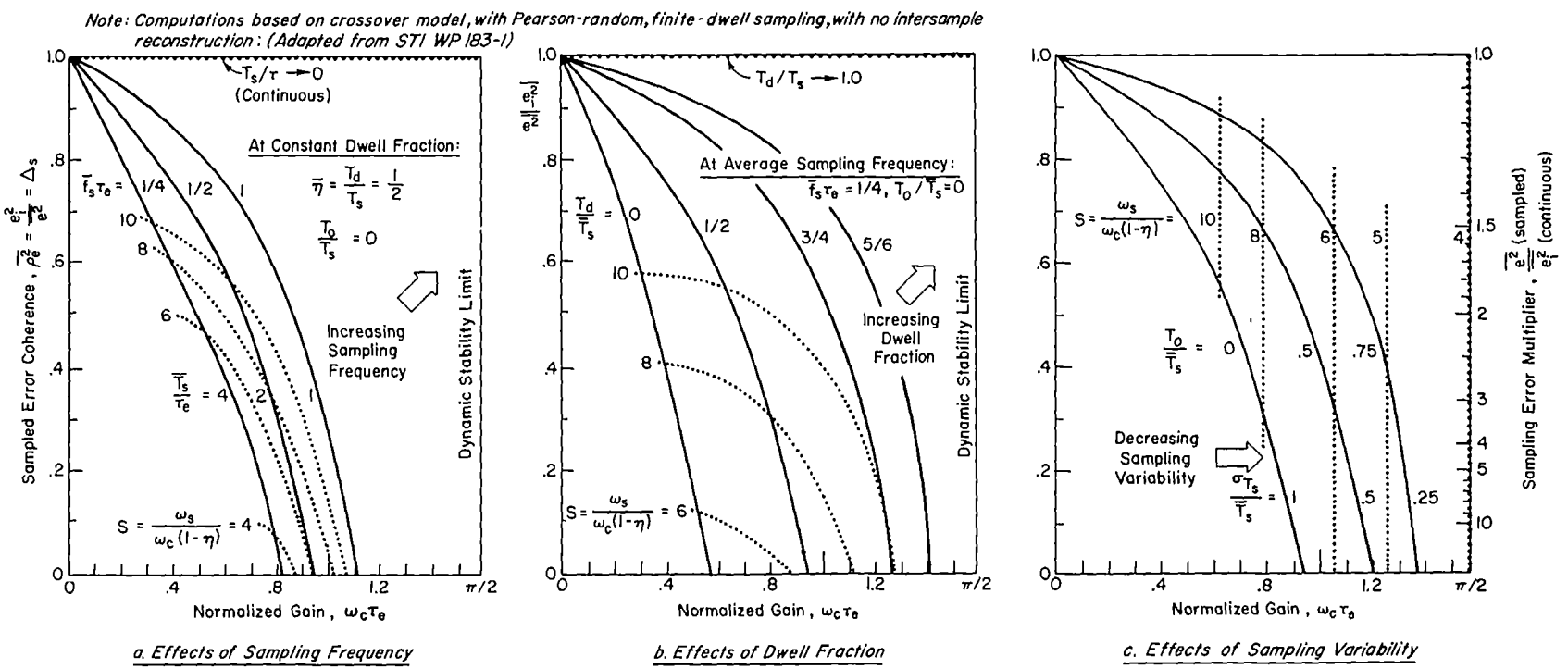

Figure 7. Effects of Random Finite-Dwell Sampling on Closed-Loop Error Coherence

In an effort to coalesce the effects of the several variables, a unifying parameter combination was sought. One such combination appears in several derivations for finite-dwell sampling and will be termed the "Sampling Frequency Parameter" S:

$$S \equiv \frac{\omega_s}{\omega_c(1-\eta)} \tag{7}$$

where: ω_s/ω_c = ratio of sampling-to-crossover frequencies

$\eta = \overline{T_d}/\overline{T_s}$ = dwell fraction

Denoting the average nonfixated period by $\overline{T_\Delta} = \overline{T_s} - \overline{T_d}$, and the crossover period as $P_c = 2\pi/\omega_c$, algebraic manipulation of the above expression gives the simpler expression: $S = P_c/T_\Delta$. This suggests a simple physical meaning for S, as the ratio of the crossover period relative to the time-away from the display. This ratio should be large to minimize scanning remnant effects. Dotted curves of constant S have been put on Fig. 7a, b, c. For reasonable combinations of dwell fraction, sampling frequency, and sampling variance, these computations show that values of S between 4 and 8 are required to keep sampling remnant within reasonable bounds.

The effects of crossover gain on the net errors with random finite-dwell sampling were also computed in Ref. 52. In addition to the normal influence of input bandwidth, ω_i, time delay τ_e and gain ω_c, there are complex additional effects due to dwell and sampling intervals and sampling variability. A typical case is sketched in Fig. 8, for continuous versus sampled loop closures. Notice that sampling effects

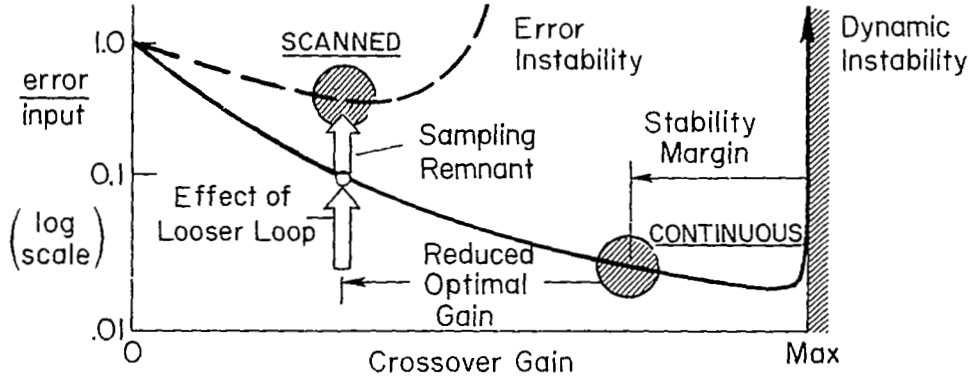

Figure 8. Sketch of Scanning Implications on Gain and Performance

penalize tracking performance two ways: by reducing the permissible crossover gain, and by adding the sampling remnant.

D. EXPERIMENTAL IMPLICATIONS

If these simple analytical models for sampling and reconstruction can be validated experimentally, then we will have a powerful tool for understanding, analyzing, and predicting performance of multi-instrument displays. Three aspects should be tested; verifying the basic assumptions, observing if the predicted qualitative interactions between sampling and loop closure variables occur, and checking the accuracy of the computed performance curves.

The following key assumptions must be checked:

1. Do different pilots adopt the same average scanning, sampling, and reconstruction strategy?
2. Are the sampling intervals randomly distributed about some mean value?
3. Is the sampling frequency high enough to justify a describing function representation?
4. Does the form of the perceptual describing function fit Eq. 1?
5. Is the sampling remnant broadband?
6. To what extent does reconstruction take place between fixations?

In regard to the last item, there are two more-or-less alternative strategies which the human might adopt: simple-finite-dwell-sampling versus finite-dwell-sampling-with-reconstruction. Table II points up some of the theoretical implications of each. Because of conflicting tradeoffs between remnant, time delays, and the perceptual reconstruction "load," it is not yet possible to <u>a priori</u> select the likely reconstruction mode.

To test the accuracy of the crossover model computations, one must force a range of perceptual scanning behavior, covering independent variations in scanning frequency, dwell time, input bandwidth, and

TABLE II

IMPLICATIONS OF ALTERNATIVE SAMPLING MODES

TYPES OF SAMPLING	CROSSOVER GAIN	EFFECTIVE DELAY		REMNANT	
None (continuous)	High	Small		Small	
Simple Finite Dwell	Low	Small		Large	
Finite-Dwell plus Reconstruction	Medium	$\dot{R} \doteq 0$ Large	$R \gg 0$ Small	$\dot{R} \doteq 0$ Medium	$R \gg 0$ Small

crossover frequency. Measurements of fixation statistics and describing functions are necessary, as well as overall performance.

We now have an empirical, conceptual and theoretical foundation on which to construct the experimental program, to be described next.

SECTION III

EXPERIMENTAL PROGRAM

A. PURPOSE

One objective of the present research is to obtain a sorely lacking data base for the basic sampling and reconstruction processes and remnant changes occurring when a pilot is required to scan and sample complex displays. The experiments include the investigation of interactions between scanning and sampling, and the role of parafoveal vision on scanning effectiveness in a high workload environment.

B. APPROACH

The experiments were conducted in three phases:

1. Preliminary tests were performed to determine the best means for inducing realistic scanning by the pilots.
2. A training phase was conducted to stabilize the subject's scanning behavior and to reveal the most fruitful experimental conditions.
3. Data were collected in a formal experiment.

C. TRACKING TASKS

The pilot/subject's primary task was tracking with a compensatory display and a first order (K/s) controlled element as shown in Figs. 9 and 10. The K/s controlled element was chosen to minimize the operator's adaptation requirements under nonscanning conditions, since past research has shown that lead or lag equalization is minimal in this case. Controlled element effects were <u>not</u> a factor in these experiments.

Input forcing functions of three different bandwidths were used. The inputs were composed of eight nonharmonically spaced sine waves with amplitudes shaped according to a double-lag, double-lead spectral envelope. The line spectra of the 0.5, 1, and 2 rad/sec bandwidth inputs used in the experiment are shown in Fig. 11. The root mean-square amplitude

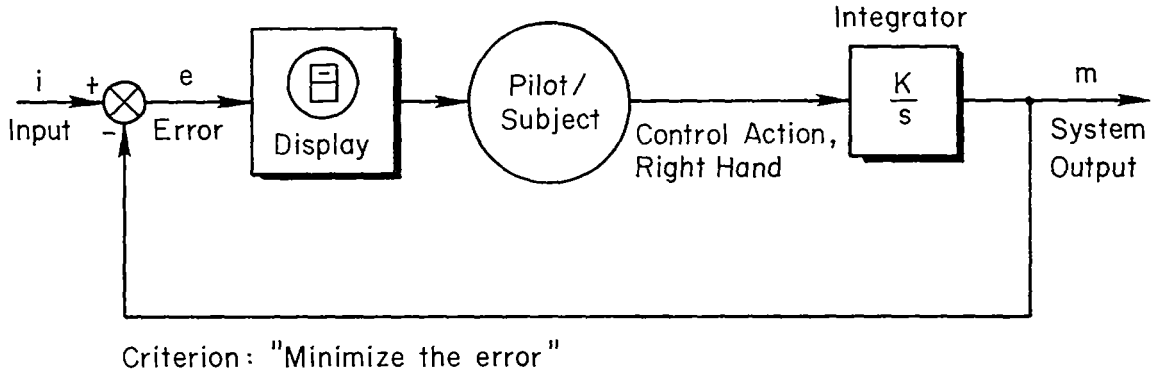

Criterion: "Minimize the error"

a) Primary control task, a compensatory tracking loop

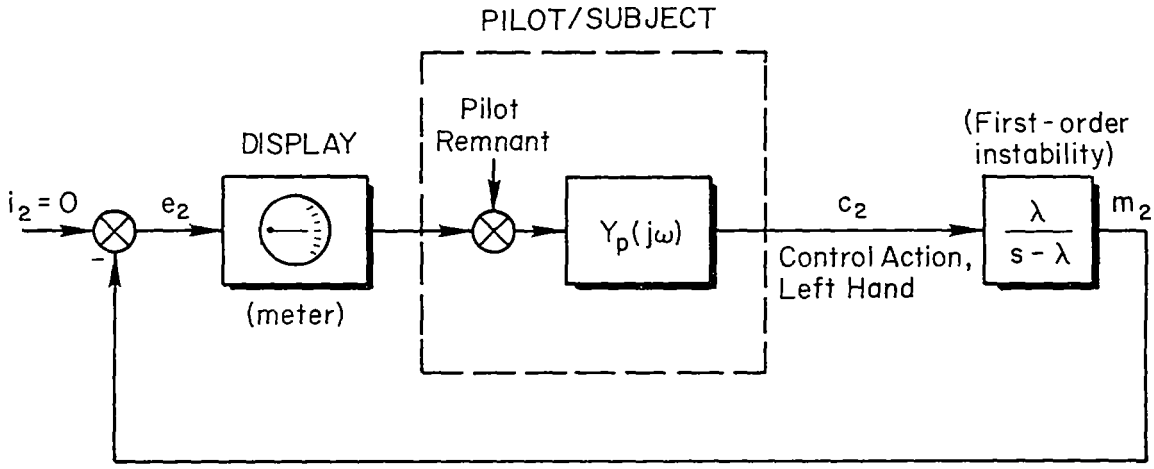

Note: Pilot's remnant provides excitation
Criterion: "Stabilize the loop"

b) Secondary control task, a tracking loop with first-order divergent controlled element

Figure 9. Main and Secondary Control Tasks

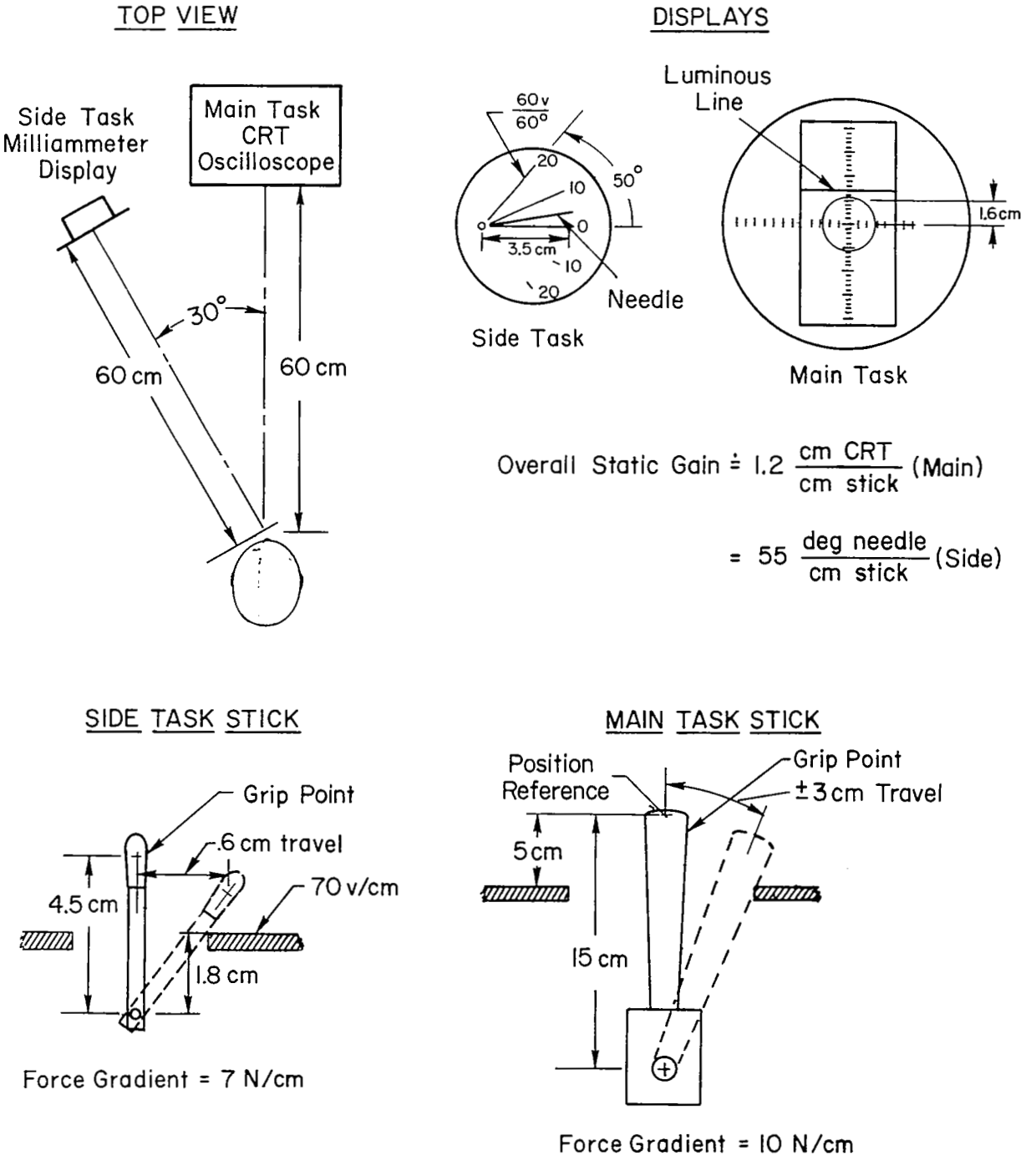

Figure 10. Displays and Controls

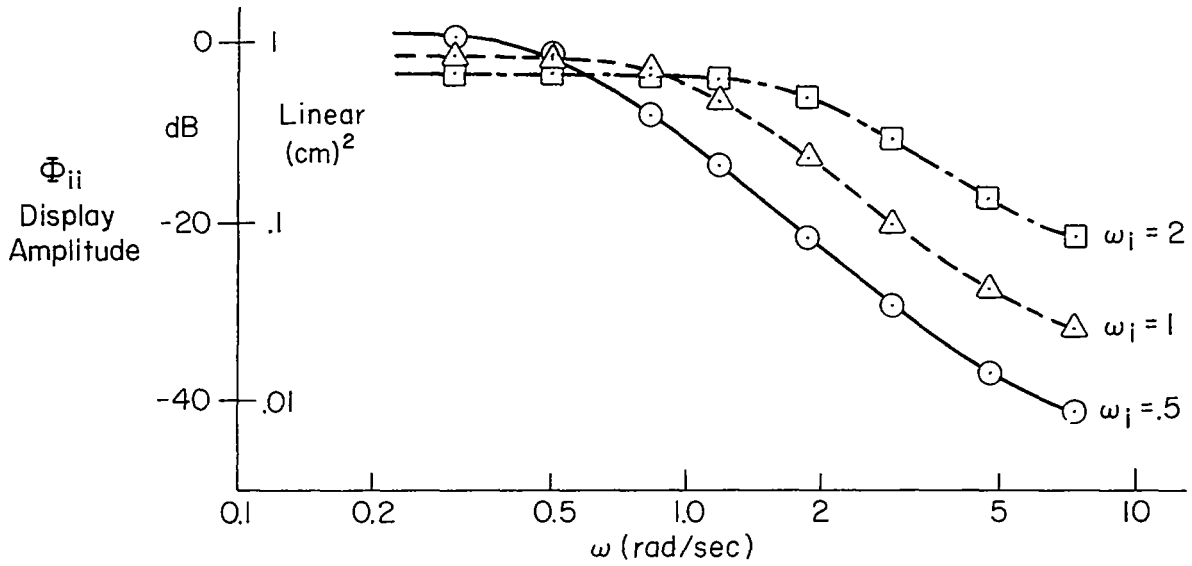

Figure 11. Forcing Function Input Spectrum Envelope

of the displayed input was set at $\sigma_i = 1.0$ cm. Table III gives the input frequencies and Table IV describes the spectral envelope parameters of the three inputs. The second-order lag/lead envelope was chosen: 1) to provide a main input band plus a shelf-like extension; 2) to avoid the sharp shelf discontinuity which has caused data reduction artifacts in some past experiments; 3) to have an analytically tractable envelope for computation; and 4) to permit shaping of a prerecorded sum-of-unit-sinusoids input tape by an easily mechanized filter.

TABLE III

FORCING FUNCTION INPUT SINE WAVES

COMPONENTS	FREQUENCY (rad/sec)	NUMBER OF CYCLES IN 100 SEC
1	0.314	5
2	0.503	8
3	0.816	13
4	1.19	19
5	1.89	30
6	2.89	46
7	4.76	76
8	7.35	117

TABLE IV

INPUT FORCING FUNCTION SPECTRAL ENVELOPE

FORCING FUNCTION SPECTRAL ENVELOPE:

$$\Phi(\omega) = K \left| \frac{\left(\frac{j\omega}{\omega_1}\right)^2 + \frac{2\zeta}{\omega_1} j\omega + 1}{\left(\frac{j\omega}{\omega_2}\right)^2 + \frac{2\zeta}{\omega_2} j\omega + 1} \right|^2_{\zeta = 0.71}$$

Forcing Function Bandwidth ω_i (rad/sec)	Lag Break Frequency ω_2 (rad/sec)	Lead Break Frequency ω_3 (rad/sec)
0.5	0.5	6.3
1	1	6.3
2	2	6.3

Two secondary tasks were tried to force the pilot/subject to realistically scan and sample the primary task display. The first attempt to induce scanning used a signal light 30 deg to the left of the main task display. The light turned on and off in a random sequence and the subject was instructed to look at it when it was on. This method of forcing scanning behavior met with limited success, as will be explained later. Finally, a secondary control task was employed that demanded the subject's attention in a more natural manner. An experienced instrument pilot was used to help develop a realistic scanning situation.

The secondary control task required the subject to stabilize an unstable first-order controlled element with no forcing function other than his scanning remnant, as shown in Fig. 9. The secondary task display was placed 30 deg to the left of the main task display so as to require a definite scanning action by the subject in order to control both tasks. The subject controlled the secondary task with his left hand by manipulating a small side stick. Reference 53 describes this technique in more detail.

The side task was designed to terminate the run if the error exceeded the display limits, thus placing a small performance demand, but a large motivational demand, on the subject.

The attentional demand of the side task could be varied by changing the time constant of the unstable controlled element. A decrease in the time constant, T_λ (or increase in $\lambda = 1/T_\lambda$) decreases the time at which the error diverges to the display limits, so that the subject must pay more frequent attention to the secondary task in order to prevent termination of the run.

D. EXPERIMENTAL MEASUREMENTS

Two categories of experimental measurements were made: (1) online measures computed during the run and recorded at the end of each run, and (2) measures obtained through digital computer analysis of data tape recorded during the experiment.

The online measures given in Table V were used for two purposes: (1) to analyze the scanning process adopted by the pilot/subjects and determine the performance interaction between the primary and secondary tasks, and (2) to indicate which experimental trials would yield the most fruitful results from the digital data analysis.

The measurements obtained through digital computer analysis are also given in Table V. The digital computation measures are divided into three general categories: (1) statistics, (2) describing functions, and (3) raw power spectra and power spectra with remnant averaged over frequency bands between input correlated components.

As noted from Table V, the describing function measures give a fairly complete description of the open-loop and closed-loop response of the main task control system, in addition to yielding the pilot's frequency response, closed-loop remnant, and correlated error.

E. EQUIPMENT

Tracking Station. The top view of the tracking station shown in Fig. 10 gives the important dimensions of the experimental equipment and layout. Basically, the same setup and pilots were used as in Ref. 44. The main

TABLE V

EXPERIMENTAL MEASURES

ONLINE MEASURES
Sampling Behavior
• Number of scans per 100 sec trial (100 f_s)
• Integrated main task dwell time per 100 sec trial (100 T_d/T_s)
Performance Measures (Main and Secondary Tasks)*
• Absolute Integrated Error per 100 sec trial (100 $\overline{\lvert e \rvert}$)
• Absolute Integrated Control Action per 100 sec trial (100 $\overline{\lvert c \rvert}$)
DIGITAL DATA ANALYSIS MEASURES
Statistics
• Sampling and dwell-time histograms
• Amplitude and First Difference Probability Distribution Histograms for error and controller output signals
• Input correlated and total mean-square value of error and controller output signals
Spectra
• Complete signal spectra
• Signal spectra with remnant averaged between input correlated components
Describing Functions
• Error-to-input describing function $[E(j\omega)/I(j\omega)]$
• Open-loop describing function $[Y_pY_c = M(j\omega)/E(j\omega)]$
• Pilot describing function assuming normalized controlled element gain $[Y_p = C(j\omega)/E(j\omega)$, where $Y_c = 1/s]$
• Closed-loop describing function $[M(j\omega)/I(j\omega)]$

*A bias type nonlinearity near null in the absolute value circuit was discovered following the program. Therefore, $\overline{\lvert e \rvert}$ and $\overline{\lvert c \rvert}$ measures may be in error at the smallest levels recorded.

task display was a 5-in. CRT oscilloscope with a reticle design as shown in Fig. 10. A polarized viewer was placed over the CRT reticle to reduce reflections of the surround. The display cursor was generated by applying a 500 Hz sine wave voltage to the horizontal sweep of the oscilloscope, so that the display could be interrupted, or "blanked," by removing this excitation voltage.

The **main task hand control** was a finger operated, fairly stiff, spring restrained side stick with minimal friction, viscous damping, and inertia. The stick characteristics are listed in Fig. 10 along with the display/control gain.

Two types of **side task display** were used. For the forced scanning trials the side task consisted of a randomly illuminated pilot light with a red cover glass. In the natural scanning tests the light was replaced by the secondary control task display. The display was a Weston microammeter meter with a white face design shown in Fig. 10. A first-order lead circuit was used to compensate for the meter's dynamic lag through the crossover frequency region. The secondary task display face was dark under ambient room lighting. This "blanked" state was achieved by a pair of polarizing filters in front of the dial. The display could be illuminated by instrument lights mounted between the display and polarizing filters. Thus, the secondary display information could be interrupted by merely switching off the display illumination.

A finger operated, spring restrained hand control was used for controlling the secondary task. The control's characteristics and the display/control gain are given in Fig. 10. Both displays were of high contrast and about equally prominent. The CRT line and side task meter needle were the same length and thickness. Seldom was more than one saccade necessary to fixate each display.

Eye Movement Instrumentation. The pilot/subject's scanning behavior was determined through continuous measurement of eye movements with a Biosystems Model SGHV-2 eye movement monitor. The monitor includes infrared sensing of the boundary of the cornea and sclera, using lightweight sensors mounted on a spectacle frame. The SGHV-2 yields voltages proportional to eye position in both the vertical and horizontal planes. Because the displays for the two tasks used in this experiment were in a horizontal plane the vertical sensor axis was not used.

The main purpose was to determine whether the subject was looking at the secondary task display (left) or the primary task display (right). Preliminary trials indicated that although the subjects moved their head slightly while tracking and scanning, the eye movement signal alone could clearly differentiate between fixations on the left and right displays. Thus head movement was neither artificially restrained nor measured.

To deny parafoveal viewing of the nonfixated display in one set of conditions, it was switched off while the display to be fixated was switched on as the eye movement signal passed the halfway point. Thus, the desired display was always "there" when fixated, yet the blanking per se could not be detected.

Simulation Equipment. The control loop dynamics and online performance measures were mechanized on a conventional analog computer. The various tracking loop signals and a 40 Hz digitizing signal were FM tape-recorded (at 1-7/8 in./sec and 1.6875 KHz center frequency) on a Minneapolis Honeywell Model 7600 tape recorder.

The main task input forcing functions and 40 Hz digitizing signal were recorded on and replayed from an Ampex FL-100 tape loop machine with Honeywell 7600 record/reproduce electronics. The inputs were generated by summing sine waves that had been precisely generated on a digital computer, converted to analog form in synchronism with the prerecorded 40 Hz digitizing signal and recorded on a master input "repertory" tape. The original 40 Hz digitizing signal was also recorded on this repertory tape and formed the time base for all subsequent data processing. Thus, low frequency tape speed variations and drifts were removed as a source of timing errors.

Digitally computed spectra and describing functions were obtained by digitizing the FM analog signals and using selected BOMM language subroutines (Ref. 54) on a CDC-3600 digital computer.

F. PILOTS

Two light plane pilots with previous tracking research experience were employed as subjects, Ref. 3. A resume of their flying experience is given in Table VI. The pilot/subjects had previously performed in

TABLE VI

PILOT SUBJECT STATISTICS

PILOT	AGE	AERONAUTICAL RATINGS	TOTAL FLIGHT HOURS	INSTRUMENT HOURS
1 (RH)	23	Commercial; Instructor; Instrument	2,800	175
2 (PH)	24	Instructor; Multi-engine; Instrument	1,700	50

over 100 2-min tracking trials involving K/s and K/s^2 controlled elements in both compensatory and pursuit display dynamics, and had reached asymptotic performance on the apparatus.

G. PRELIMINARY EXPERIMENTS

Forced Scanning. The first attempt at inducing scanning behavior in the pilot/subjects was to have them look 30 deg away from the primary display at a "distraction light" when this light was "on." The distraction was commanded at random intervals, having a mean interval of 0.7 sec and a standard deviation of 0.2 sec. The off-time of the light was held constant at 0.5 sec which was felt to be long enough to allow the subject to directly perceive error displacement and rate on the main task display.

A typical time history from a tracking trial is shown in Fig. 12. Note that the subject's eye-point-of-regard (EPR) correlates very poorly with the commanded sampling behavior. The pilots claimed that forced scanning was extremely unnatural and difficult to follow. It was concluded that scanning would have to be induced naturally in order to obtain meaningful results.

Natural Scanning. To induce natural scanning the pilot/subject was required to stabilize an unstable secondary axis of control, as described in Section III.C, in addition to the primary tracking task. The subjects were instructed to minimize the main display error, but no performance

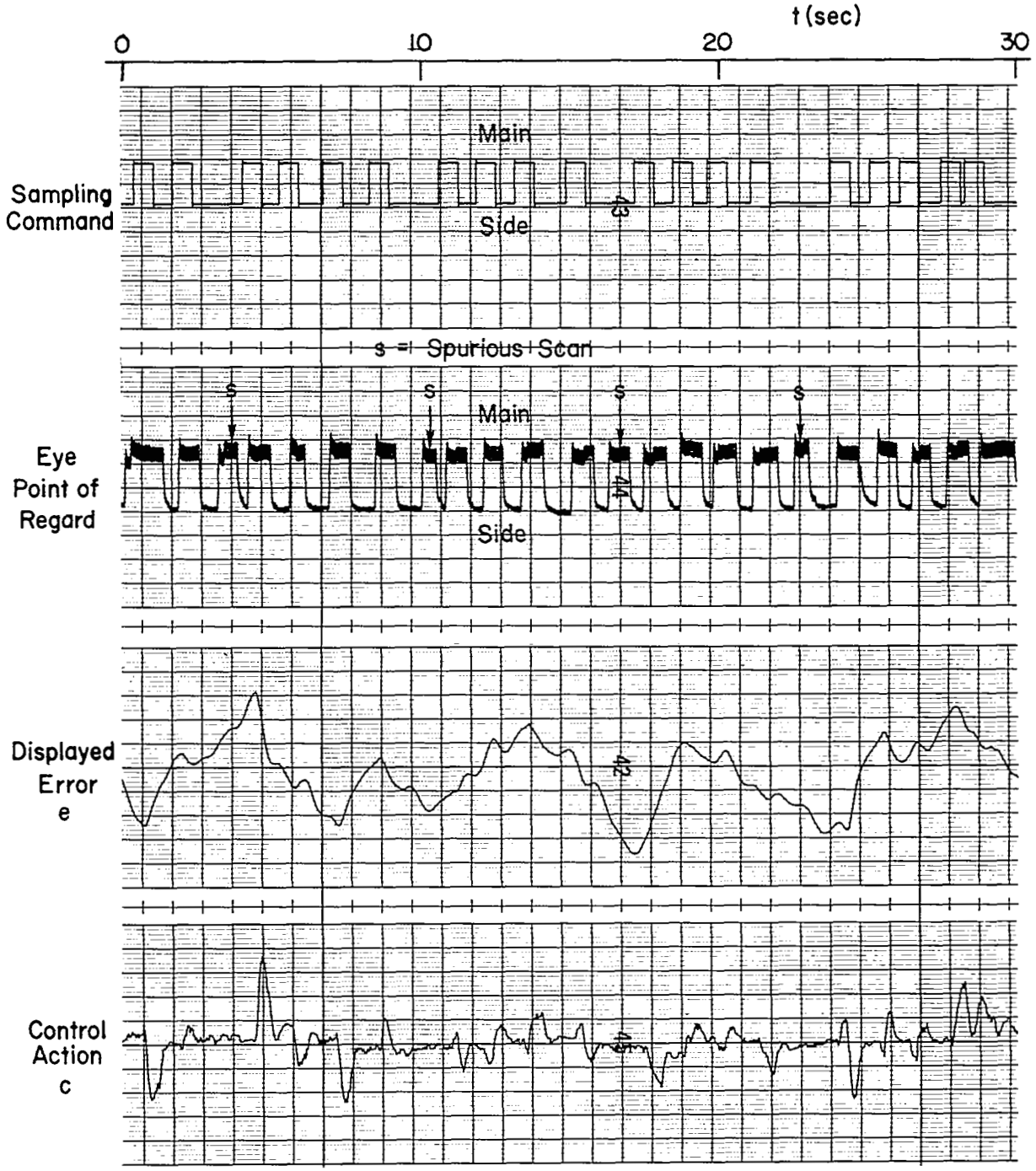

Figure 12. Time History with Sampling Command Light Showing Poor Correlation of Scanning with Commands

criterion was placed on the side task other than to keep error within the display limits in order to avoid terminating the run.

By using various combinations of main task input bandwidth ($\omega_i = 0.5$, 1, or 2 rad/sec) and side task instability ($\lambda = 0.5$, 1, and 2 rad), it was found that a wide range of scanning rates and dwell times could be invoked in all subjects. This is a useful technique since it permits testing of the theoretical models over a range of subject-governed scanning policy.

Blanking of Parafoveal Information. In order to assess the importance of parafoveal cues on tracking behavior while scanning, either the main task or secondary task display was blanked out when it was not being foveally viewed by the subject. The subjects did not find this condition too disconcerting. Some changes in performance and scanning behavior were caused by the display blanking, so this condition was included in the formal experiment.

Blanking to Prevent Direct Rate Perception. To deny the subjects direct error rate perception from the main task display, an attempt was made to apply a zero-order hold to the main task error when the subject foveally viewed the main task display. The subjects commented that this was a completely unnatural condition because it denied them immediate feedback on their main task control response. This condition probably opened up the internal stimulus/response loop in the subjects, involving proprioceptive feedback, and they found it very disconcerting.

A successful alternative was to truncate the main task display "on" time, thereby limiting the perceptual dwell time. Under this condition the subject was still allowed to choose his own scanning policy; however, the nonfixated display was blanked and in addition the main display information was only presented for 0.25 sec. This value was selected on the basis of previous work showing an eye movement refractory time on this order, and on the basis of the minimal time for an accurate judgment of analog position to be made (Ref. 44) thereby allowing no time for a judgment of error rate to be made. The subjects were able to accommodate this condition and offered the comment that the main task display cursor appeared as though it "jumped" from one sample to the next. This technique formed the fourth sampling treatment in the formal experiment.

Parafoveal Tracking. Tracking with pure parafoveal viewing (eye fixated 30 deg from the display) was also tested in the preliminary experiment. The subjects were told to continuously observe the side task display while performing the main task (the side task was not being performed). Performance was severely degraded over foveal tracking, as found in Ref. 7. The subjects commented that during pure parafoveal tracking they lost track of the zero reference line. This was evident in the oscillograph recordings of the error signal which exhibited large random drifts. This effect was minimized by carefully lining up the zero reference lines of both displays in the same horizontal plane and placing a zero reference marker midway between the displays. We decided to include pure parafoveal tracking in the foveal experiment, both as a tie-in with the research of Levison and Elkind, and to assess the importance of parafoveal cues in our experimental context.

Pilot Dither. Some stick "dither" in the pilots' main task control movements was noted during preliminary parafoveal tracking. Dither was also apparent in some of the scanning conditions. When questioned, the pilots replied that dither enhanced parafoveal perception because the display cursor moved more quickly.* Since dither was not used routinely by pilots in flight, and because it would interfere with the Fourier analysis measures to be applied to the data, the pilots were asked to minimize their dither.

H. TRAINING ON THE NATURAL SCANNING TASK

Training on the natural scanning task was started before the design of the formal experiment was completed, because certain conditions that were extremely difficult at the beginning yielded useful results when trained.

Table VII gives the number of two-minute tracking trials performed by each of the pilot/subjects for various experimental conditions. The total training time on conditions requiring scanning exceeds 2-1/2 hours.

*Parafoveal perception is more sensitive to rate than displacement when compared with foveal perception.

TABLE VII

NUMBER OF TWO-MINUTE TRAINING TRIALS
AT VARIOUS EXPERIMENTAL CONDITIONS

SCANNING CONFIGURATION		PILOT-SUBJECT					
		No. 1			No. 2		
		INPUT BANDWIDTH (α_i)			INPUT BANDWIDTH (α_i)		
		0.5	1	2	0.5	1	2
No Scanning Pure Foveal Viewing "F"			5	2	2	8	
No Scanning Pure Parafoveal View "P"			11	11	2	10	9
Natural Scanning with Parafoveal Viewing Allowed "SP"	$\lambda = 0.5$		3	7		3	4
	$\lambda = 1$		13	3		7	2
	$\lambda = 2$		13	3		12	
Natural Scanning with Parafoveal Cues Blanked "SB"	$\lambda = 0.5$	4	2		2	5	
	$\lambda = 1$		7	6		6	
	$\lambda = 2$	4	2		7	6	
Natural Scanning with Parafoveal Cues Blanked and Main Task Dwell Truncated to 0.25 sec. "$SB_{.25}$"	$\lambda = 0.5$	12			13	7	
	$\lambda = 1$		3			4	

Training results indicated that the pilots' sampling behavior and tracking performance had reached stable levels prior to the formal experimental trials. The pilots commented that the combination of exercise and learned technique caused only nominal eye fatigue.

I. EXPERIMENTAL DESIGN

Design. Figure 13 gives a resume of the experimental conditions used in the formal experiment. On the basis of results from the training phase it was decided to use the combination of 1.0 rad/sec main task input

SCANNING MODE	TASK VARIABLES	CONFIGURATION CODE
1. No scanning; full continuous foveal viewing of main task display	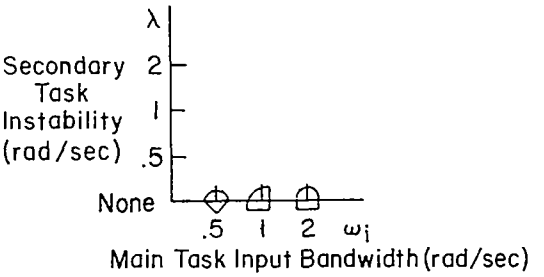	F
2. No scanning; continuous parafoveal viewing (30° off-fovea) of main task display	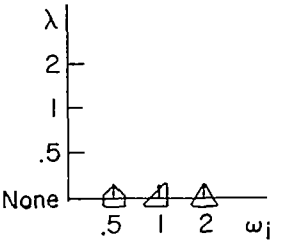	P
3. Natural scanning, with parafoveal perception of nonfixated display	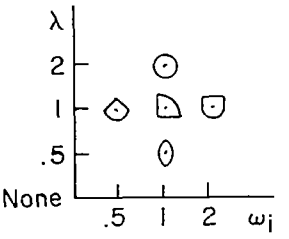	SP
4. Natural scanning, with nonfixated display blanked to preclude parafoveal utilization	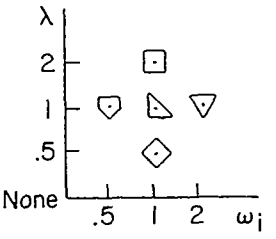	SB
5. Natural scanning, with nonfixated display blanked and the main display blanked after 0.25 sec to preclude rate perception	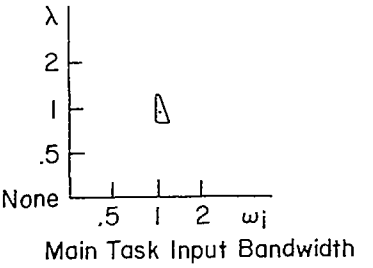	$SB_{.25}$

Figure 13. Experimental Design

bandwidth and secondary task instability of 1.0 rad/sec as the standard scanning condition in the blanked, unblanked and truncated main task dwell display configurations. Various other combinations of main task input bandwidth and side task instability were included to determine the influence of these parameters.

Full foveal viewing of the main task was used as the reference condition from which the changes due to scanning could be compared.

Table VIII gives the order in which the experimental conditions were administered to the subjects. Two replications were run for each condition, and the presentation order was counterbalanced between the two subjects. The large number of experimental conditions necessitated presenting them in two sessions, so an attempt was made to present an equal number of easy and difficult conditions in each session.

Procedure. The formal experimental trials were conducted in two 2-1/2 hour sessions for each subject. Two warm-up runs were given at the beginning of each session, consisting of a base foveal tracking condition and a condition requiring scanning. Each experimental condition was replicated twice. At the midpoint of each session the subjects were given a 10 min break. Each tracking run lasted about 2-1/2 min. The last 2 min were tape recorded for digital data analysis, while the online performance measures were obtained over the last 100 sec of each trial.

TABLE VIII

EXPERIMENTAL CONDITION PRESENTATION ORDER

	DAY 1			DAY 2		
	MAIN TASK INPUT BANDWIDTH (ω_i)	SCANNING CONFIGURATION CODE	SIDE TASK INSTABILITY (λ)	MAIN TASK INPUT BANDWIDTH (ω_i)	SCANNING CONFIGURATION CODE	SIDE TASK INSTABILITY (λ)
RH	1	F	—	0.5	F	—
	1	P	—	0.5	P	—
	1	SP	1	1	SP	0.5
	2	SB	1	1	SP	2
	1	SB.25	1		Break	
		Break		1	SB	1
	1	SB	2	0.5	SP	1
	0.5	SB	1	2	P	
	1	SB	0.5	2	F	
	2	SP	1			
PH	2	F	—	2	SP	1
	2	P	—	1	SB	0.5
	0.5	SP	1	0.5	SB	1
	1	SB	1	1	SB	2
		Break			Break	
	1	SP	2	1	SB.25	1
	1	SP	0.5	2	SB	1
	0.5	P	—	1	SP	1
	0.5	F	—	1	P	—
				1	F	—

SECTION IV

PRESENTATION OF RESULTS

This chapter contains various presentations of on-line and reduced describing function data and some statistical analyses between certain variables. However, the interactions between these experimental variables and the resulting scanning and tracking performance are so complex that no simple data presentation can be made to clarify them. Consequently, correlation of the data with the theory of Section II is deferred to Section V.

First, the data from on-line performance measurements will be reviewed, starting with time histories, scanning statistics, and performance. The latter half of the chapter contains describing function measurements and remnant computations.

A. ON-LINE SCANNING AND PERFORMANCE MEASURES

1. Typical Time Histories

To obtain a feel for the types of display, control, and scanning behavior being analyzed in these sections, consider the typical time histories presented in Figs. 14, 15, and 16. Figure 14 compares compensatory tracking when regarding the display with **full foveal** attention, versus the **full parafoveal** case, where the subject was looking 30 deg to one side. The eye movement trace at the bottom of Fig. 14 is not the true eye-point-of-regard (EPR) since it has not been corrected for head movements, which cause the slow drifts noted thereon. Nevertheless, the eye movements show that the subject did not look at the main display under the full parafoveal condition. The quick pulses on the EPR trace are blinks, as noted thereon. The salient points to be gleaned from Fig. 14 are as follows:

- The error and control signals are fairly random-looking and probably have a reasonably Gaussian distribution.

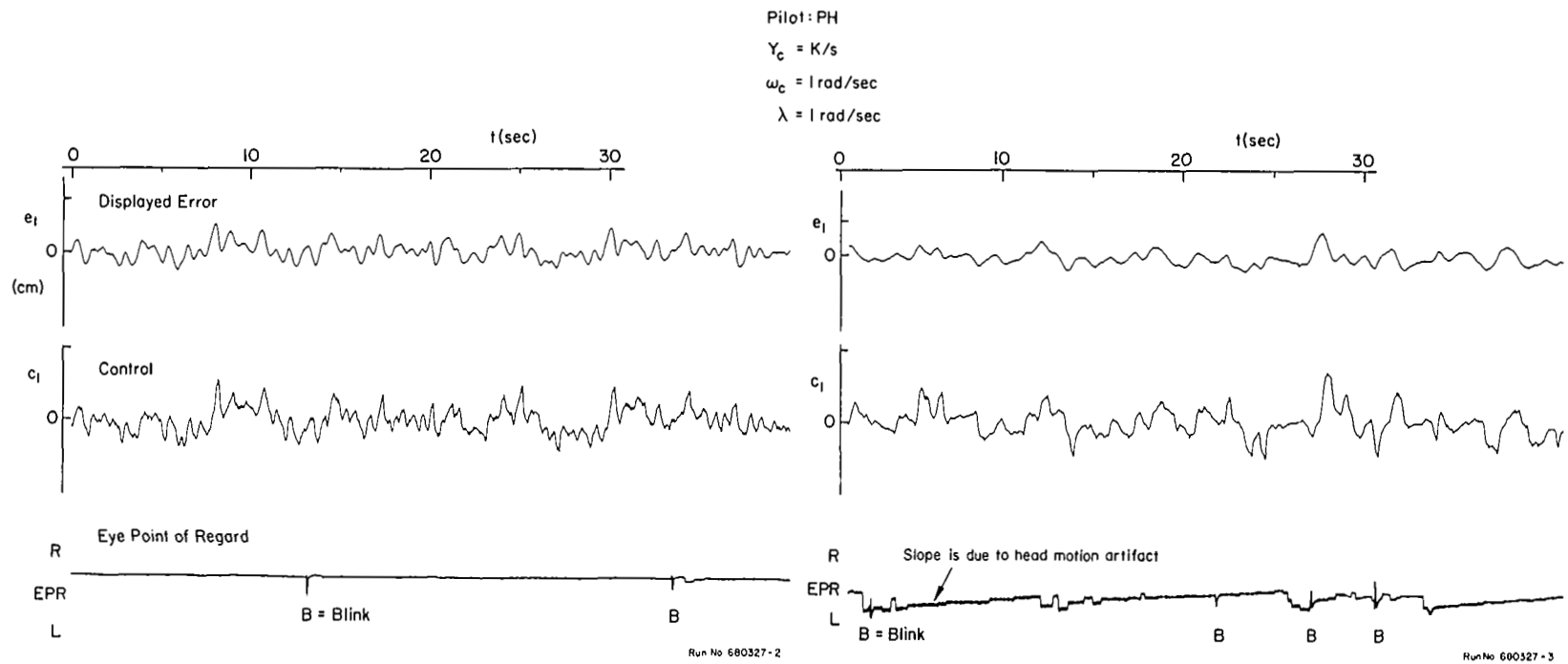

a) Foveal Tracking (Fixation to Right)

b) Parafoveal Tracking (Fixation to Left)

Figure 14. Time Histories of Foveal and Parafoveal Tracking

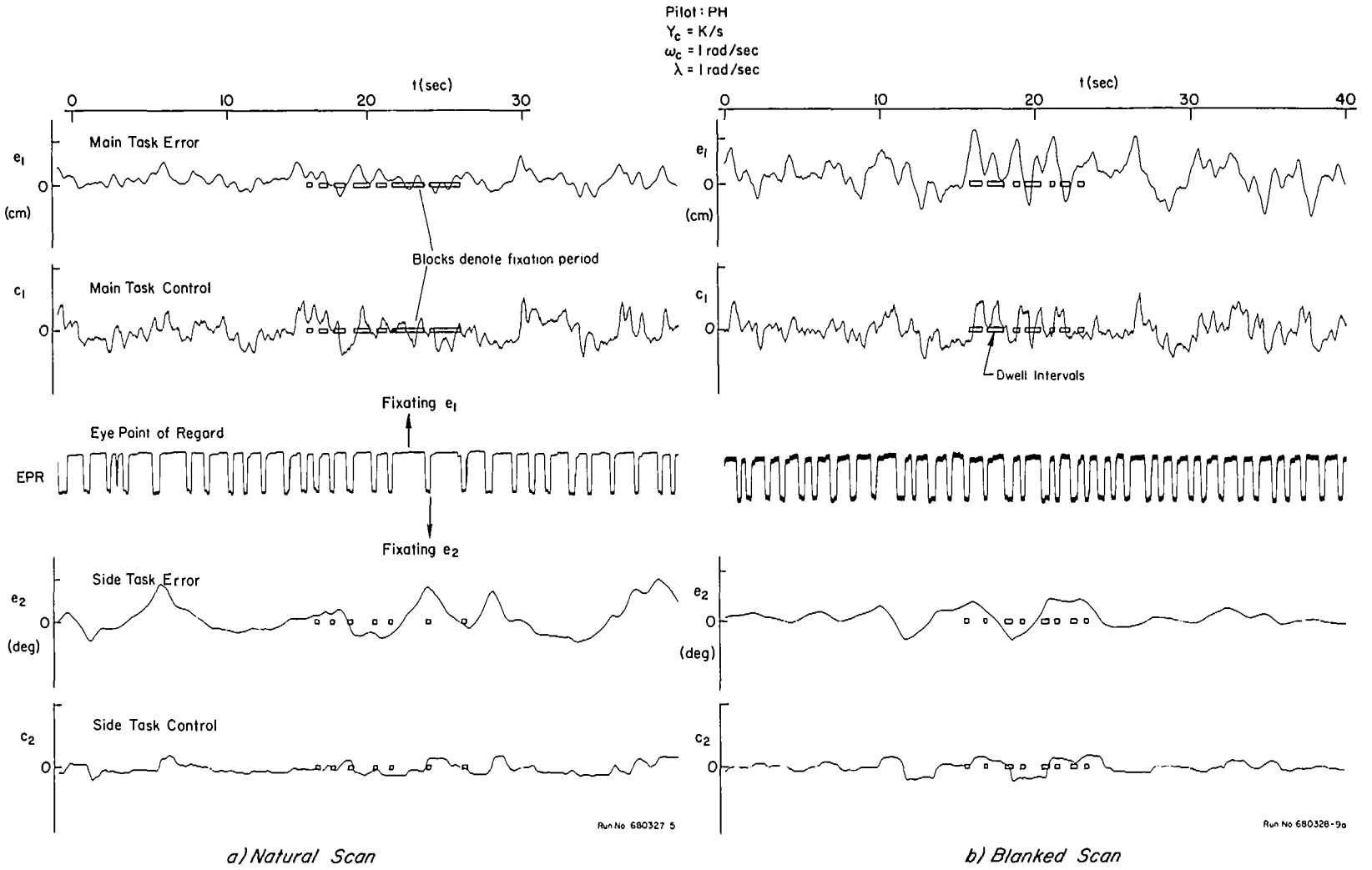

Figure 15. Time Histories of Natural and Blanked Scan Tracking

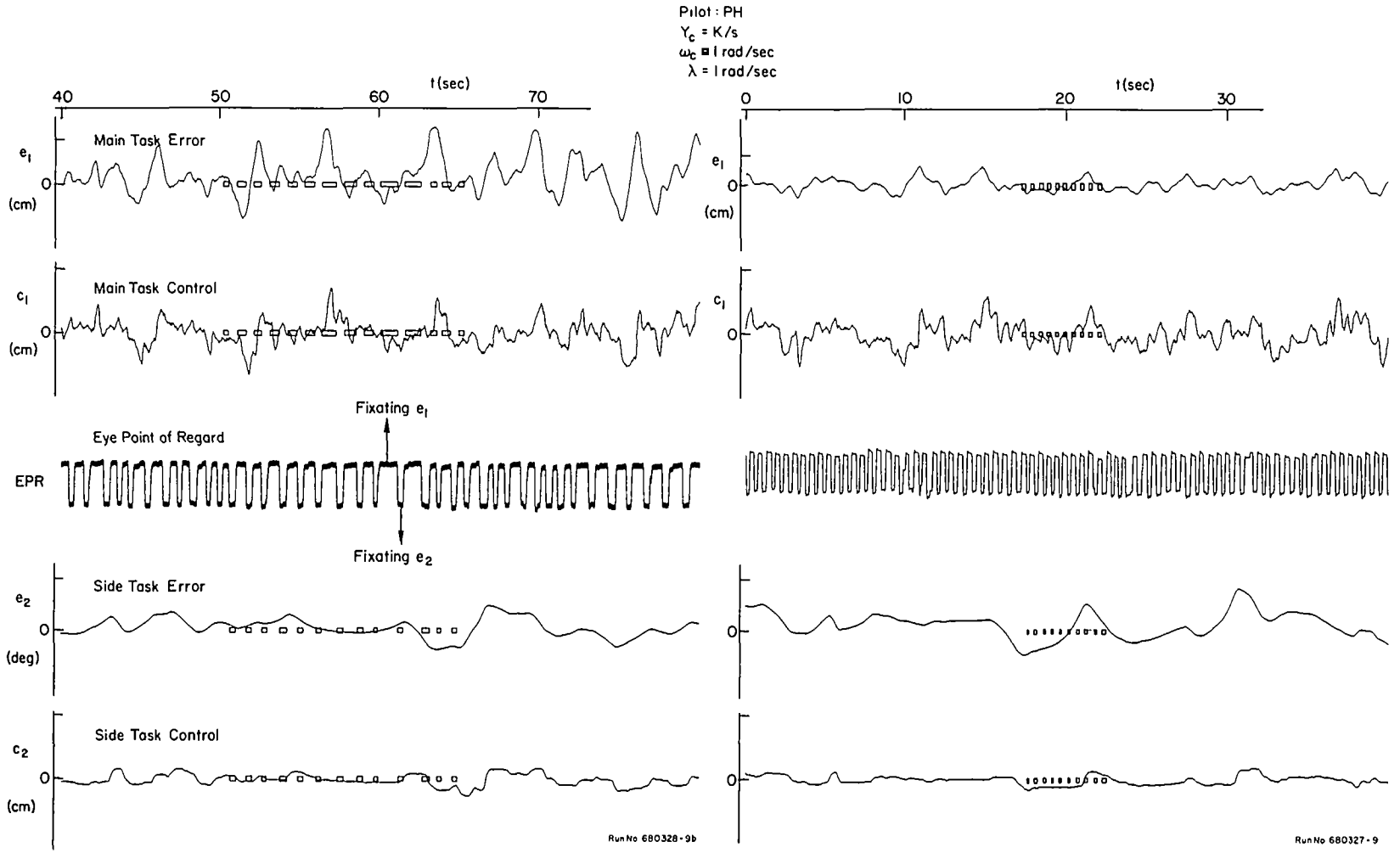

a) Blanked Scan

b) Blanked Scan with Main Display "on" Dwell Time Limited to .25 Seconds

Figure 16. Time Histories of Blanked and Truncated-Blanked Scanning

- Parafoveal-case error is substantially larger than the foveal case (note the increased scale).
- In either case, the control signal is fairly continuous and roughly proportional to the error signal.
- There appears to be less high-frequency control activity in the parafoveal case, with a tendency to larger, more discrete control actions.

The above results are consistent with a quasi-linear tracking model involving substantially lower effective gain in the parafoveal situation, as will be shown by the describing function data. These data verify the pioneer work in Ref. 7 which indicated that continuous parafoveal tracking was possible.

The time history shown in Fig. 15 compares natural and blanked-scanning behavior for one pilot. The main task error and control are shown at the top, the eye-point-of-regard at the middle, and the side task error and control at the bottom. Regarding the side task first, it can be seen that the error tends to diverge off-scale unless prevented from doing so by suitable (roughly proportional) control action. Looking at the main task traces, it is apparent that the error and control signals are roughly similar, albeit somewhat larger than full foveal tracking. The eye movement signal shows clearly that the majority of the scan time is spent fixating the main task display, with frequent, short fixations on the side task. These side dwells are consistently just under 0.5 sec. The sampling intervals have a readily apparent average, but intervals well above and below this average are also obvious. Histograms of these intervals are presented later.

Behavior during the blanked-display case is similar to the natural scanning case, except that the errors are larger, the scanning is more frequent, and the control behavior appears somewhat more pulsed.

Dark lines have been added to a portion of the error traces to define those periods when that display was being fixated. From these it is obvious that the display is regarded not only when it exceeds a given threshold in either position or rate. Occasionally there is a correlation between some of the control action peaks and a slightly prior

fixation on that display (e.g., the c_1 trace around $t = 15 - 20$ sec in Fig. 15a and also Fig. 15b during the same period). This sort of action is consistent with the model of finite-dwell signal reconstruction ahead of the neuromuscular system. Generally, however, there is no obvious relationship of control pulses and dwells.

Finally, let us contrast the type of scanning adopted in the simple blanked scan case with that adopted when the on-time of the main display is truncated to only 0.25 sec. This is shown in Fig. 16b (Fig. 16a is a continuation of the run shown on Fig. 15b). It is readily apparent that a much faster scanning mode is adopted in this case. Because the main display only stays "on" for a time too short to perceive its rate, the pilot can neither reconstruct the effective input signal between scans, nor can he perceive the actions of his own control. Consequently, he is forced to adopt the technique of very high frequency sampling. This even forces a shorter dwell time on the secondary task. Nevertheless, this scanning mode does not seem to have affected the main task tracking error very significantly (note the change in scales).

As in the previous cases with scanning, there appear to be a number of pulsatile control actions correlated with the slightly prior fixation. (For example, notice the 10-second period centered around $t = 20$ sec on Fig. 16b.) An interesting observation from the bottom of this figure is that in the rapid sampling case there appears to be <u>less</u> side task control activity.

The foregoing observations from the time traces are supported by various scanning and performance measures taken both on-line and through describing function computations. These will be presented next.

2. Overview of Main Effects

Next we will present the effects of the three dimensions of task variables (scanning mode, secondary display workload, and input frequency) on the average dwell times, sampling intervals, tracking error, and control activity, which were measured on-line during each run. A gross survey of the effects of the applied task variables is shown in Figs. 17 and 18. Figure 17 shows the effects of the various scanning modes with other test variables held

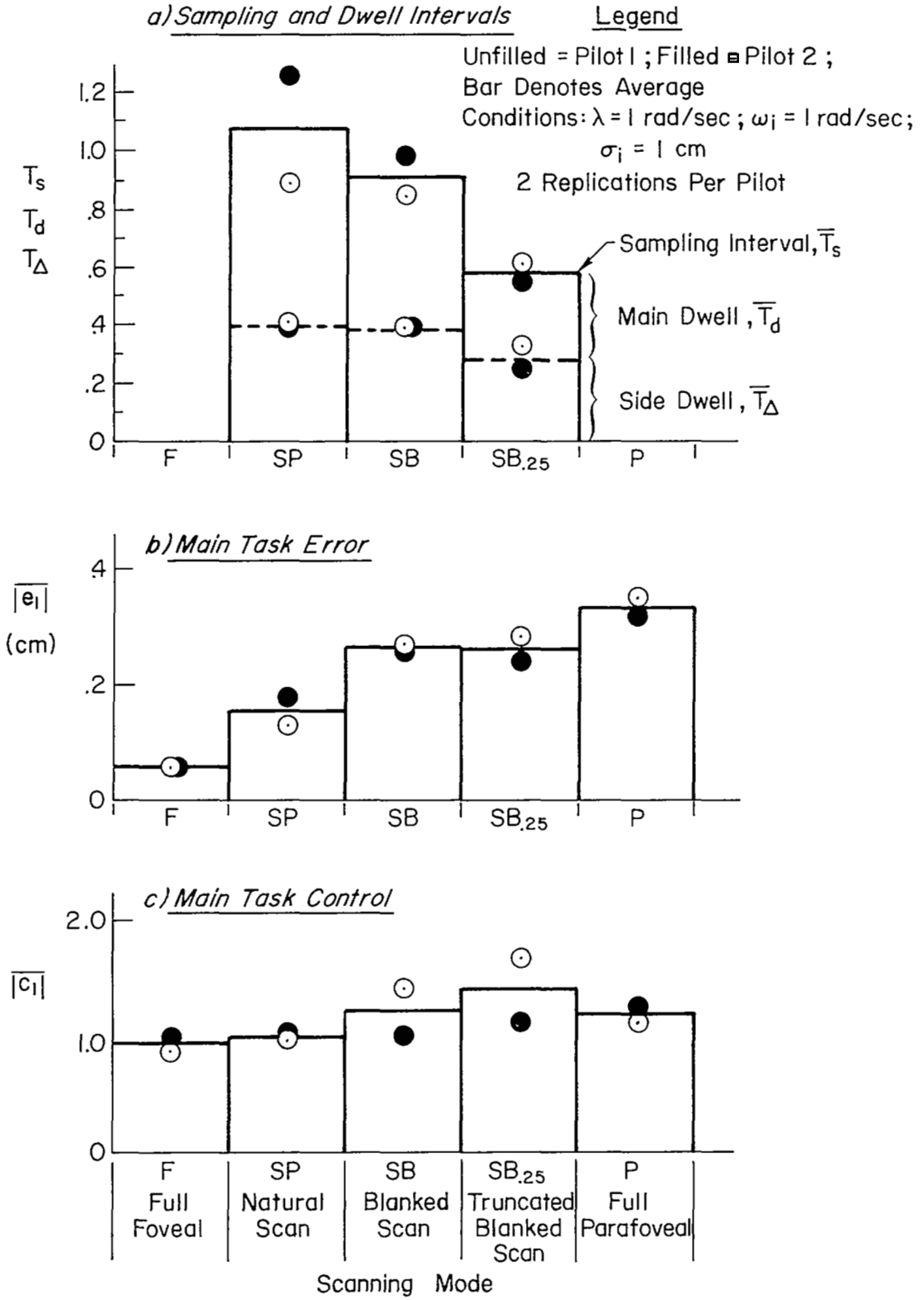

Figure 17. Effects of Scanning Mode at Reference Task Conditions (ω_i = 1.0, λ = 1.0)

constant at the standard condition of $\omega_i = 1$ rad/sec, $\lambda_2 = 1$ rad/sec. Each pilot's two-run average is shown as a separate symbol, while the mean value is shown by the bar. It is obvious from this figure that a wide range of scanning behavior and performance can be induced by the applied experimental scanning condition. Salient points on Fig. 17 are:

- The two pilots behave similarly, therefore justifying averaging their data in most of the subsequent data presentations. The within-pilot variance was generally less than the between-pilot variance, implying that stable and asymptotic performance had been reached.

- Conditions are arranged along the abcissa in order of increasing difficulty. Plot "a" shows that the average scanning frequency increases (sampling interval, T_s, decreases) as the more difficult, blanked scanning conditions are imposed. As noted in the time traces (but not anticipated a priori) the side task dwell, T_Δ, remained fairly invariant over a wide range of scanning conditions except for the truncated-blanked case. These effects will be discussed more fully later.

- Plot "b" shows that the error increased severalfold when progressing from the full foveal through natural, blanked, and truncated-blanked scanning to full parafoveal viewing.

- Plot "c" shows that, at constant input frequency, the average control effort does not increase in proportion to the error. This point is discussed later on.

Figure 18 is a summary plot for the corresponding data versus all other conditions. The two left-hand columns show the effects of input frequency on both the nonscanned and scanned situations. As might be expected, parafoveal errors were much larger than the foveal case, although the control activity was not proportionally larger. This, plus the roughly linear increase of errors with input frequency, is consistent with the conventional crossover model (operating at a reduced effective gain in the parafoveal case).

Next, consider the center column of Fig. 18 which shows the effects of input bandwidth, when the side task loading is held constant at $\lambda = 1$.

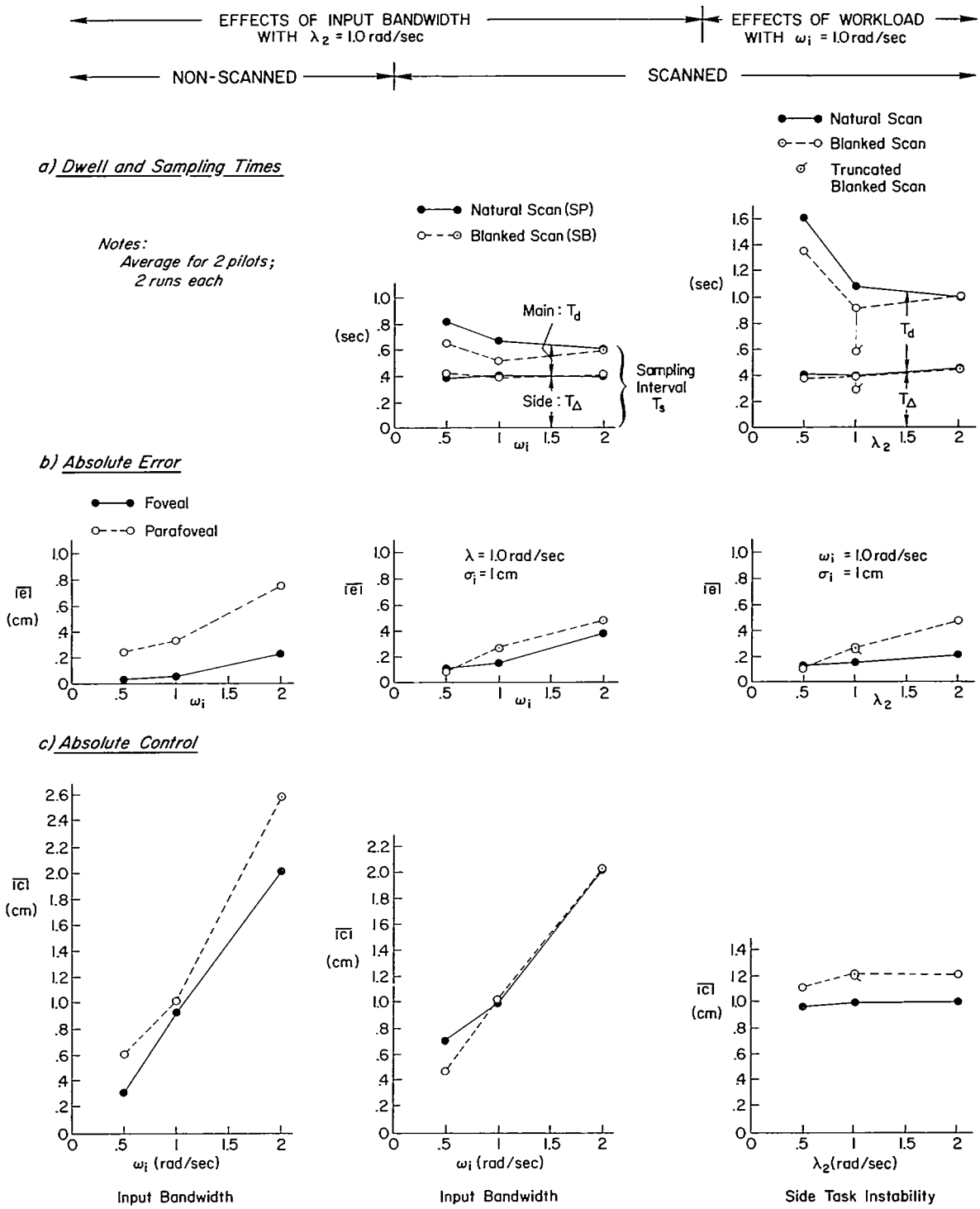

Figure 18. Summary Plots of Scanning Behavior and Tracking Performance

First, it is apparent from the sampling interval plot that increasing the input bandwidth did not result in a corresponding increase in sampling frequency, which would be evidenced as a decrease in the sampling interval, T_s. The constancy of the side task dwell is also readily apparent. In both cases the error increases with input bandwidth, with the blanked scan having worst performance. The control effort also increases linearly with ω_i, with little difference between the two scanning modes.

Turning now to the right column of Fig. 18, we see the effects of the side task difficulty on the corresponding performance measures. Added to this figure is a tagged point corresponding to the truncated-blanked scanning situation. The gross effects of increasing side task instability were to radically decrease the sampling interval (as expected) with only a slight increase in the side task dwell time (unexpected), and significant decrease in the main task dwell time. This result was the same for either scanning mode, with the blanked case having slightly faster scanning on the average. Under natural scanning conditions, the error did not increase linearly with λ_2, while in the blanked scan case, it increased at a greater rate. The average control effort was about the same in all cases. Interestingly, even though the sampling and dwell intervals were greatly reduced for the truncated-blanked scanning mode, the resulting error and control measures were not significantly worse.

In view of the significant effects of the different scanning modes on the error performance, it may seem surprising that the control activity was not sensitive to scanning mode or side task difficulty, while it was linearly affected by input frequency. This phenomenon has been observed in other experiments, e.g., Ref. 3. It turns out that there is a perfectly reasonable explanation for the apparent paradox (when the plant is a K/s). When the input bandwidth is constant and the closed-loop output is made to follow the dominant low frequency portions of the input, it can be shown that the major portion of the control action required to provide this output motion [$C(j\omega) \doteq 1/m(j\omega)$] will be proportional to rms magnitude and bandwidth of the input. Meanwhile, the smaller errors (which are the small differences between the two large input and output quantities)

can vary significantly without proportionately affecting the total amount of control effort required. Consequently, the average control activity is sensitive to input bandwidth mainly, while the error may be sensitive to many other variables, as well.

Now let us examine some of the effects revealed by this overview in more detail, starting with the scanning statistics.

3. Scanning Statistics

A number of EPR traces, such as those previously given in Figs. 15 and 16, were analyzed in detail to give information on the dwell times and sampling interval statistics. Some of the more interesting of these are given in Figs. 19 through 21, covering natural, blanked, and truncated-blanked scanning modes, respectively. The histograms in these figures show the fraction of total fixations or scans having intervals within the 0.1 (or 0.05) sec interval indicated. Looking first at the natural-scanning case shown in Fig. 19, the following points are readily apparent:

- The sampling interval for Pilot 2 was significantly longer than that for Pilot 1. This is apparently due to an increased main task dwell time because the side task dwell times were approximately equal.

- The very narrow range of side task dwells centered around 0.4 sec is readily apparent in the bottom left of Fig. 19. This distribution is also highly skewed, with no dwells shorter than 0.3 sec being observed, while intervals as large as 0.8 sec are occasionally observed.

Figure 20 shows that roughly similar scanning statistics resulted from the blanked scanning mode. The distribution of side task dwell times is again concentrated sharply near 0.4 sec, and the distribution shows significant skewness, as before. The much shorter dwell times and sampling intervals allowed by the truncated-blanked scanning mode are readily apparent in the histograms of Fig. 21. Here Pilot 2 decreased his main task dwell (and thereby his sampling interval) much more than Pilot 1.

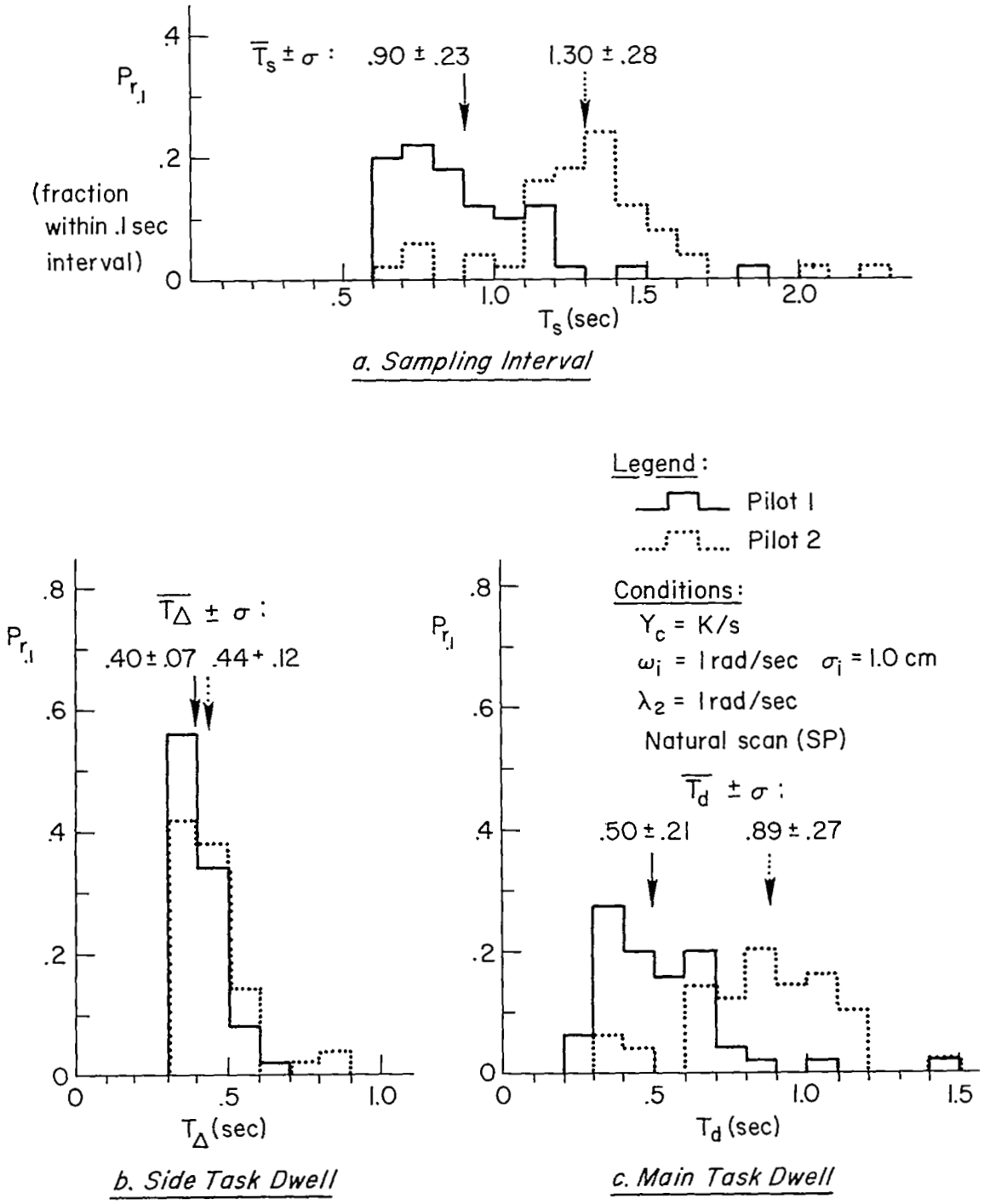

Figure 19. Sampling and Dwell-Time Histograms for Natural Scanning

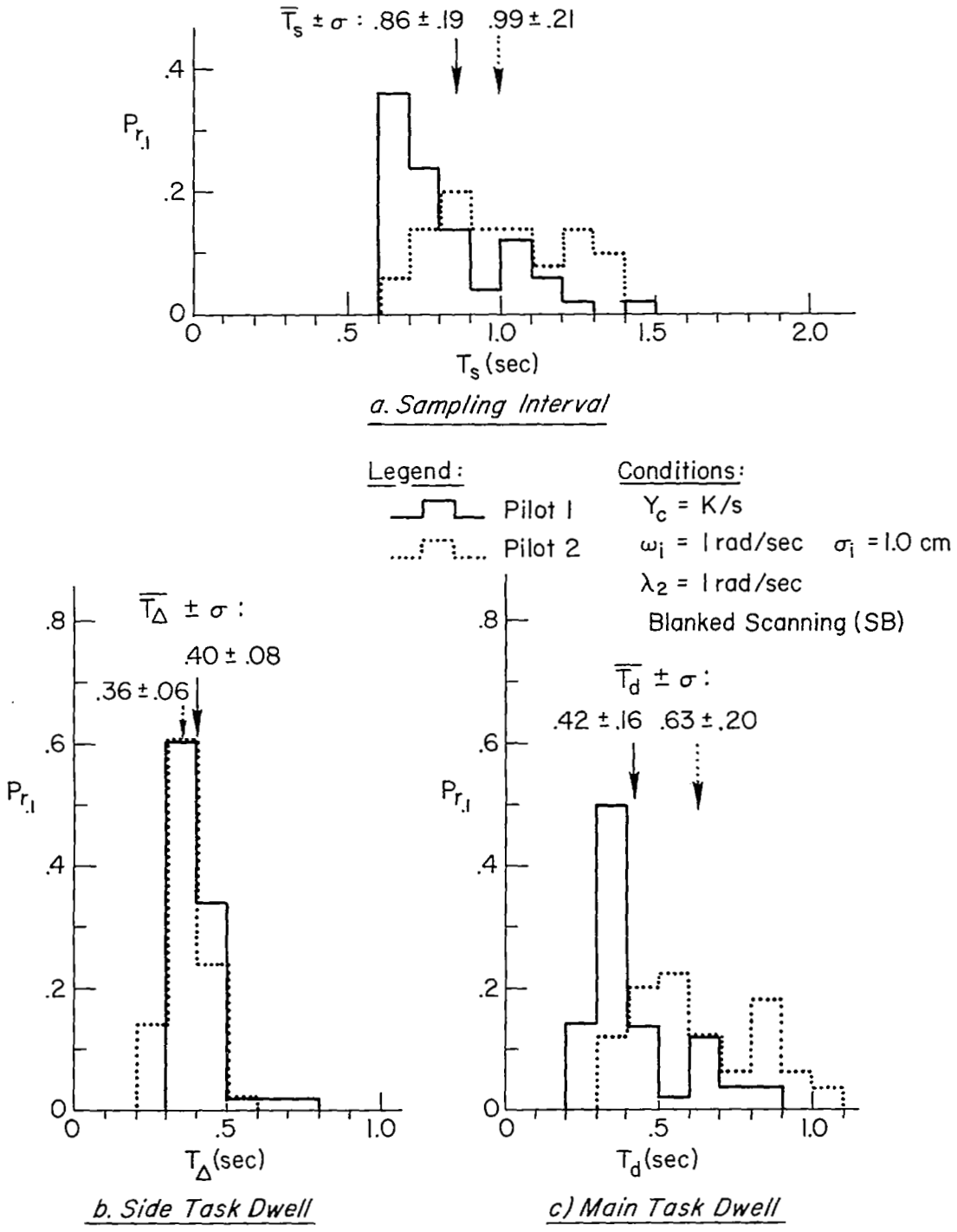

Figure 20. Sampling and Dwell Time Histograms for Blanked Scanning

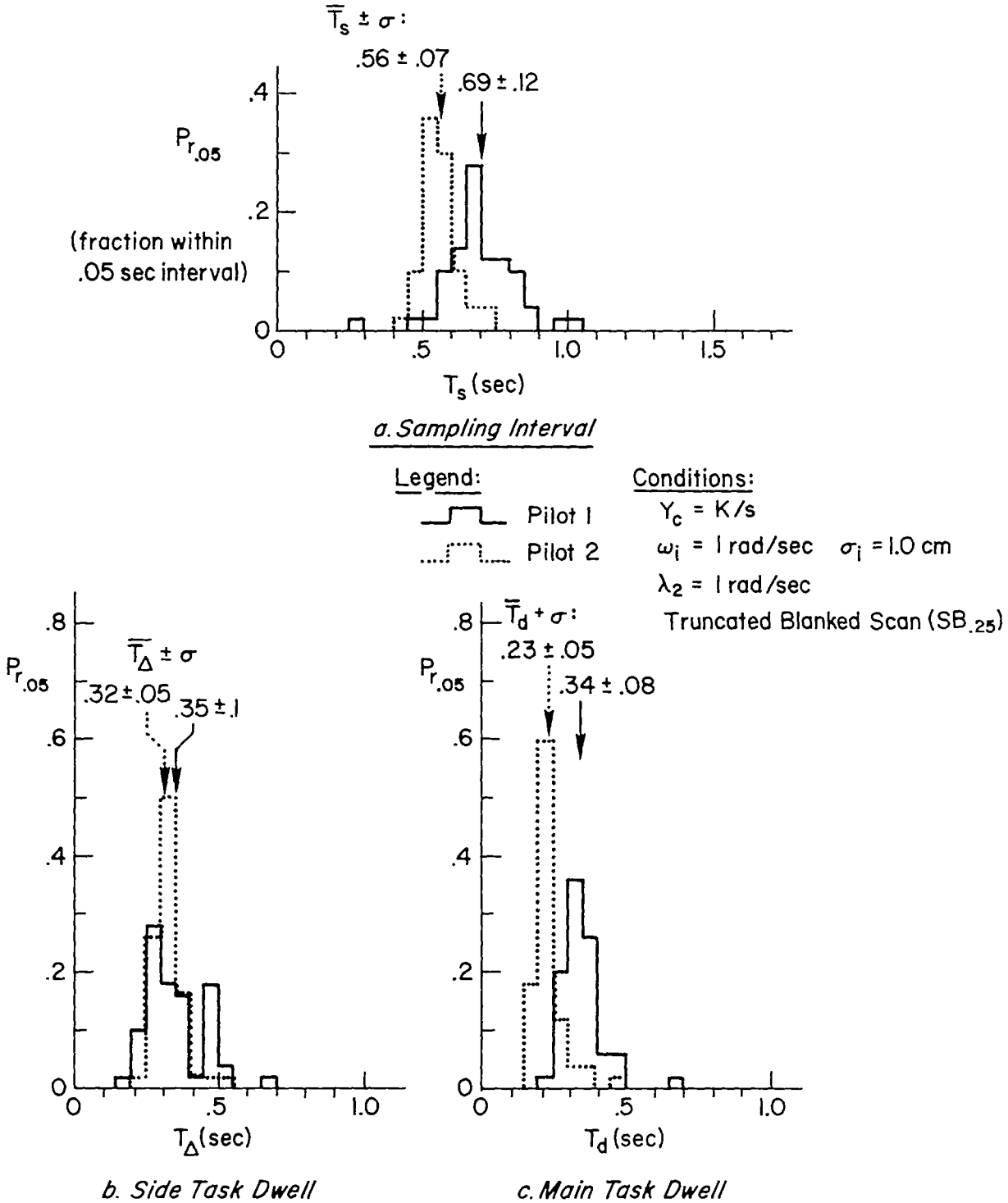

Figure 21. Sampling and Dwell Time Histograms for Truncated-Blanked Scanning

It is interesting to note that the relatively skewed sampling histograms for each individual operator observed throughout these experiments do not show the Gaussian-like distribution presented by Levison, et al., in Ref. 7. However, their sampling interval distribution curve was averaged over a few subjects, which would therefore tend to centralize and normalize the distribution of the ensemble. On the other hand, the distribution of sampling intervals is not exponential as assumed in Bergen's random sampling theory, Ref. 51. Sampling intervals less than 0.5 sec were never observed (except for the SB.25 case), nor were there many beyond 2.0 sec.

A possible bimodal distribution of main dwell times and sampling intervals is apparent in Fig. 20. To show this more clearly, the distributions of deviations from the mean dwell time have been plotted in Fig. 22. For the blanked scan case, both pilots show a pair of peaks centered roughly at 0.2 sec above and below the mean dwell time. A roughly similar pair of peaks can be discerned for Pilot 1 in the natural scanning case. Taken together, the invariant $T_{\Delta} \doteq 0.4$ sec and the bimodal T_s and T_d peaks separated by roughly 0.4 sec are highly suggestive of a time-quantized scanning situation. Many previous investigators have sought or asserted this, and a similar inference has been drawn by Clement in Ref. 2 based on groupings of mean-dwell intervals from in-flight eye movement data. Further "microanalysis" of eye-fixation data such as that presented here will be required to thoroughly explore this observation.

Examinations of the time histories shown previously do not reveal any obvious correlations between the length of dwell of one instrument and that on another. Nevertheless, this was checked by calculating the sample correlation coefficients for the foregoing data. No significant correlation could be found between main task dwell and side dwell, at least on a scan-by-scan basis.

We have noted that the side task dwell tended to remain relatively constant despite changes in main task dwell and corresponding changes in sampling interval. Figure 23 shows this more dramatically. For <u>each run</u> in the main experiment, the mean-side task dwell has been plotted versus the mean-sampling interval for <u>that</u> run (the different symbols correspond to the configuration code of Fig. 13). Two interesting results are illustrated in Fig. 23:

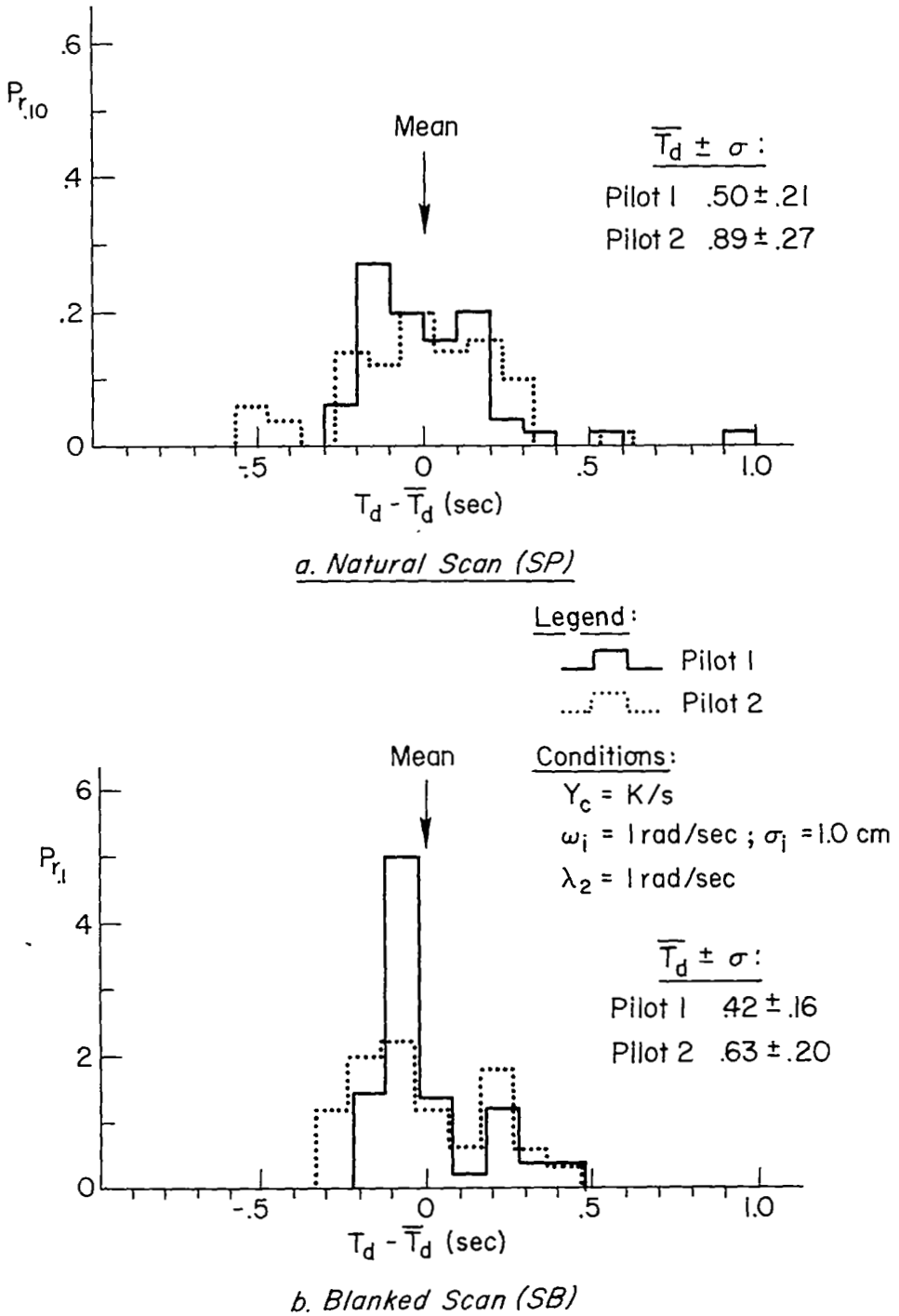

Figure 22. Comparison of Dwell Time Histograms for Two Pilots, Shifted to a Common Mean Value

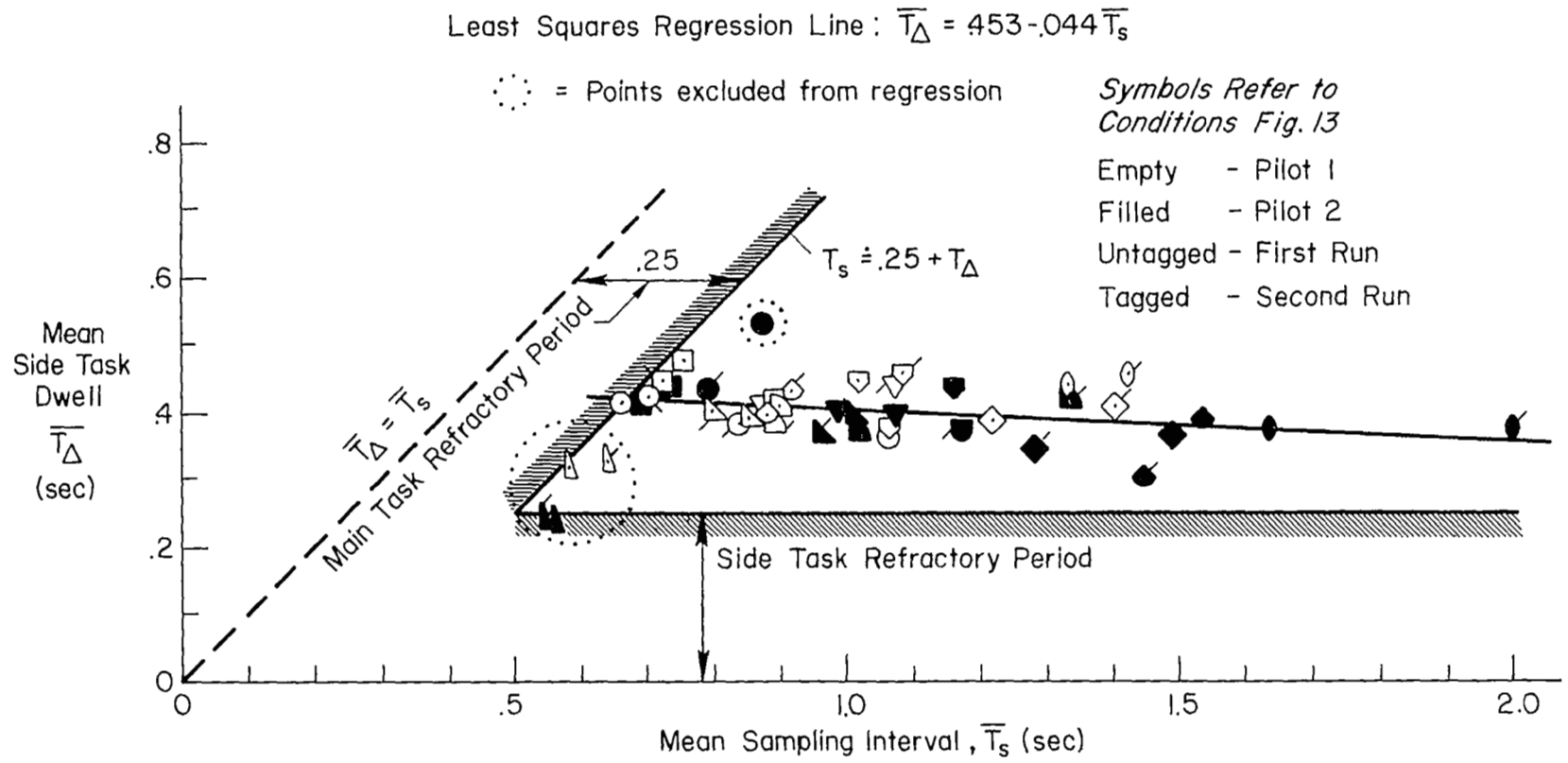

Figure 23. Side Task Dwell as a Function of Sampling Interval

- The average side task dwell time is on the order of 0.4 sec for a wide range of sampling behavior. However, the truncated blanked condition does not fit the regression line well (⍓).

- The side and main task average dwell times were never below 0.25 sec. Boundaries corresponding to this minimum are shown in Fig. 23 as a "refractory interval."

It is theorized that the 0.4 sec average dwell interval is the length of time required to fixate on the side task and obtain error magnitude and rate information. 0.4 sec is also the dwell time found by Senders, Ref. 33, and Clement, Ref. 5, for loosely controlled loop closures for monitoring tasks. The 0.25 sec lower bound on the dwell times is thought to represent a "scanning refractory period;" the minimum time required to move the eye to a display, fixate there, perceive an analog magnitude, and start to move elsewhere. This value is similar to the value of 0.3 sec found in Ref. 55 as the minimum tachistoscopic presentation time for the accurate reading of analog scales requiring an eye movement to fixate. When fixated, the minimal glimpse time to obtain position information is much less than 0.25 sec, as previously shown in Fig. 2.

Now that we have seen that the side task dwell remains roughly constant under the various externally imposed conditions, the question remains; what caused the large changes in scanning interval? It is hypothesized that the divergent time constant sets an upper bound on the permissible time away from the secondary task, i.e., the main dwell time. This is because a side task would diverge off-scale within a time on the order of $T_\lambda = 1/\lambda$ if the control were held constant. Consequently, the pilot must observe and correct the side task within the interval T_λ. (For more details on the principle behind this assertion, the reader should consult Ref. 53.) Figure 24 supports this hypothesis. It can be seen that the plotted values for main dwell times all lie below the bounding line given by $T_d = T_\lambda$. The data may be fitted by a straight line of the form

$$\overline{T_d} \leq KT_\lambda \quad ; \quad (K \doteq 0.6 \text{ for natural scan}) \qquad (8)$$

or

$$\overline{T_d} \leq 0.6/\lambda$$

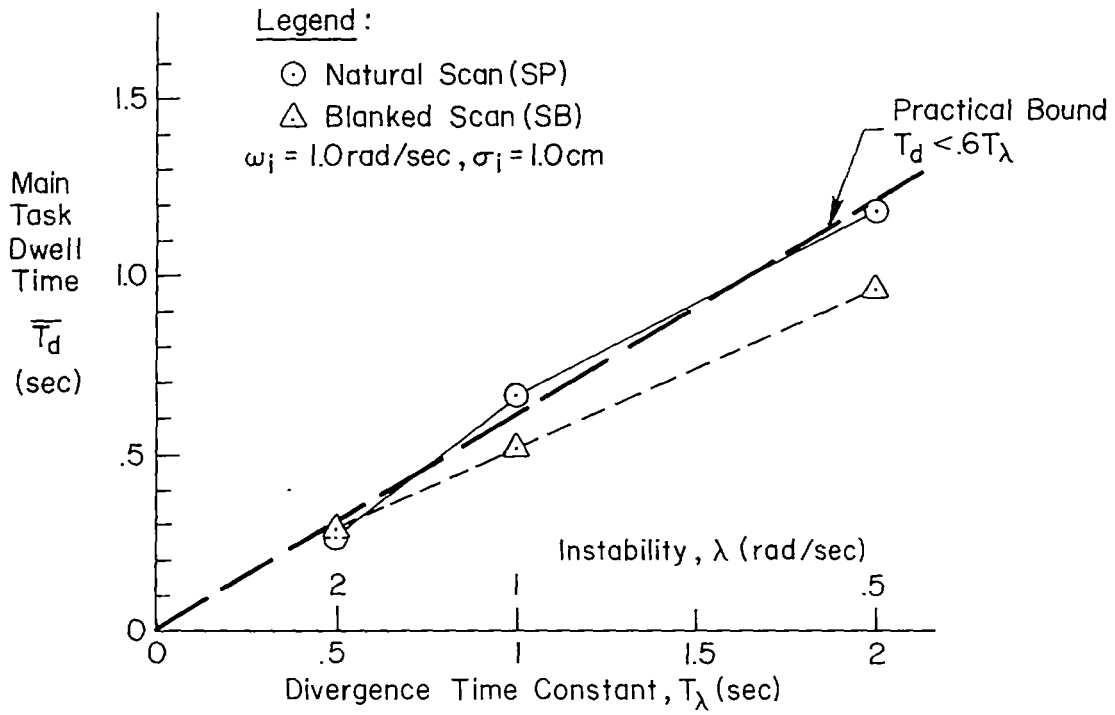

Figure 24. Main Task Dwell Time as Limited by the Side Task Divergence Time Constant

Noting that the allowable scan interval is $T_s = T_d + T_\Delta$ and that T_Δ is roughly constant at 0.4 sec, gives the following expressions for the maximum allowable scan interval and main task dwell fraction as a function of the side task instability for two-display situations:

In terms of:	$T_\lambda = \lambda^{-1}$	λ	
$T_{s_{max}} \leq$	$.6T_\lambda + .4$	$\frac{.6}{\lambda} + .4$	(9)
$f_{s_{min}} \geq$	$\frac{1}{.6T_\lambda + .4}$	$\frac{\lambda}{.6 + .4\lambda}$	(10)
$\left[\frac{T_d}{T_s}\right]_{max} \leq$	$\frac{T_\lambda}{T_\lambda + (T_\Delta/K)}$		
$\leq$	$\frac{T_\lambda}{T_\lambda + .67}$	$\frac{1}{1 + .67\lambda}$	(11)

This interpretation has two implications: (1) the unstable side task provides a powerful control over scanning frequency, independent of other task variables, and (2) the scanning frequencies adopted by the pilot in these experiments are <u>not</u> necessarily correlated with the main task display bandwidth.

That the scanning frequency does not increase in proportion to command input bandwidth is shown in Fig. 25. Within the constraints imposed by the secondary task time constants, the scanning frequency must be adjusted by other considerations, such as achievable crossover frequency, sampling remnant, and the like. These factors will be untangled in the next chapter, when a comparison is made with the finite-dwell theory.

It is interesting to examine the effectiveness of the subcritical instability as a secondary display task loading in producing the decrement in attentional demand to the primary task. One measure of scanning workload

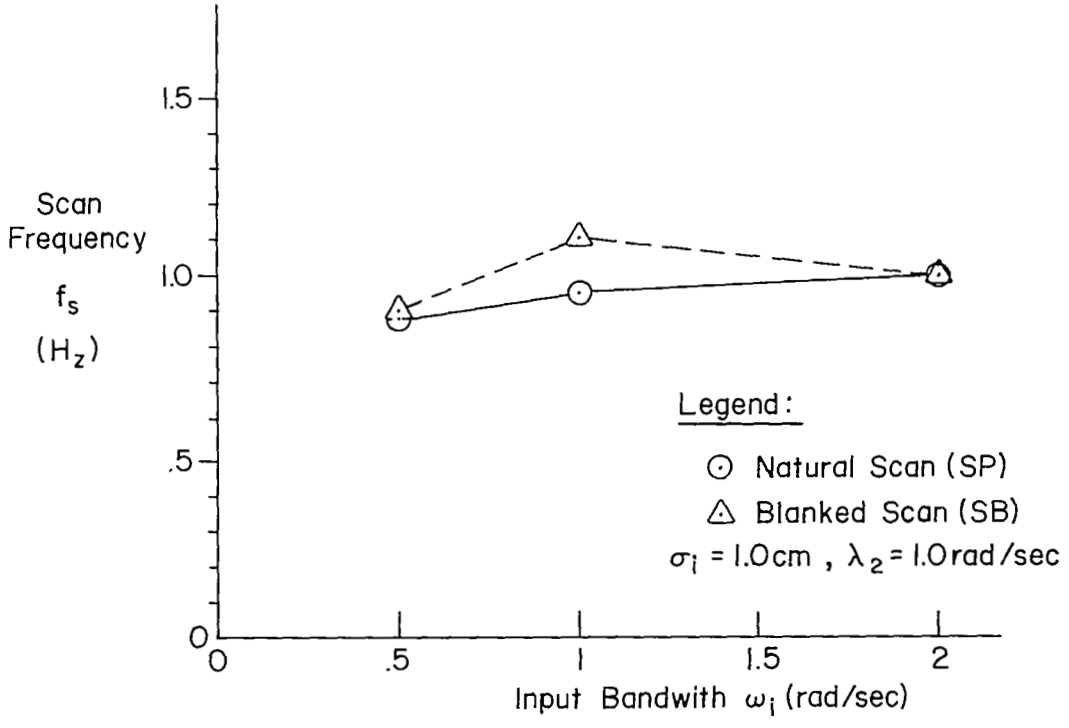

Figure 25. Sampling Frequency Versus Input Bandwidth

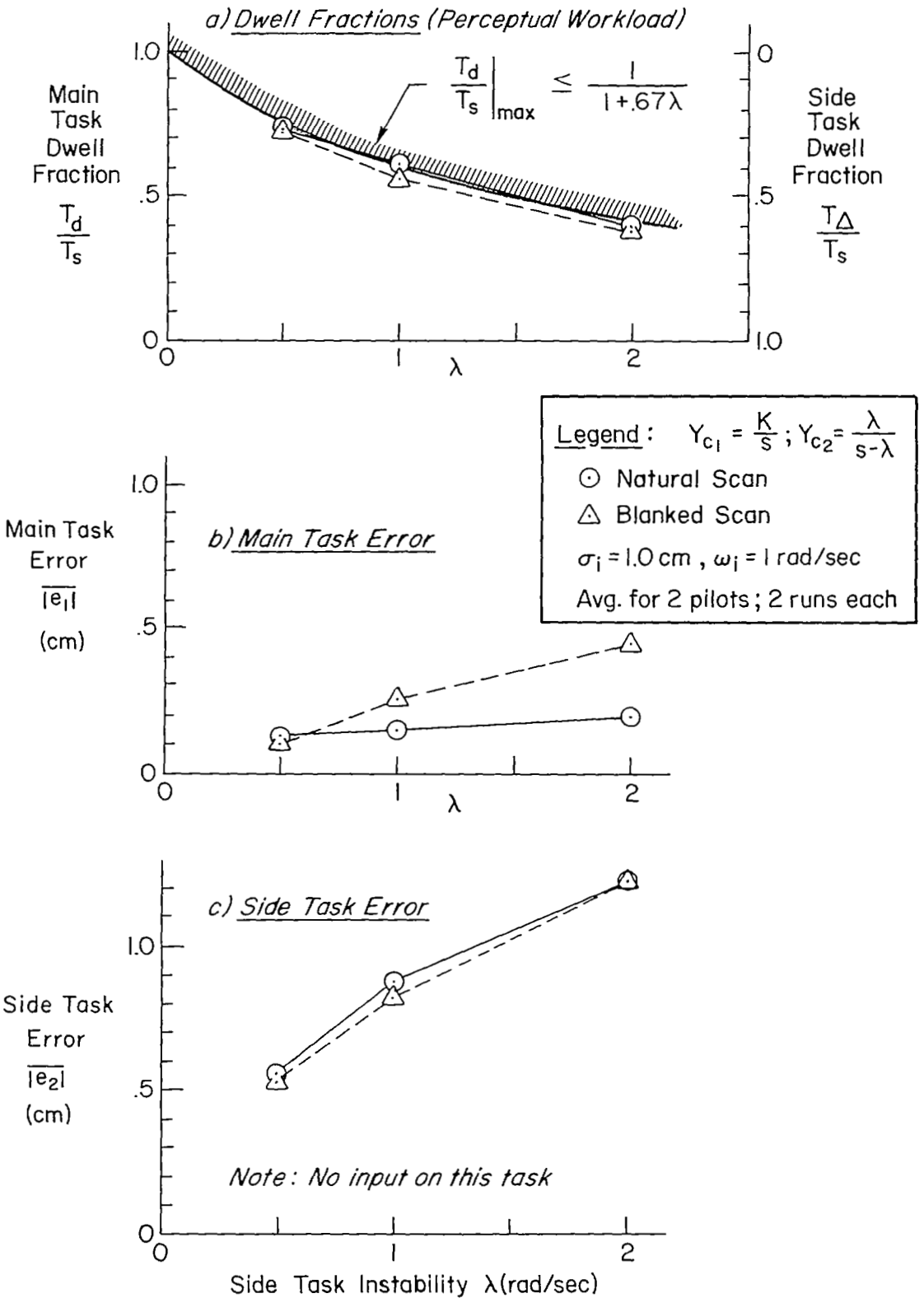

Figure 26. Main Task Dwell Fraction and Tracking Performance as a Function of the Side Task Unstable Root

on a given task has been defined in Ref. 2 as the fraction of time spent on that display. This is also equal to the average dwell fraction, $\overline{T_d}/\overline{T_s}$. Figure 26a shows how the attentional demand shifts between the main and side tasks as λ is increased. The analytical upper bound $T_d < .6/\lambda$ is a plot of Eq. 11 for the average conditions of this experiment. This simple analytical expression fits the data quite well.

B. DIGITAL DATA ANALYSIS

Due to time and money limitations we could not digitally analyze all the recorded data. The on-line performance and scanning behavior measures indicated that the second trial for each condition gave consistent data, and that the conditions involving the 1 rad/sec main task input bandwidth gave a wide range of scanning behavior. Thus for the sake of efficiency the digital data analysis was generally limited to the above cases.

1. Describing Function Data

The forward-loop describing functions, $M(j\omega)/E(j\omega)$, obtained for the basic (foveal) tracking conditions are compared in Figs. 27 and 28 with earlier, unpublished data obtained on the same pilots. A rectangular input spectrum with a 2.9 rad/sec bandwidth was used in the "previous" case with a −20 dB shelf. Both sets are for compensatory tracking. The data appear relatively consistent in the crossover frequency region; however, the present data seems to deviate from past data in two ways: (1) a consistent gain slope slightly greater than 20 dB/decade, and (2) relatively large phase lags at frequencies below 3 rad/sec. King-Smith (Ref. 56) has proposed a slope modification to the conventional crossover model of the form:

$$Y_p Y_c = \frac{K_1 e^{-j\tau_e \omega}}{(j\omega)^r} \qquad (12)$$

In this case the actual crossover frequency is $\omega_c = K_1^{1/r}$. The effect of the parameter, r, is to increase the slope of the Bode (magnitude) plot and to shift the phase due to $1/(j\omega)^r$ from 90 deg to:

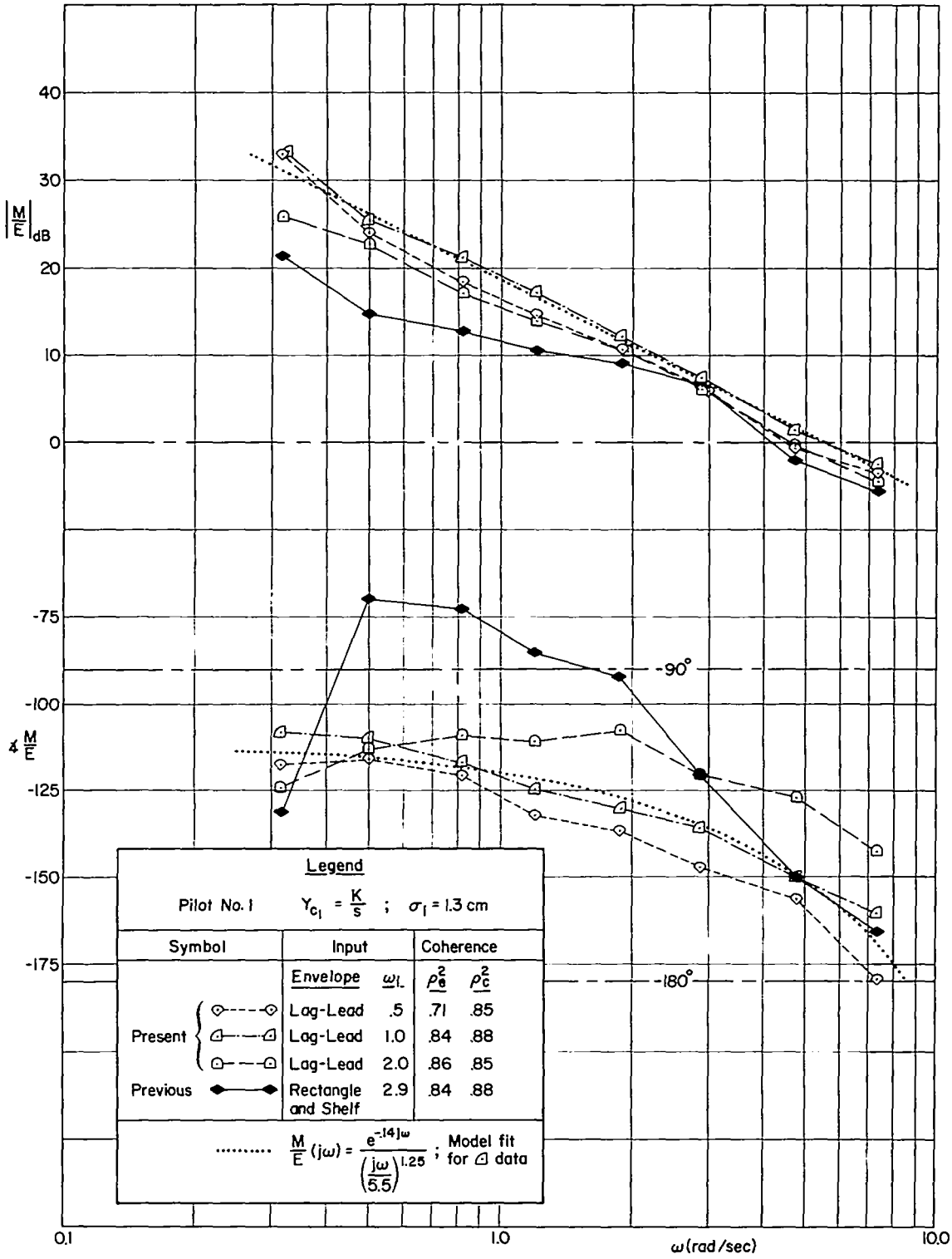

Figure 27. Comparison of the Present and Previous Describing Functions of the Pilot-Subject 1 for Various Input Forcing Function Spectra, Full Foveal Tracking; $Y_c = K/s$

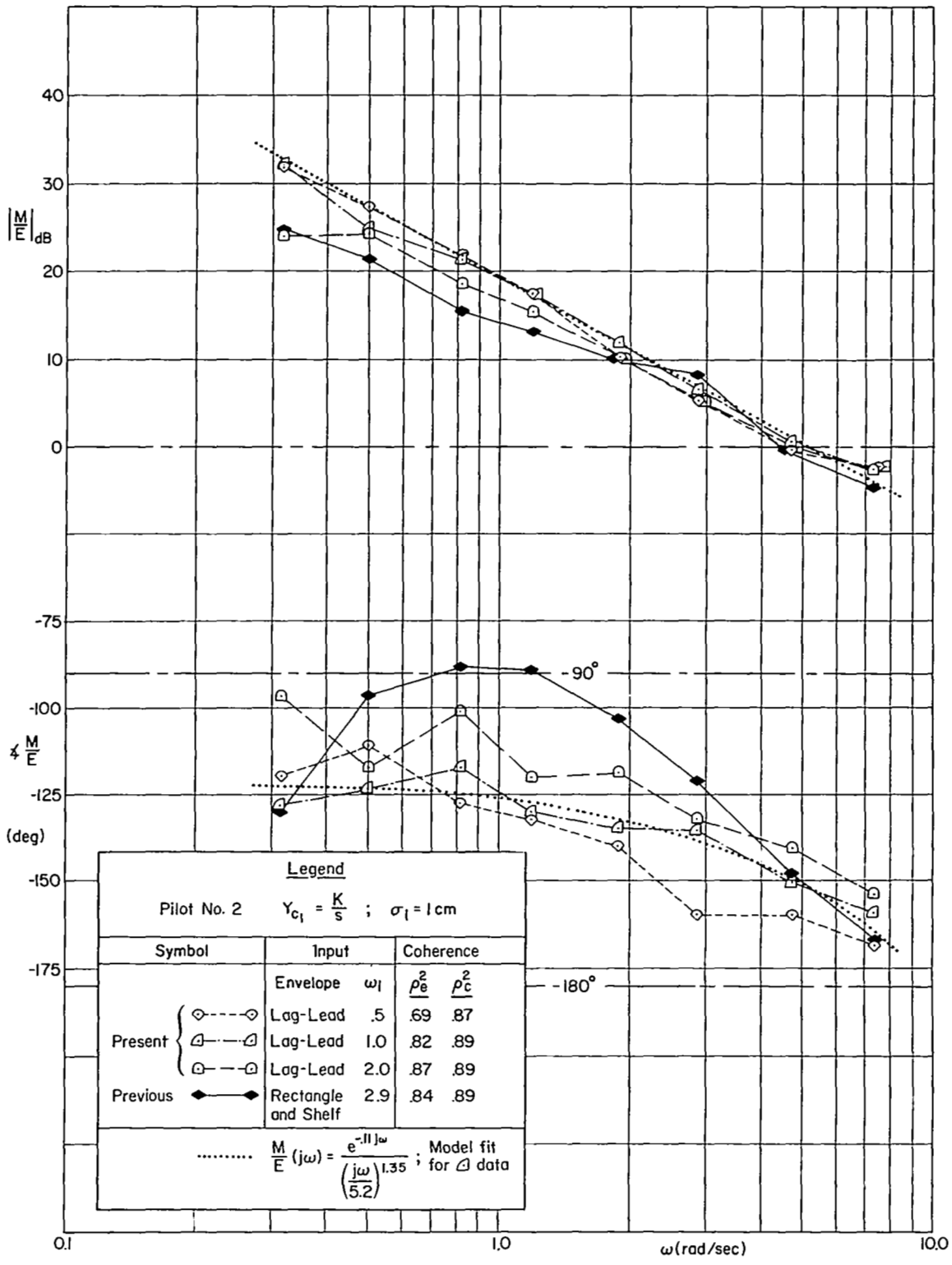

Figure 28. Comparison of Present and Previous Describing Functions of Pilot-Subject 2 for Various Input Forcing Function Spectra, Foveal Tracking; $Y_c = K/s$

$$\angle\,[1/(j\omega)^r] = (\pi/2)r \quad \text{[radians]}$$
$$= (90^\circ)r \quad \text{[degrees]} \qquad (13)$$

Thus, less time delay is required to fit a given set of phase data if $r > 1.0$

The effects of scanning and sampling on the describing functions are shown in Fig. 29 where two sampling conditions are compared with the pure foveal and parafoveal tracking conditions. Scanning and pure parafoveal viewing cause the open-loop gain (and thus the crossover frequency) to decrease. Increased high-frequency phase lag is evident for the blanked display and parafoveal viewing cases but scanning with parafoveal viewing caused no significant phase penalty over pure foveal tracking.

The simple-crossover-model parameters* were computed for all available runs and are presented in Fig. 30. Figure 30 shows the effect of scanning mode on ω_c and τ_e at the reference conditions of $\omega_c = 1.0$ rad/sec and $\lambda_2 = 1.0$ rad/sec. The regression of crossover frequency is readily apparent. Only the blanked scan cases show a significant increase in τ_e, and this is a small fraction of the sampling interval, shown at the bottom of Fig. 30. It is also apparent (remembering that sampling frequency is the inverse of $\overline{T_s}$) that, as sampling frequency increased, crossover frequency decreased for these conditions. Thus these data do not support the simple notion that crossover and sampling frequencies should vary directly. There may be mitigating circumstances, though, because we have just shown (e.g., Eqs. 8-11) that the sampling is controlled, here, mainly by the constant level of T_Δ and the constraint of $T_d \leq \lambda^{-1}$, rather than by the frequency content of the input or error per se. Even though ω_c governs the bandwidth of the error signal, the other scanning demands can overpower this effect.

*Despite the slightly better fit of the modified crossover model of Eq. 12, only the simple crossover model ($r = 1$) was assumed for these fits for consistency with past practice.

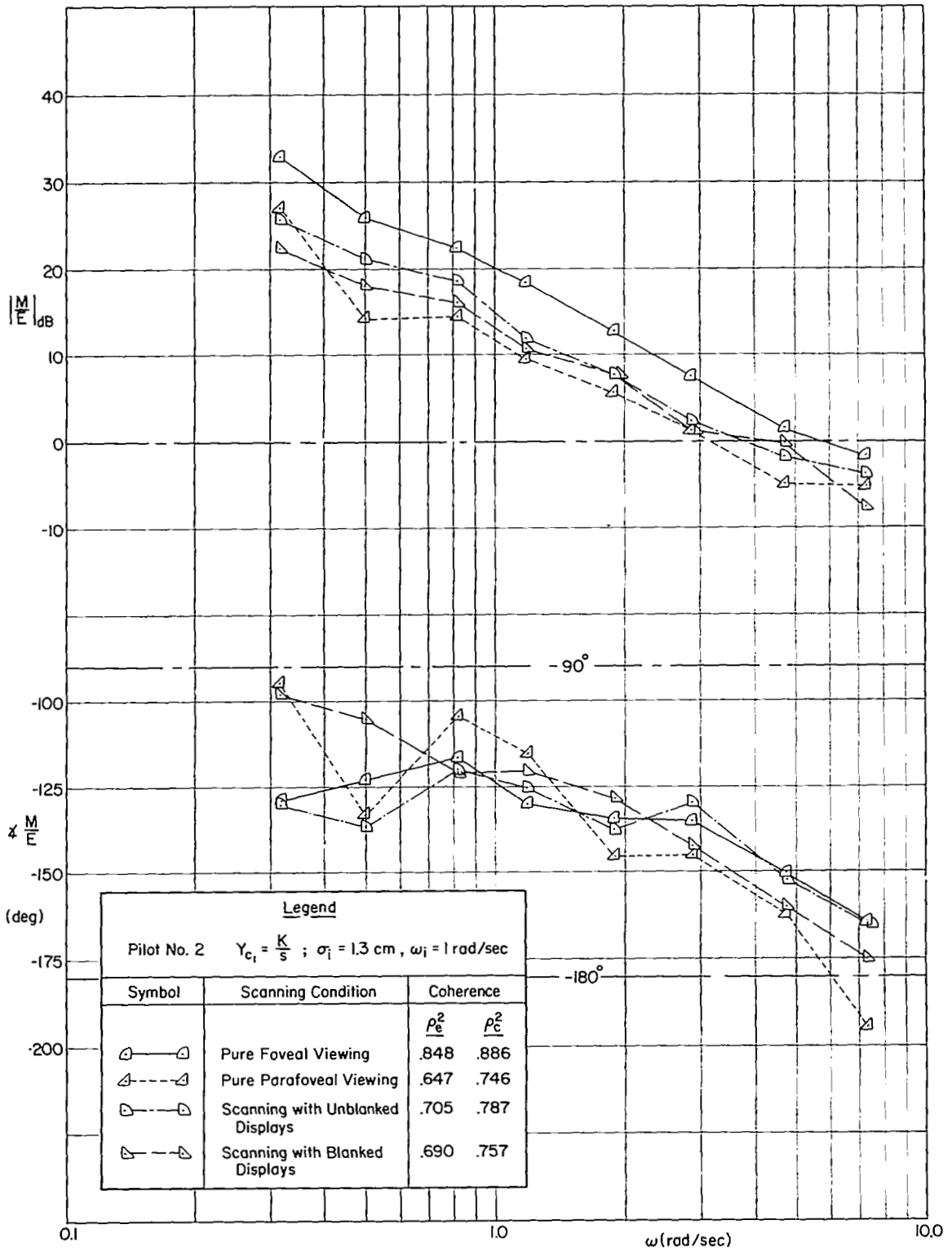

Figure 29. Comparison of Describing Functions Under Scanning and No-Scanning Conditions

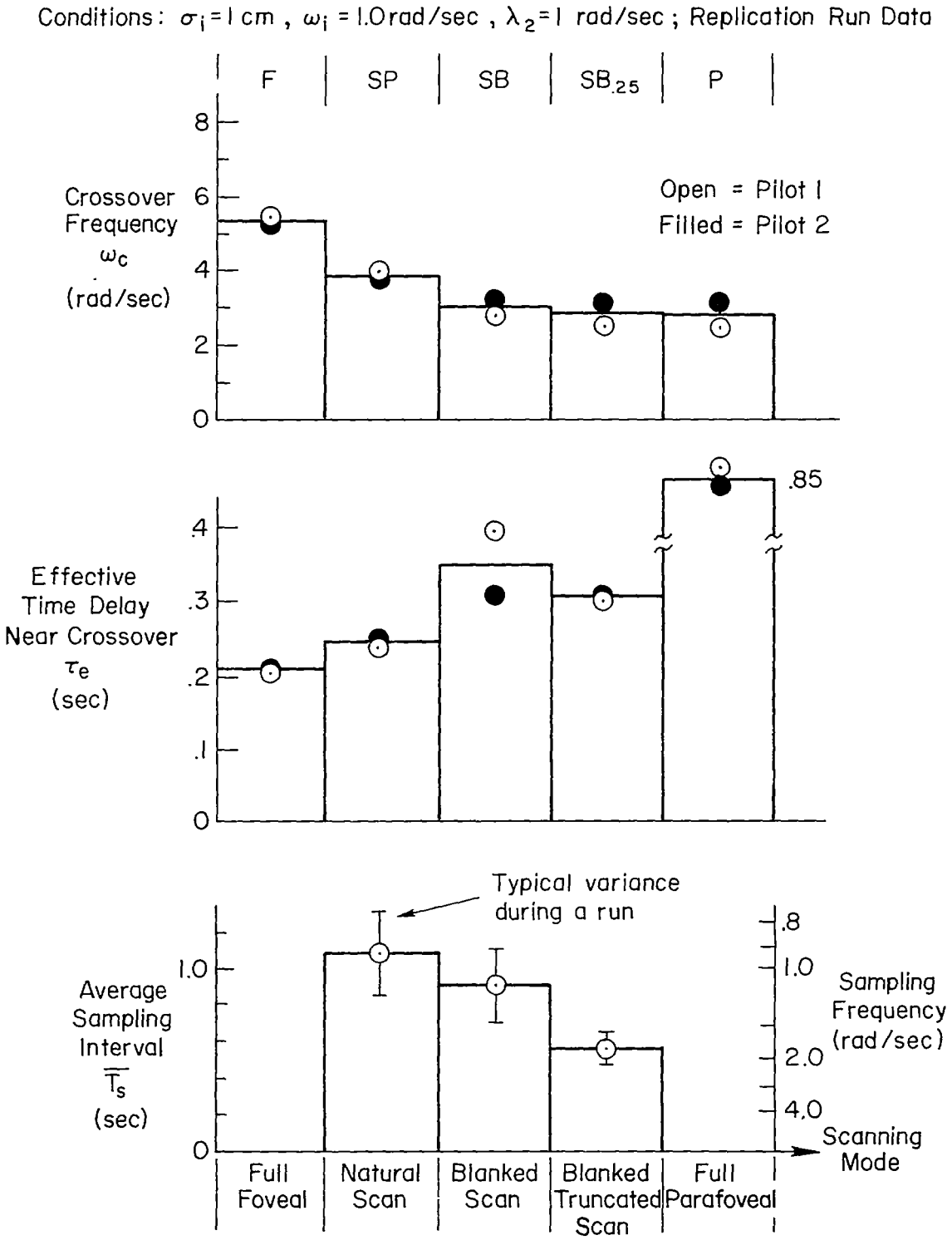

Figure 30. Summary of Effects of Scanning Mode on Open-Loop Describing Function Parameters

Closed-Loop Describing Functions — Typical overall closed-loop describing function data [$Y_{CL}(j\omega) = M(j\omega)/I(j\omega)$] are shown on Fig. 31 for the four key scanning modes. The input frequencies did not extend far enough to show the ultimate attenuation at higher frequencies, but the phase curves show that the closed-loop bandwidth regressed with scanning. Taking the frequency for 90 deg phase lag as a metric, the closed-loop bandwidths appear to be in the region from 3 to 6 rad/sec. The lowest closed-loop bandwidth occurs for pure parafoveal tracking, as would be predicted from previous figures.

2. Remnant Data

As explained in Section II, scanning leads to greater remnant because of drastically increased amounts of erratically jagged control output power circulating around the loop and giving rise to a wideband remnant signal input. Ultimately, this results not only in larger remnant errors but in increased correlated errors as well, due to the need for gain regression under these high-remnant conditions.

Typical closed-loop error spectra for several scanning modes are shown in Fig. 32. On this figure, the stepped lines correspond to remnant levels averaged over the indicated bandwidths, while the isolated points represent the error power at the input frequencies.* Note that the input components of the error spectrum lie considerably above the corresponding remnant level in each case. This implies a high signal/noise ratio at each input frequency, and insures that the describing functions are accurate measures of pilot behavior and are not biased by the noise content.

It is immediately apparent that there is a great increase in remnant for either of the scanned conditions, the increase being of the order of 20 dB (a factor of 10 increase) over the nonscanned foveal case. The

*To provide compatible scaling, the error power concentrated at each input frequency is assumed to be spread over a narrow frequency band of $\Delta\omega = 2\pi/\text{run length}$. Since the run length is 100 sec, $\Delta\omega \doteq .063$ rad/sec.

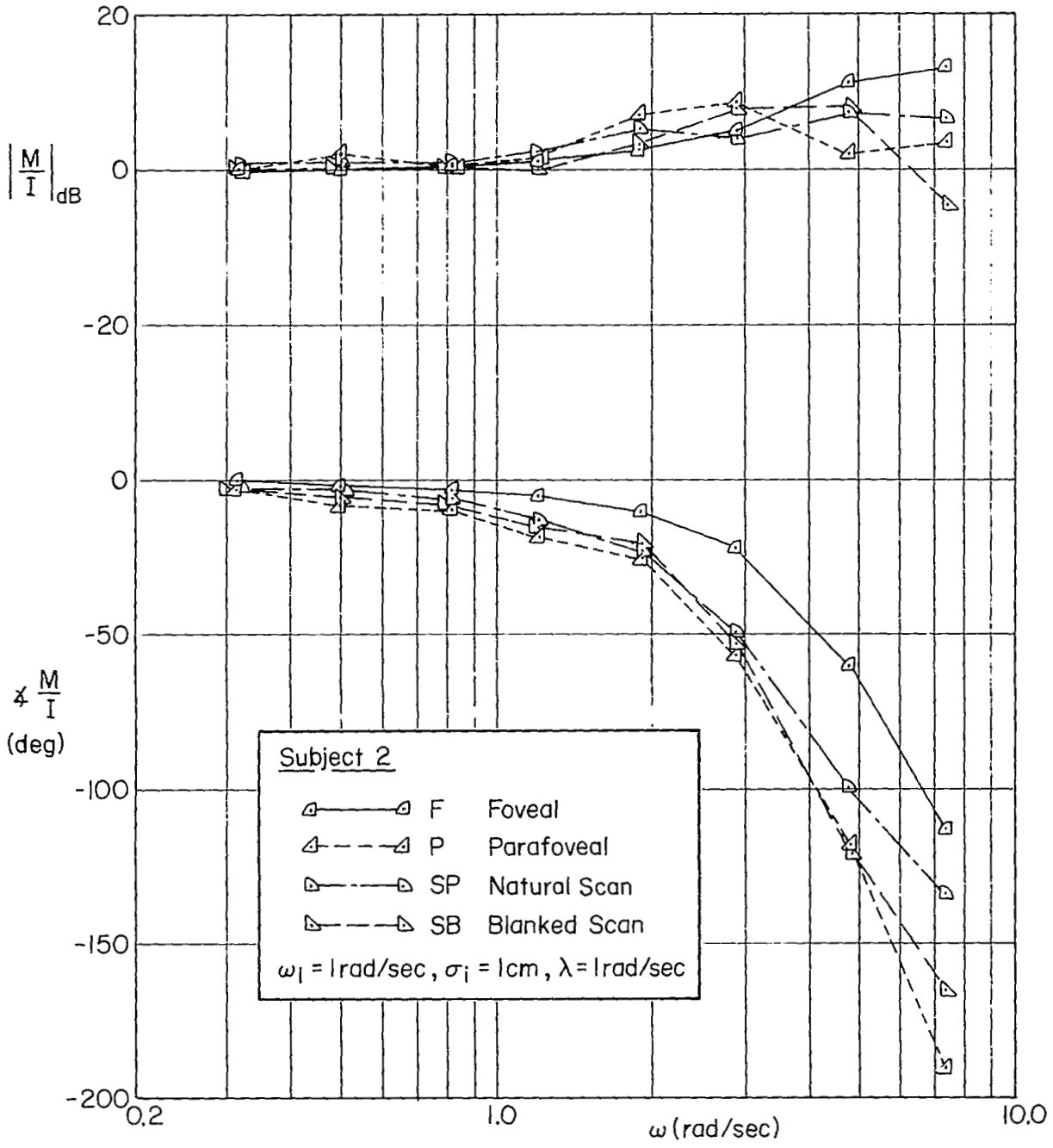

Figure 31. Closed-Loop Describing Functions for Various Scanning Conditions

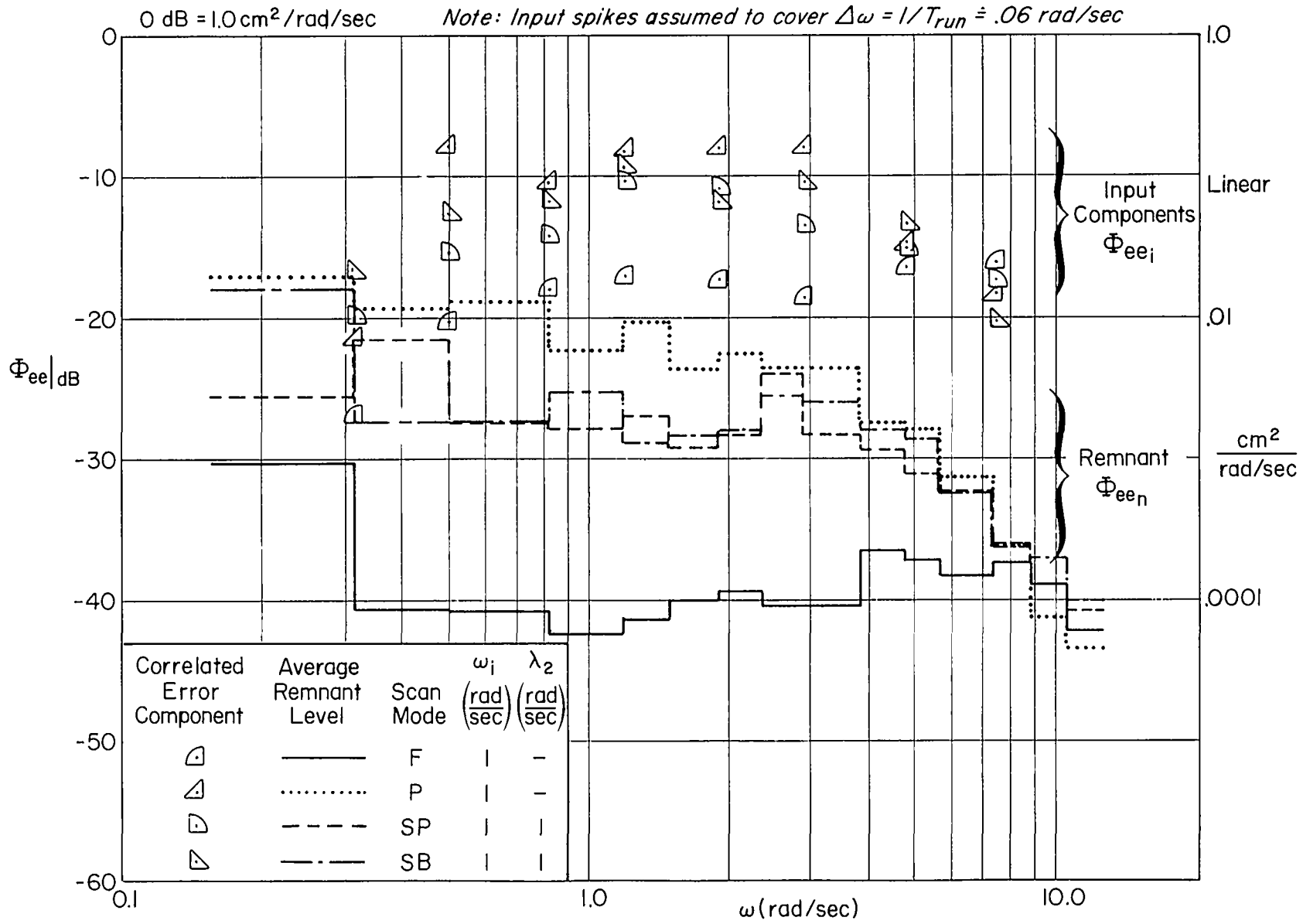

Figure 32. Closed-Loop Error Spectra for Various Scanning Modes

correlated errors increase correspondingly, although not by such a high factor. The worst errors occur in the full parafoveal condition, for both remnant and correlated components.

A significant feature of the remnant spectra on Fig. 32 is the smooth envelope in the frequency region below the closed-loop frequency, i.e., below 3 to 6 rad/sec. The attenuation and coalescing of the remnant spectra at higher frequencies is due to the attenuating effect of the limited closed-loop bandwidth. To the extent that remnant may be considered as an uncorrelated "noise" signal injected at the error perception point (as suggested in Refs. 7 and 60), then the injected remnant acts like another input signal. The resulting closed-loop remnant will then be attenuated by the closed-loop bandwidth of the pilot/vehicle system. This effect is clearly evident in Fig. 32. Comparison of the shapes of the remnant portion of the spectrum in Fig. 32 with the closed-loop describing functions of Fig. 31 reveals a rough correspondence between the remnant rolloff and closed-loop bandwidth.

A simple, overall measure of relative remnant is the error power coherence $\overline{\rho_e^2}$, or fraction of input-correlated power in the error signal. This is given by:

$$\overline{\rho_e^2} \equiv \frac{\overline{e_i^2}}{\overline{e^2}} = 1 - \frac{\overline{e_n^2}}{\overline{e^2}} \qquad (14)$$

A corresponding coherence, $\overline{\rho_c^2}$, exists for the operator's output.

Figure 33 shows the error- and control-power coherence as a function of the several task variables. Figure 33a shows that the error relative remnant is about the same for both pilots. The control coherence differs appreciably, being generally lower than $\overline{\rho_e^2}$ for Pilot 1 and higher for Pilot 2. Nevertheless, the average coherences are roughly comparable and their ranking is the same with respect to scanning mode. The power coherence for foveal tracking of $\overline{\rho_e^2} = 0.8$ to 0.9 is comparable to other investigations with Y_c = K/s. Blanked scanning or parafoveal tracking reduces this to about $\overline{\rho_e^2} \doteq 0.6$ at the reference conditions.

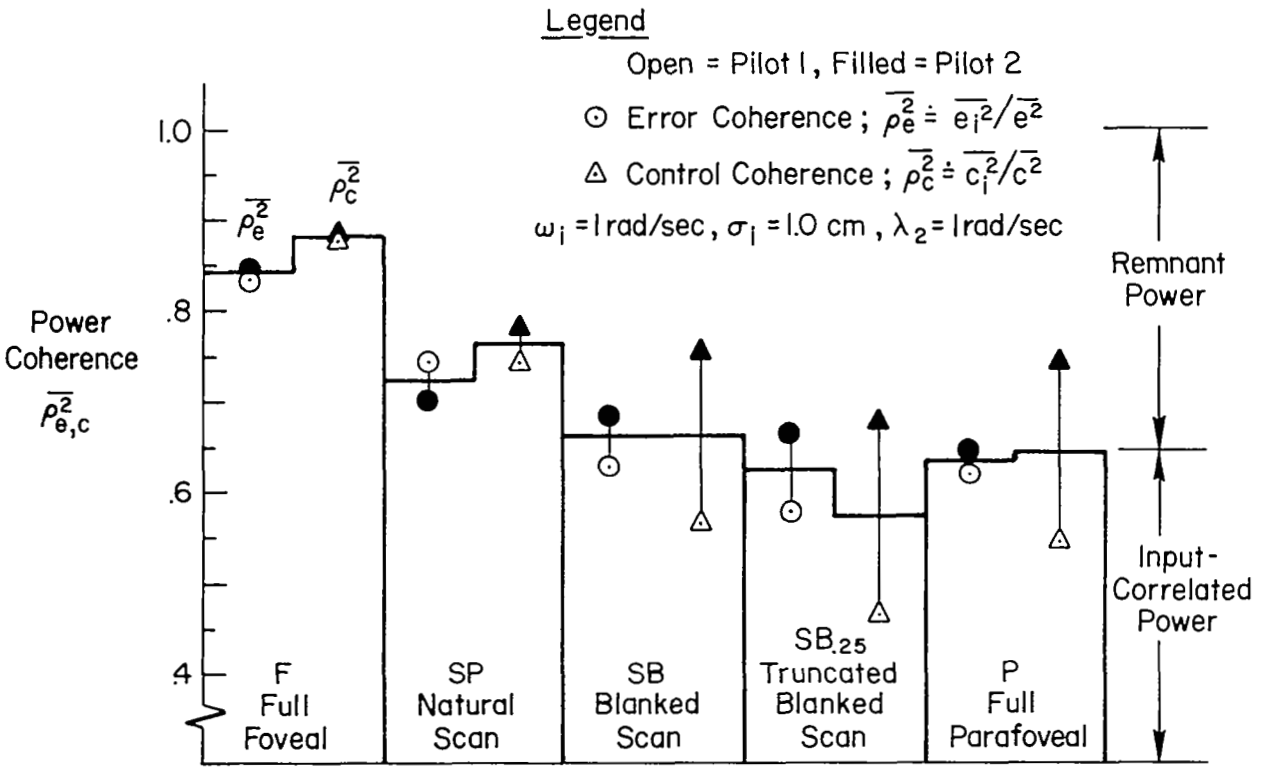

a) Scanning Mode (at reference conditions)

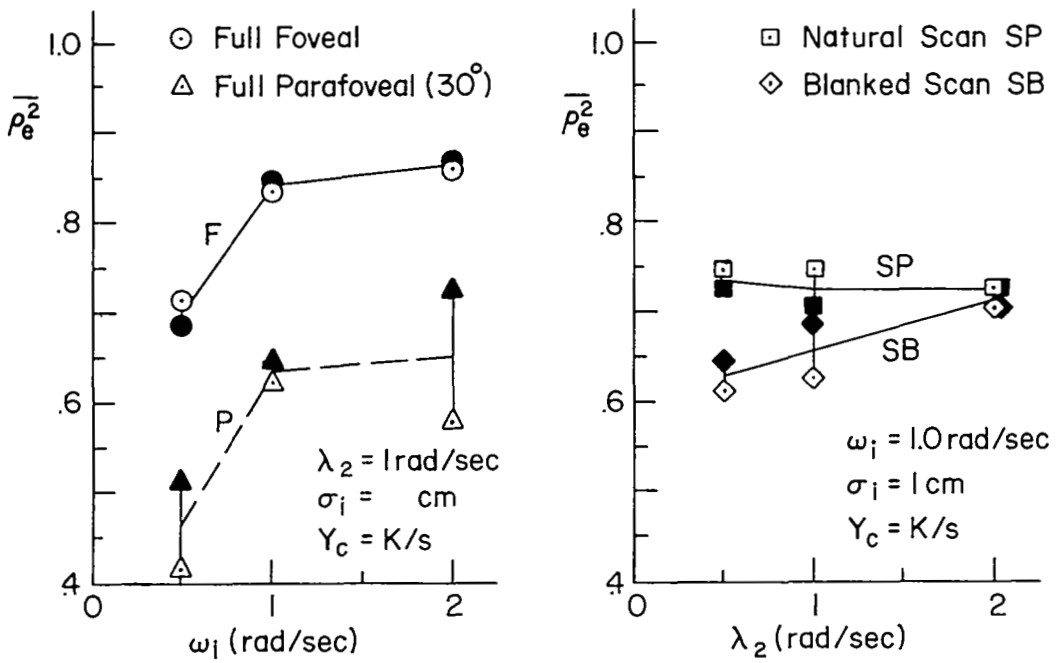

b) Input Bandwidth

c) Side Task Instability

Figure 33. Relative Remnant (Power Coherence) of Error and Control Signals for Various Scanning Modes and Conditions

The effect of input bandwidth on $\overline{\rho_e^2}$ is significant, as shown in Fig. 33b. The sharp dropoff in $\overline{\rho_e^2}$ at low input bandwidths (an easier task) is probably due to the fact that the input-correlated errors become very small while a certain amount of "residual-remnant" remains, thereby reducing the ratio of correlated-to-total errors.

According to the data in Fig. 33c, varying the secondary task difficulty did not have a strong effect on $\overline{\rho_e^2}$, which stayed within the range 0.70 ± 0.10 for both natural and blanked scanning conditions. As shown in Section II, several scanning parameters affect $\overline{\rho_e^2}$, and some of these are compensating in this case. Further discussion is in Section V.

One inference which is tentatively drawn from these coherence data is that the relative scanning remnant power is not allowed to reach more than about 50 percent of the total — this being accomplished by suitable adjustments of scanning frequency and dwell time within the constraints allowed by the other task variables.

Some correlations were attempted between the various normalized error measures to see if a simple functional relationship were evident. About the best one that was obtained is shown in Fig. 34. Here is plotted the total remnant power, $\overline{e_n^2}$, as a function of the correlated error power, $\overline{e_i^2}$ (both normalized with respect to the input, which was constant). All of the symbols shown correspond to the reference conditions of $\sigma = 1$ cm, $\omega_i = 1$ rad/sec and $\lambda = 1$ rad/sec. The bounding lines shown in Fig. 34 indicate that the remnant power for this particular combination of input frequencies and scanning conditions increases somewhere between the first and second power of the correlated error, the exponent being approximately 1.2 in this case. Further discussions of the relationship of the remnant to the scanning are contained in the next chapter, which interprets some of these data in the light of recent theoretical models.

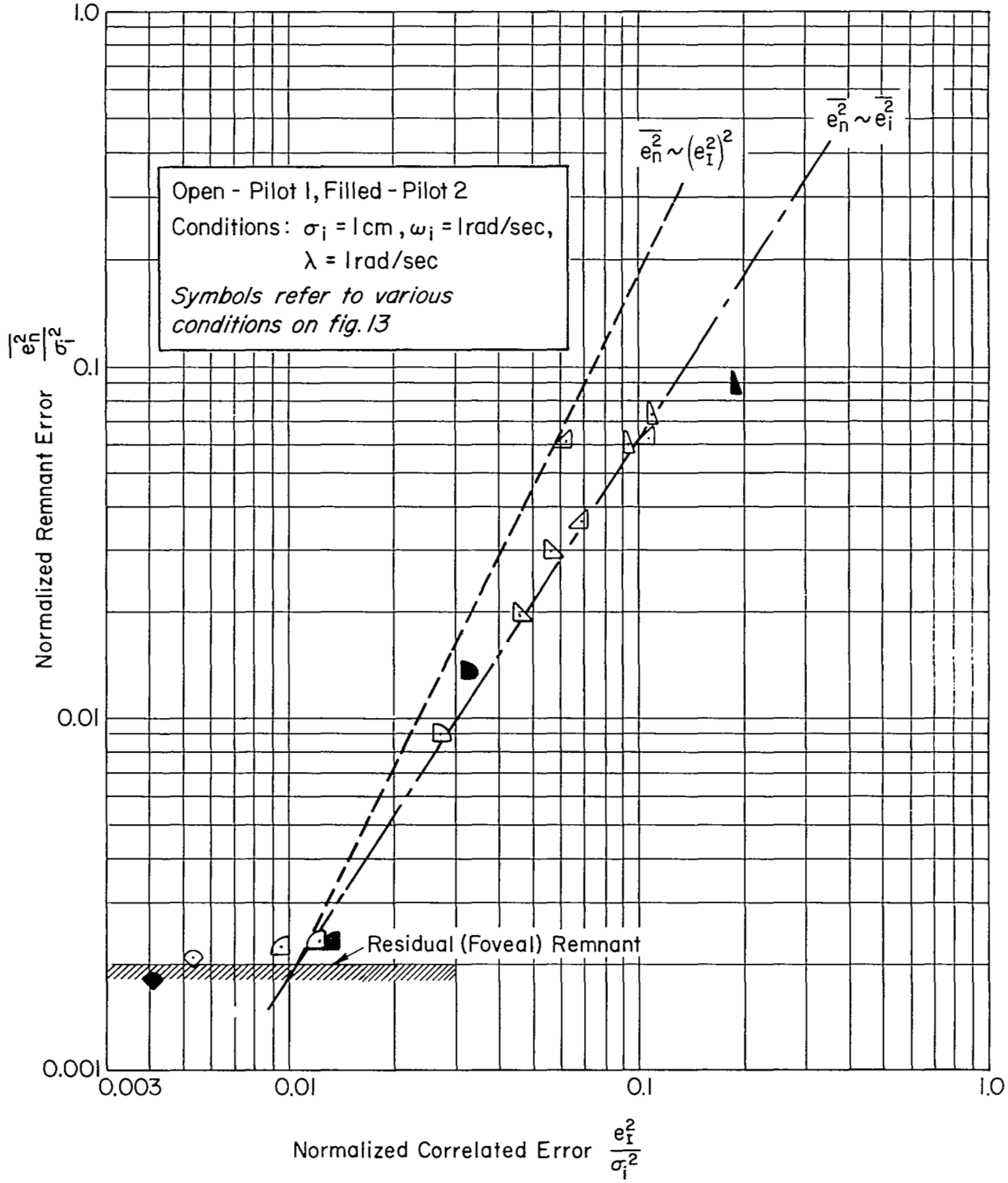

Figure 34. Remnant Error Versus Correlated Error

In concluding this presentation of the basic data, the following general observations are made:

- Both pilots show generally the same behavior. The measures which differed most were those open to individual choice and style, rather than those affected by the closed-loop effects (e.g., scanning interval or primary task dwell time). It is therefore felt that these results are generally applicable to other pilots with similar instrument flight background and training.

- The following order of increasing difficulty and decreasing performance was generally observed in all measures: foveal, natural-scan, blanked-scan, truncated blanked-scan, and full parafoveal viewing.

- Small but consistent differences did exist between the viewing conditions where parafoveal view was allowed and those where it was denied. To the extent that multi-display scanning may more closely approach the blanked-scan conditions of this experiment, then one must be careful in applying the data from scanning with parafoveal viewing to display situations where it may not be available.

- A wide range of scanning conditions could be forced by the experimentally imposed variables. However, it is shown that the use of the variable side task instability served to control mainly the time away from the subsidiary task, and thereby the main task dwell. This, in turn, was a primary governor of the scanning frequency. Therefore, one should be cautious in interpreting the ratio of scan frequency to closed-loop bandwidth under these forced conditions, with those which might occur under more free conditions.

In the next section, we will interpret these data in the light of the scanning and sampling theory.

SECTION V

COMPARISON WITH THEORY

In this section we will interpret our results in terms of the theory in Section II. First, data relating to validation of the basic assumptions will be presented. Then the effectiveness of the theory predicting overall performance measures will be assessed.

A. VALIDATION OF ASSUMPTIONS

At the end of Section II, a list of basic assumptions to be validated by the experiments was presented. This list will now be evaluated.

1. Do different pilots adopt the same average scanning, sampling, and reconstruction strategy?

The answer, on the basis of the two typical pilots studied herein, is generally "YES". Throughout the presentation of the data, the points for Pilots 1 and 2 have been kept separate. A perusal through the figures indicates that the general levels of each parameter, the performance measures, the trends with applied experimental variables are all remarkably similar for both pilots. Considering that the replication runs were run on different days, and the wide latitude of sampling behavior open to each pilot, the close agreement observed in these data strongly suggest that the scanning behavior adopted by the pilot is dependent primarily on the task variables and the laws governing optimum behavior under these conditions, rather than idiosyncratic pilot preferences. Compared with Pilot 1, Pilot 2 did have a significantly larger dwell time and sampling interval, but these have counteracting effects on performance.

2. Are the sampling intervals randomly distributed about some mean value?

Inspection of the various time histories (Figs. 14-16) shows that relatively random changes in the dwell times and sampling intervals occur from sample to sample. The side task dwell time was the most uniform, ranging from only 0.4 to 0.8 sec, while the main task dwell ranged over the time allowed by the secondary task divergent time constant, i.e., up

to approximately 0.6 T_λ. The observation that the mean scanning interval was governed by the sum of these two dwells, and therefore by the secondary task stability level, has been previously discussed in Section IV. Variations in sampling interval around this mean were remarkably small, ranging from 20 to 40 percent of the mean. A reexamination of past scanning data shows similar modest variations about the mean sampling interval. For example, from the series of experiments by Fitts, et al. (Ref. 23) the ratio of standard deviation-to-mean sampling interval on the cross pointer indicator was about 21 percent. The data presented by Levison, Elkind, et al., in Ref. 7 also show a variance of approximately 30 percent of the mean. The mean scanning frequencies for each of these references are quite similar, ranging from 1.0 to 1.5 looks/sec.

It is necessary to obtain a satisfactory analytical expression for the observed sampling distributions to permit the sampling remnant to be computed. During the examination of the preliminary data from these experiments, the Pearson Type III distribution function was found to fit the data satisfactorily (Ref. 58). Typical fits to previously presented data for the blanked-scanning case are shown in Fig. 35. A main feature of the fitted functions is that all distributions are sharply truncated at a "lower bound", T_o. In certain cases a truncated Poisson distribution was satisfactory, but, for most others, higher order terms of the Pearson Type III formula were required. The "variability parameter" $\delta = T_o/\overline{T_s}$ has important effects on the level of the random sampling remnant, as explained in Section II. Increasing T_o towards $\overline{T_s}$ reduces the sampling interval variance, σ_{T_s}. As the ratio of $\sigma_{T_s}/\overline{T_s}$ becomes smaller, the random sampling contributions to remnant are reduced, while the contributions at near-harmonics of the sampling frequency become more pronounced. The measured and fitted histograms and parameters are summarized in Table IX.

In the face of the foregoing data of our own and others, we conclude that sampling intervals are randomly distributed about a fairly stable mean, but that they are not widely distributed and cannot be considered as purely Poisson distributed. An important feature of the measured sampling interval histograms is their truncation at a fairly well defined lower bound, T_o. A satisfactory analytic function to fit the observed distributions is the Pearson Type III (gamma) probability density function.

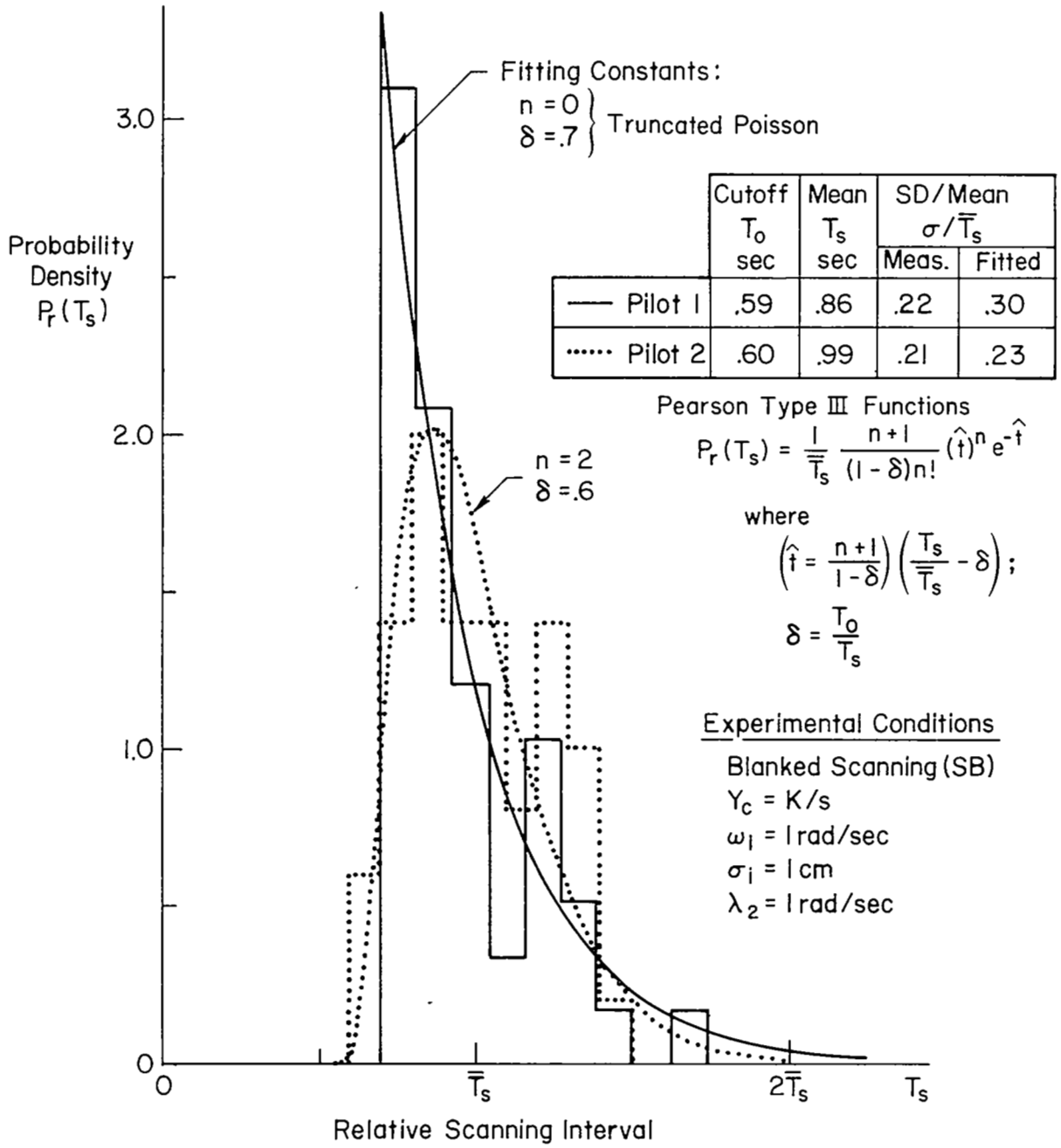

Figure 35. Pearson Type III Distribution Function Fits to the Sampling Interval Histograms for Blanked Scanning

TABLE IX

TYPICAL SAMPLING DISTRIBUTION PARAMETERS

EXPERIMENTAL CONDITIONS AND PILOT (Y_c = K/s, λ_2 = 1 rad/sec, ω_i = 1 rad/sec, σ_i = 1 cm)	MEASURED FROM HISTOGRAMS					APPROXIMATE PEARSON TYPE III PARAMETERS	
	MEAN SAMPLING INTERVAL $\bar{T}_s$ (sec)	STANDARD DEVIATION σ_{T_s} (sec)	STD. DEV. / MEAN $\sigma_T/\bar{T}_s$	LOWER BOUND T_o (sec)	RELATIVE LOWER BOUND $T_o/\bar{T}_s$	SKEWNESS FACTOR n	VARIABILITY FACTOR $\delta = T_o/\bar{T}_s$
Natural Scan, SP:							
Pilot 1	0.9	0.23	0.26	0.6	0.7	2	0.6
Pilot 2	1.3	0.28	0.22	0.6	0.46	45*	0*
Blanked Scan, SB:							
Pilot 1	0.86	0.19	0.22	0.6	0.7	0	0.7
Pilot 2	0.99	0.21	0.21	0.6	0.6	2	0.6
Truncated Blanked Scan, SB:							
Pilot 1	0.69	0.12	0.17	0.25	0.36	20	0.36
Pilot 2	0.56	0.07	0.13	0.4	0.7	4	0.7

*This combination of n, δ results in an "apparent" value of $T_o/\bar{T}_s \doteq 0.5$, which approximates the observed ratio, 0.46. The large value of n is necessary to approximate the low skewness of the observed distribution for this configuration.

Pearson Type III Distribution:

$$P_r(T_s) = \frac{1}{\bar{T}_s} \frac{n+1}{(1-\delta)n!} (\hat{t})^n e^{-\hat{t}}$$

where $$\hat{t} = \left(\frac{n+1}{1-\delta}\right)\left(\frac{T_s}{\bar{T}_s} - \delta\right)$$

$$\delta = \frac{T_o}{\bar{T}_s}$$

3. Is the sampling frequency high enough to justify a describing function representation?

We will show that the answer is yes. Before proceeding with this discussion, the reader should recall the sampling and reconstruction portion of Section II (i.e., Figs. 3 and 14). The main implication of the theory was that, for short dwell fractions (approaching impulsive samples), the sampling rate should be much higher than the signal bandwidth to be passed, to prevent the remnant contribution from exceeding the level of the describing function component. For longer dwell fractions, longer sampling intervals can be tolerated while maintaining a reasonable coherency (signal-to-noise ratio). The computed results indicated that a scanning frequency parameter, $S = \omega_s/\omega_c(1 - \eta)$, related these variables, and that it should lie in the range of 4 to 8 to keep the scanning remnant within reason.

Let us examine some of the separate components of scanning frequency parameters first. Figure 36 shows cross plots of scanning frequency, dwell fraction, and the error coherence versus crossover frequency for a number of the scanned conditions at constant input bandwidth. Crossover frequency was chosen as the abscissa as an indicator of displayed signal bandwidth, on the basis of the closed-loop error spectra. At the top, Fig. 36a shows that the ratio of scanning-to-crossover frequency ranges from approximately 1 to 4 with no general trend apparent. Remember that the scanning frequency in these experiments is governed primarily by the side task dwell, and not by the operator's free choice of a scanning frequency. Nevertheless, the attentional demand of the side task is thought to be similar to that encountered in true instrument flight operation. Figure 36b, in the center, reveals a fairly systematic trend in the dwell fraction versus crossover frequency. Further implications of this trend are discussed later, but some correlation is apparent. Distinct "foveal" and "parafoveal" branches are suggested. Finally, consider Fig. 36c, at the bottom, which gives the error coherence versus ω_c. A rather definite trend is apparent, with the lowest crossovers resulting in the lowest percentage of input-correlated error. It is also obvious that the display conditions are well separated on the basis of "parafoveal", "unblanked displays" and

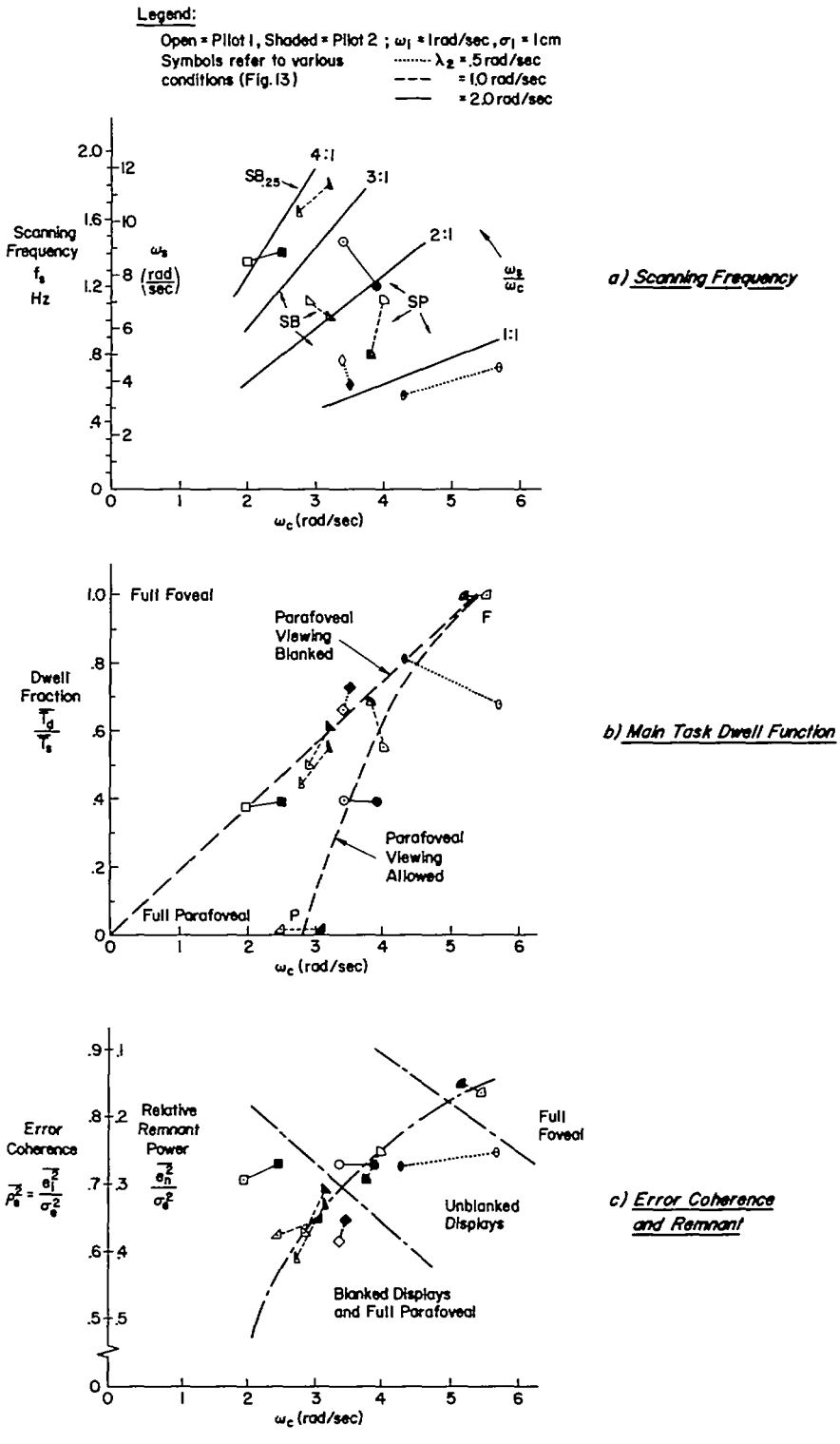

Figure 36. Crossplot of Scanning Frequency, Dwell Function and Error Coherence versus Crossover Frequency

"blanked displays". It is worth noting that, despite the extremely difficult scanning conditions here, the error coherence did not drop much below 0.6, which means that the describing function still accounts for about 60 percent of the error power, and the scanning remnant only 40 percent or less. On this basis alone, we would expect the describing function model to be a reasonably valid representation. Neither the scanning frequency nor dwell-fraction alone correlate with the coherence, however.

Now let us see how the scanning frequency parameter $S = \omega_s/\omega_c(1-\eta)$ fares. Figure 37 shows a cross plot of this parameter versus the scanning-to-crossover frequency ratio. While the scanning-to-crossover frequency ratio varies over a 4:1 range, the scan frequency parameter range only varies over a 2:1 range, right in the predicted region of 4 to 8.

On the basis of the good error coherence and large scanning frequency parameter observed, these experiments strongly validate use of quasi-linear describing functions to model the closed-loop aspects of scanning and reconstruction process.

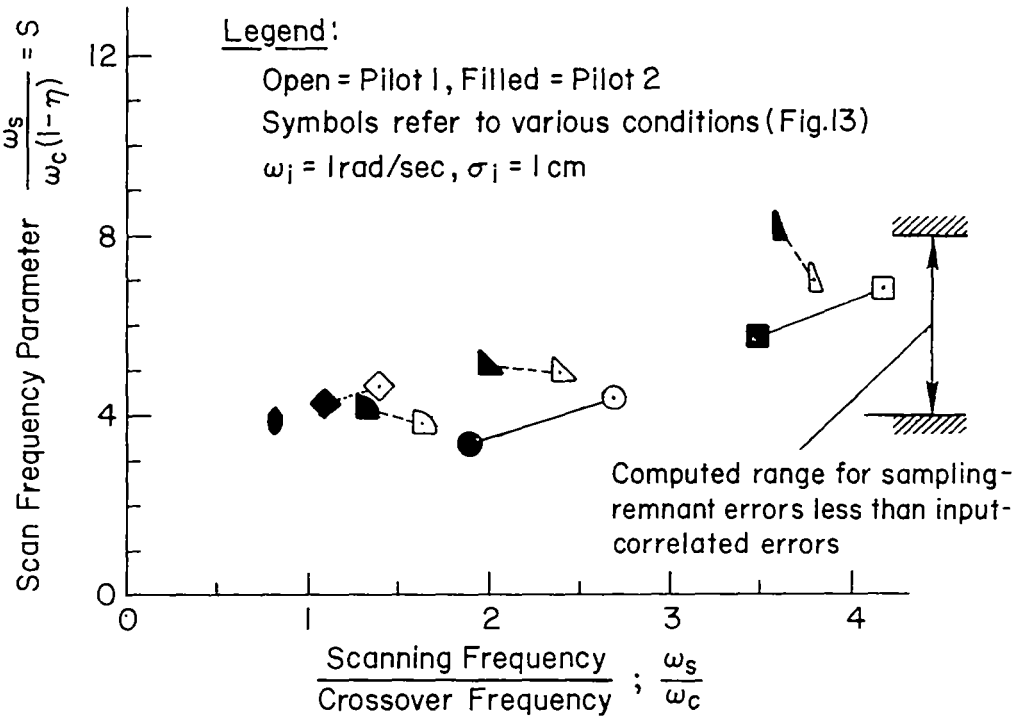

Figure 37. Scanning Frequency Parameter Versus Ratio of Scanning-to-Crossover Frequency

4. **Does the form of the scanned, sampling, and reconstruction describing function fit Equation 1?**

Equation 1 of Section II indicated that the describing function attributed to sampling, scanning, and reconstruction could be adequately represented by an attenuation factor, K_h (independent of frequency), and an incremental sampling time delay increment, τ_s:

$$Y_H(j\omega) \doteq K_h e^{-j\omega\tau s} \qquad \text{(See Eq. 1)}$$

In order to determine this "perceptual describing function" Y_H, the pure foveal gain and phase measurements were subtracted from those at various sampling and scanning conditions, using each pilot's own foveal data as a reference level. The results are given in Fig. 38 (the scatter is due to the small difference between larger quantities). For the unblanked display conditions (Fig. 38a) there are no apparent phase penalties due to sampling, but the differential gain curves have a decrement ranging from −3 to −6 dB (at 1 rad/sec), and a slightly positive slope (about 2 dB/decade). For the blanked display cases (Fig. 38b) the differential gain curves show similar gain decrement (−2 to −10 dB) and positive slope (2 dB/decade). Here, the differential phase curves show some evidence of phase lag penalties due to sampling. Even so, the worst phase shifts only correspond to roughly a 0.15 sec delay, which is a small fraction of the typical sampling interval of 1 sec. Inspection of these shows that they roughly fit the predicted describing function, i.e., the attenuation factor <u>is</u> very nearly independent of frequency and the phase differences <u>can</u> be fairly well represented by a small time delay increment. The slight positive slope noted in the describing function difference is mainly attributed to the higher-than-unity slope of the foveal describing function. Since the scanned describing functions actually show a closer fit to the simple crossover model, this improves the validity of the pure-attenuation-plus-delay model for $|Y_H|$, at least for display system analyses.

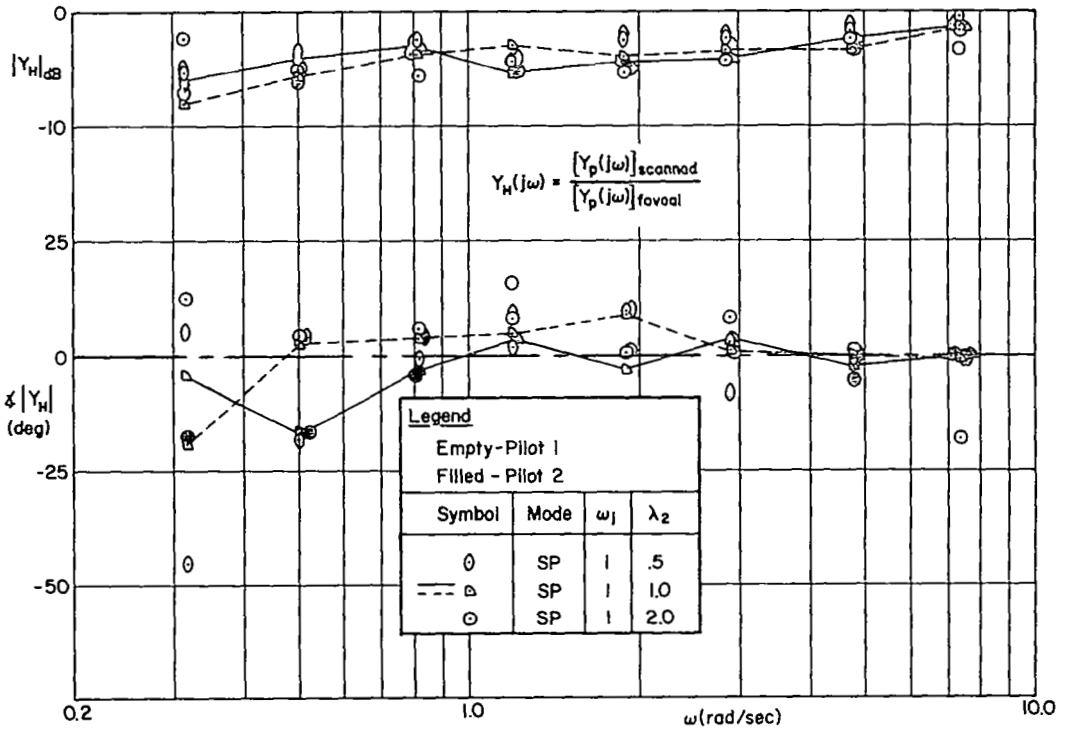

a) Natural Scan Conditions

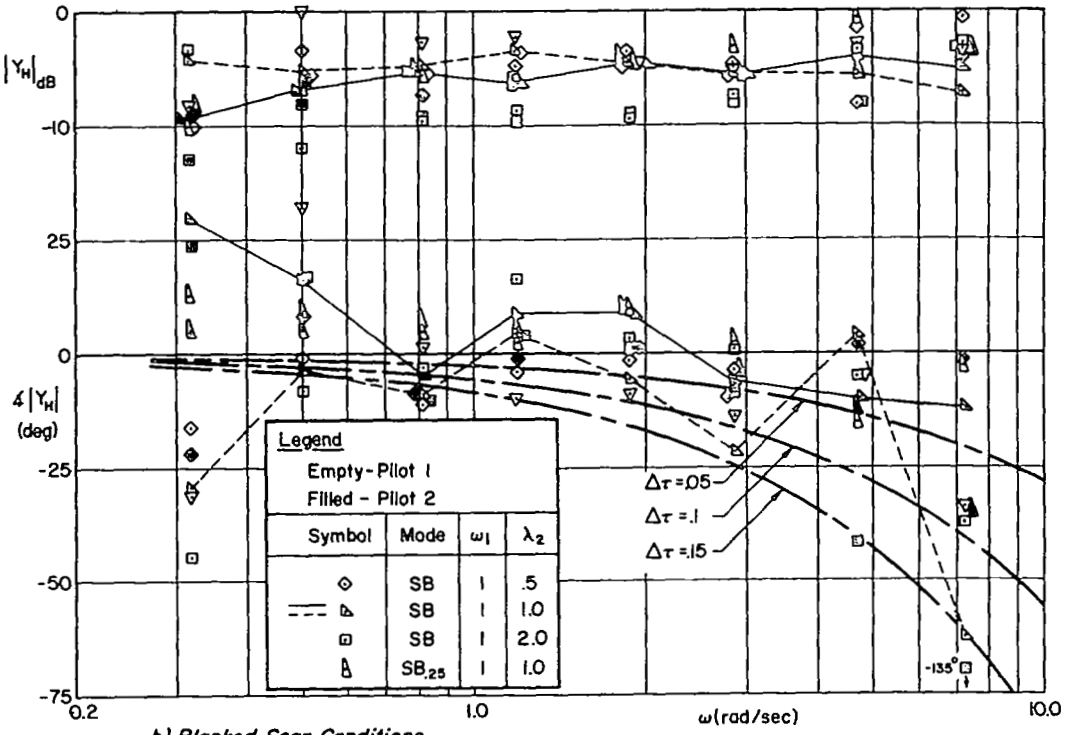

b) Blanked Scan Conditions

Figure 38. Apparent Describing Function Due to Scanning and Reconstruction

5. Is the sampling remnant broadband?

Because closed-loop system performance (e.g., tracking errors) are important outputs from pilot/vehicle analyses, attention has been focused on the error spectrum. The sampling remnant theory in Ref. 47 shows that two general types of sampling remnant exist. Perfectly periodic sampling results in remnant at harmonics of the sampling frequency, with very little in the input passband. As sampling becomes more random, a certain proportion of this high frequency power is "demodulated" to the input passband and appears as broadband "observation" noise. The experimental data bearing on this assumption was presented in Fig. 32 of the previous section. Inspection of this figure shows that the error remnant spectra due to the various scanning modes are quite smooth across the input bandwidth and are fairly flat up to the closed-loop cutoff frequency (as indicated by the 90 deg phase point of the closed-loop describing function. Beyond this frequency it continues to be smoothly attenuated up to the limit for which our data were reduced. Thus, any sampling harmonic components which may have been present in the control spectrum at sampling frequencies were strongly attenuated by the closed-loop cutoff, which, in turn, is limited by the crossover frequency.

The theory of Section II, e.g., around Eqs. 2 and 3, indicates that the sampling remnant (considered as an injected noise) has a power spectral density level which scales with the mean-square displayed error;

$$\Phi_{nn_e}(\omega) \doteq \frac{\bar{T}_s \overline{e^2}(1-\eta)(1-\delta)}{\pi \left| 1 + j\omega T_d/2 \right|^2} \tag{3}$$

To validate our Eq. 3, the previously given closed-loop error remnant spectra Φ_{ee_n} of Fig. 32 were converted to remnant injected at the display point and were normalized by $\overline{e^2}$ according to the following relationship:

$$\underset{\substack{\text{Normalized}\\ \text{Injected}\\ \text{Remnant}}}{\frac{\Phi_{nn_e}(\omega)}{\overline{e^2}}} = \underset{\substack{\text{Measured}\\ \text{Closed-Loop}\\ \text{Remnant, etc.}}}{\frac{\Phi_{nn_e}(\omega)}{\left| (M/I)j\omega \right|^2 \overline{e^2}}} \tag{14}$$

Figure 39 shows the results of this computation. It can be seen that the widely different closed-loop remnant levels of previous Fig. 32 tend to coalesce when normalized by the corresponding $\overline{e^2}$. The normalized remnant for the scanned and parafoveal cases is somewhat larger than the foveal case, as might be expected. To compare these data with Eq. 3 we take the following values for the blanked display case, for which the theory is most valid: $\overline{T}_s = 0.86$ sec, $\overline{T}_d = 0.42$ sec, $\eta = 0.52$, $\delta = T_o/\overline{T}_s = 0.70$. The resulting analytical model is:

$$\left.\frac{\Phi_{nn_e}}{\overline{e^2}}\right]_{SB} = \frac{0.040}{(1+0.21j\omega)^2}\left[\frac{\text{rad}}{\text{sec}}\right]^{-1} \qquad (15a)$$

Equation 15a is shown as a solid line in Fig. 39. The fit to the corresponding data points is excellent, so our theoretical scanning remnant model seems reasonably valid.

It is interesting to note that the model for human operator basic remnant during continuous single-loop tracking given by Levison, et al, in Ref. 59, has a form identical to Eq. 3.

Present; Scanned Case

$$\frac{\Phi_{nn_e}}{\overline{e^2}} = \frac{0.040}{(1+0.21j\omega)^2} \qquad (15b)$$

Ref. 59; Foveal Case

$$= \frac{0.035}{(1+0.3j\omega)^2}\left[\frac{\text{rad}}{\text{sec}}\right]^{-1} \qquad (15c)$$

The model of Ref. 59 (Eq. 15c) is shown dashed in Fig. 39. Perhaps fortuitously, it comes close to our scanned remnant equation and data, but it does not fit our foveal remnant data, as it should. The reason for the disagreement is not known, but it is not considered very serious at this time because data on subject-to-subject variability are not yet available.

Thus the answer to Question 5 is: **Yes, the remnant due to scanning, sampling, and reconstruction is broadband and it can be modeled by a first-order filtered noise model per Eq. 3.**

	Main Task: Y_{c_1} = K/s, σ_i = 1.0 cm, ω_i = 1 rad/sec Viewing Mode		Side Task $Y_{c_2} = \frac{1}{(s-1)}$, No Input	Main Task $\frac{\sigma_e}{\sigma_i}$	$\bar{f}_s$ (Hz)	$\frac{\bar{T}_d}{\bar{T}_s}$
●	F	Foveal	None	.12	–	–
▣	P	Parafoveal (30° horizontal and zero ref. ext.)	None	.33	–	–
◇	SP	Natural Scanning	✓	.22	1.12	.55
△	SB	Scanning, but non-fixated display was blanked	✓	.26	1.16	.52

(Data for Pilot I)

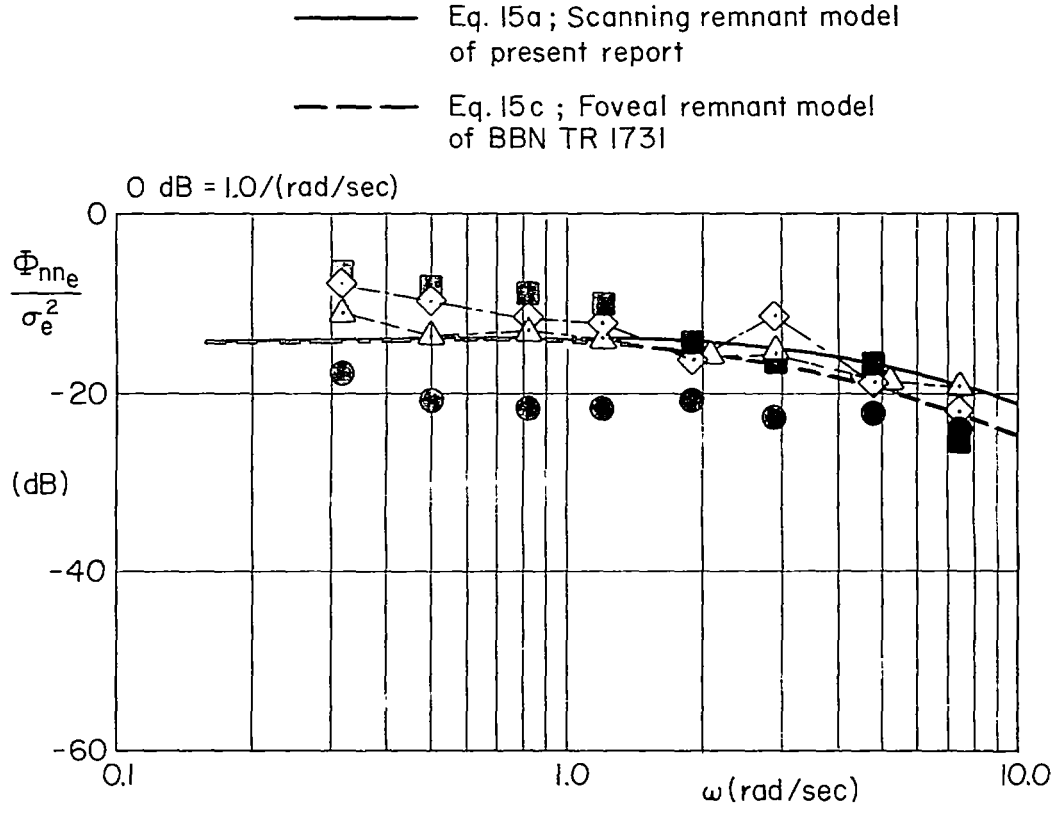

Figure 39. Normalized Injected Remnant Spectra

6. To what extent does signal reconstruction take place between fixations?

The data from these experiments indicate that reconstruction does occur in some situations but not in others. First consider the direct evidence from the time histories, and then the indirect evidence from the describing functions.

Under conditions of pure-gain pilot equalization, signal reconstruction occurs (by definition) when the operator's control output does not return to zero between each fixation dwell interval on the display in a given axis of control. As explained in Section II, a variety of signal "holds" or "weighted extrapolations" may be used to obtain a better control signal approximation between fixation dwells. Thus, no matter what the extrapolation in the case of pure-gain equalization, it qualifies as reconstruction as long as the extrapolation is not identically zero between fixations.

Figure 40 is an excerpt from previous Fig. 15b, where the nonfixated display was blanked. Heavy lines superimposed on each coordinate denote the fixation periods on either the main (tracking) or side (stabilization) tasks. Careful scrutiny of the main task control action (second time history from the top of the figure) shows that (allowing for the neuromuscular delays and dynamics) the control is frequently interrupted as the control follows the error. The control interruptions roughly correlate with the fixation interruptions on the main display and the control frequently returns to the neighborhood of zero during fixation interruptions (again allowing for the effective delays between error and control). Between fixations there is evidently a tendency to relax on the control force. This implies a decaying form of intersample reconstruction for this blanked viewing condition. There is seldom any attempt to hold the previous control signal throughout the intersample interval. When parafoveal vision is denied the operator, the decay in the control action toward zero between samples appears to be even more rapid than suggested by the truncated cardinal weighting function in Fig. 5. Thus, reconstruction on the primary task seems to be negligible.

By contrast, while stabilizing the first-order divergence (see bottom of Fig. 40), the left-hand control action remains fairly constant between fixations on the secondary task. This implies that zero-order-hold reconstruction is used on the side task (e.g., refer to Fig. 4).

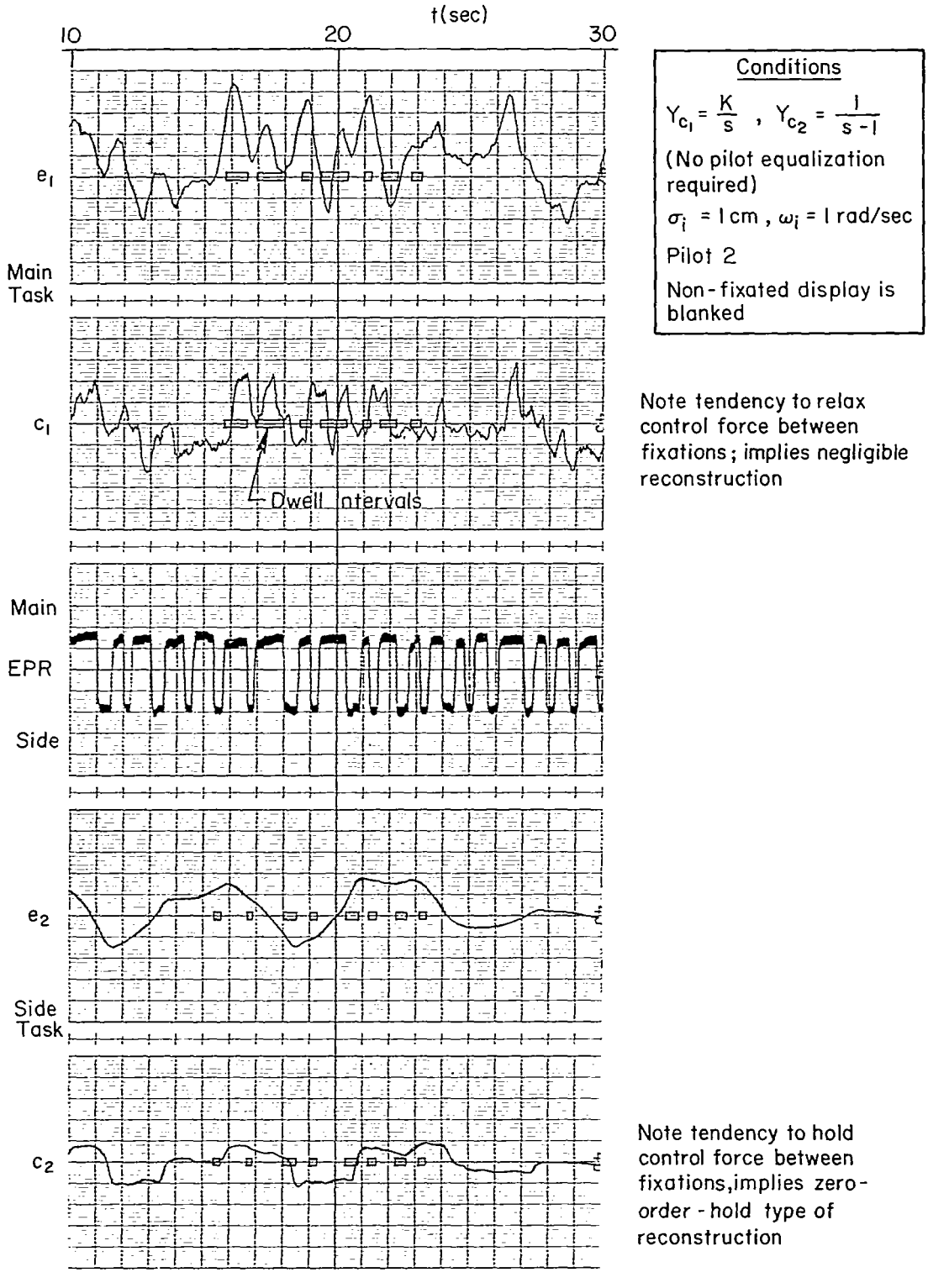

Figure 40. Excerpt from Time Traces of Fig. 15b, Showing Evidence For (Side Task) and Against (Main Task) Signal Reconstruction Between Fixations Under Conditions Requiring No Pilot Equalization

Now let us consider the indirect evidence for or against reconstruction from the describing function data. One could, in principle, take the parameters of the perceptual describing function $Y_H(j\omega)$ from Fig. 38b (the differential describing function between the foveal and various scanning conditions), ascribe the attenuation to K_h in Eq. 1, ascribe the phase lag increment to τ_s in Eq. 1 and estimate a reconstruction rate weighting coefficient R from Fig. 6. This was attempted, but not much confidence is attached to the results for a number of reasons:

- The attenuation observed in Fig. 38b need not necessarily be attributed to reconstruction since the finite dwell fraction itself will exhibit an average attenuation equal to η. Thus effects on attenuation are confounded and inconclusive at this point. However, we shall return to the consideration of gain later.
- The phase data in Fig. 38b are too scattered to obtain a precise measure of incremental time delay.
- The foveal and scanned describing functions were not fitted precisely enough to obtain reliable differences for the incremental time delay between the scanned and foveal describing functions. Furthermore, the incremental time delay depends on unreliable small differences between larger quantities.
- The use of Fig. 6 presumes a specific type of reconstruction, although inspection of the main task time histories has suggested that the intersample reconstruction is minimal. It cannot be assumed a priori that its incremental time delay will obey the relationship derived for truncated cardinal reconstruction.

The main result of this interpretation of the differential describing function data was that dwell times in excess of the 0.3 sec minimum were required to generate a larger "apparent" rate weighting coefficient R (see Section II-2 for a definition of R). The rate weighting coefficient calculated from Fig. 6 roughly matched the average relationship:

$$R \doteq 1.25(\bar{T}_d - 0.2) \qquad (16)$$

However, this alternative explanation for the low effective incremental time delays in the differential describing functions in Fig. 38b is not given much credence in view of other more direct evidence to which we now turn.

Better indirect evidence against error signal reconstruction between samples (during the main task) is given by the observed open-loop gain regression, as characterized by crossover frequencies. The simple finite dwell sampling theory without reconstruction, reviewed in Section II, predicts that the adopted crossover frequency in the primary task will be linearly proportional to dwell fraction, $\eta = \overline{T}_d/\overline{T}_s$. This is simply because the loop is assumed closed during the fixation interval and open between fixations. The time averaged open-loop gain for the finite dwell sampled crossover model is thus $\omega_c = \eta\omega_{c_F}$ where ω_{c_F} is the adopted crossover frequency for continuous foveal tracking. The operator cannot increase his gain during the dwell interval of scanned tracking because of stability constraints during foveal tracking. Consequently, one would expect the crossover gain to regress linearly with dwell fraction in the absence of control between fixations. Preliminary evidence for this has already been presented in Fig. 36b, where the data corresponding to blanked conditions were scattered along a line of perfect correlation through the origin. However, the naturally scanned data (where parafoveal viewing was allowed) did not lie on this line of perfect correlation through the origin. Instead, the scanned data with parafoveal viewing diverged toward the purely parafoveal crossover value near 3 rad/sec.

This result suggested that the dual-gain finite-dwell switching model proposed in Ref. 7 might represent foveal-parafoveal scanning observations better, by accounting for parafoveal closure of the primary task loop during the interrupt fraction $(1-\eta)$. The switched gain model is represented easily by multiplying the ratio of parafoveal gain to foveal gain by $(1-\eta)$ and adding the product to η to obtain the effective dwell fraction, viz.

$$\eta_e \equiv \eta + \Omega(1-\eta) \tag{17}$$

where $\Omega = \omega_{c_P}/\omega_{c_F}$ = ratio of crossover gains for continuous parafoveal relative to continuous foveal tracking ($\Omega \equiv 0$ for blanked scanning conditions)

$\eta = \overline{T}_d/\overline{T}_s$ = dwell fraction

Because the pilot cannot increase his gain much beyond the purely foveal level during each fixation, the switched gain model says that the ratio of scanned to foveal gains should equal η_e. Figure 41 shows this correlation, which is fairly good.* If appreciable signal reconstruction were employed during the interrupt fraction, the perceptual gain would not regress nearly as much as shown. Reconstruction is not needed to explain the higher ω_c data for natural scanning with parafoveal perception permitted, because the effective dwell fraction η_e, based on a simple switched-gain model, also correlates very well with the observed data. The value of this simple result depends on how important and variable is the parafoveal gain under realistic instrument scanning conditions. If the parafoveal gain on a particular axis (among several in a multiloop display) can be shown to be negligible, then a very simple and useful finite dwell model is possible without the need for intersample reconstruction.

The principal surprise is that display signal reconstruction apparently was <u>not</u> used in the main tracking task, although it <u>was</u> used during the secondary stabilization task. Close scrutiny of all the data, trends, and theories suggests the following explanations:

- The side task only required brief fixations and crude zero order hold reconstruction to maintain a stable closed loop since minimization of error was not required. Furthermore, the control action was the only input.

- Consequently, the main tracking task could be attended to with a relatively high dwell fraction, and any high frequency scanning remnant existing at the pilot's controls would be attenuated by the K/s dynamics. Thus, intermittent control action could be used without generating much display (error) remnant.

- Under these conditions (high dwell fraction, filtered control sampling remnant), reconstruction was not needed to achieve reasonably high error coherence, and so it was not used.

- Under conditions where the dwell fraction is very small due to other tracking demands, we would expect to see reconstruction used to lower the tracking errors. This is exemplified by the zero order hold side task control technique observed herein.

*The apparent "wild point" for ⊙ in succeeding plots is due to an anomalously high ω_c for one particular natural scanning run.

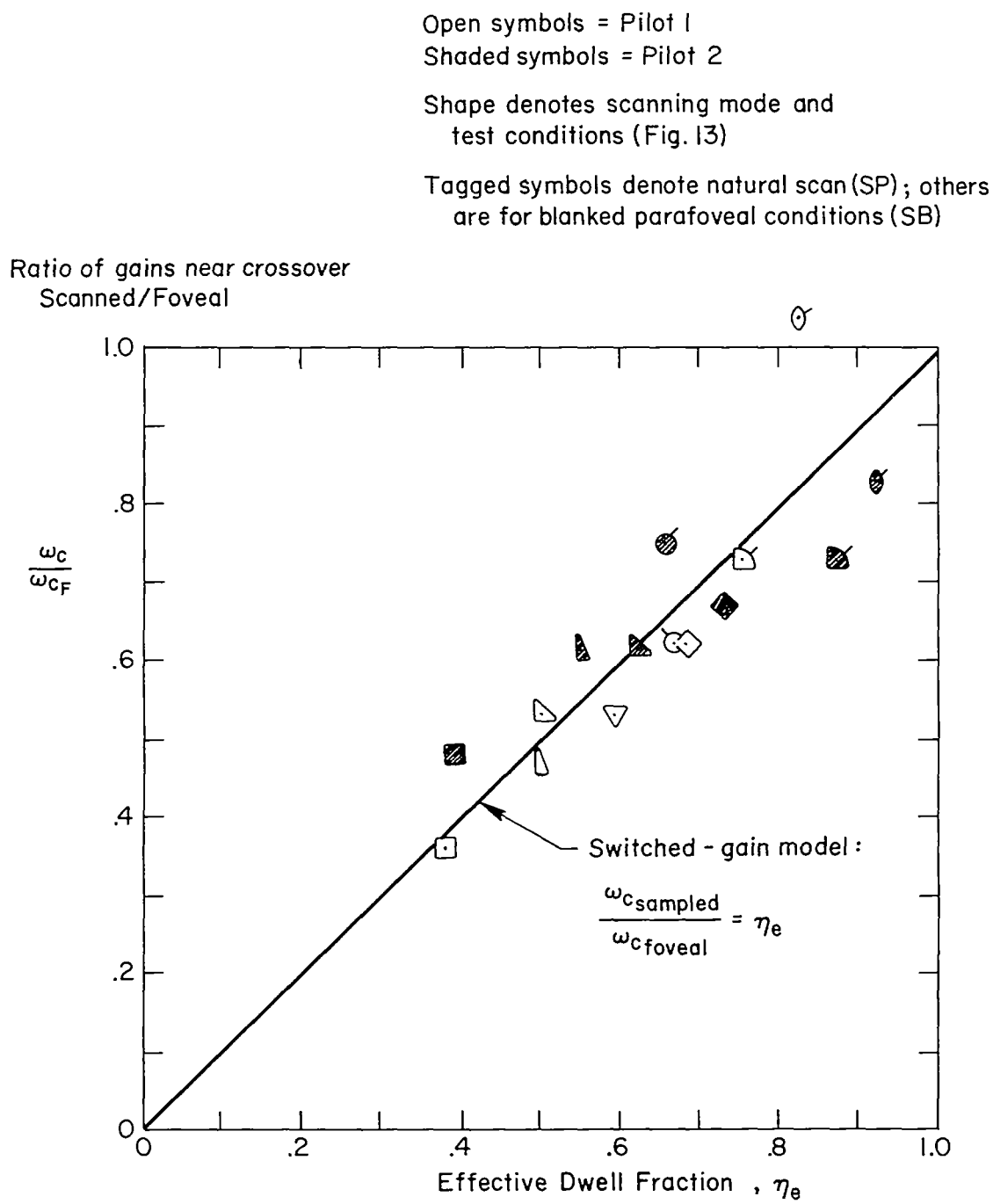

Figure 41. Crossover Gain Ratio Versus Dwell-Weighted Gain Factor

This discussion completes the rather detailed empirical assessment of numerous key assumptions and models on which our comprehensive display theory is built. All of the assumptions have been validated.

B. CORRELATION OF THEORETICAL AND MEASURED PERFORMANCE

1. Relative Correlated Error Power

Experimental measurements of the relative input-correlated power, ρ_e^2, are compared with theoretical estimates of coherence for continuous foveal and continuous parafoveal tracking in Fig. 42. In this case, the "theoretical" values are based on a remnant power spectral density in the form of Eq. 15c (originally from Ref. 59). The average foveal remnant spectrum level employed was $0.04\sigma_e^2$/rad/sec for input bandwidth $\omega_i = 0.5$ rad/sec and otherwise $0.02\sigma_e^2$/rad/sec. The observed foveal coherence in Fig. 42 correlates fairly well with theoretical values. The average parafoveal remnant spectrum level employed was $0.17\sigma_e^2$/rad/sec for $\omega_i = 0.5$ rad/sec and for one pilot, $\omega_i = 1$ rad/sec, as well. Otherwise, the parafoveal value was $0.1\sigma_e^2$/rad/sec. Figure 42 shows that there is much more variability in parafoveal coherence than in foveal coherence.

Experimental measurements of ρ_e^2 for sampled conditions are compared with theoretical calculations for sampling error determinant, Δ_s (Eq. 6) in Fig. 43 for scanning the main task with and without parafoveal perception. The effective dwell fraction, η_e, was employed in calculations with Eq. 6, where parafoveal perception of the main task was possible. The observed values of ρ_e^2 do correlate quite well with theoretical values based on random finite dwell sampling remnant in Eq. 3. Thus it appears that the observed remnant is dominated by a "sampling" remnant and that there is little evidence of the application of intersample reconstruction to increase the residual coherence above 0.8 in Fig. 41a. Instead the pilots apparently reduced their variability in sampling behavior to achieve coherences of 0.6 or more, a marked improvement in coherence over that low level which accompanies purely random finite dwell sampling.

With these rather good correlations between observed coherence and very simple theoretical measures for sampling and purely foveal remnant, we are encouraged to compare predictions and observations of mean-squared error.

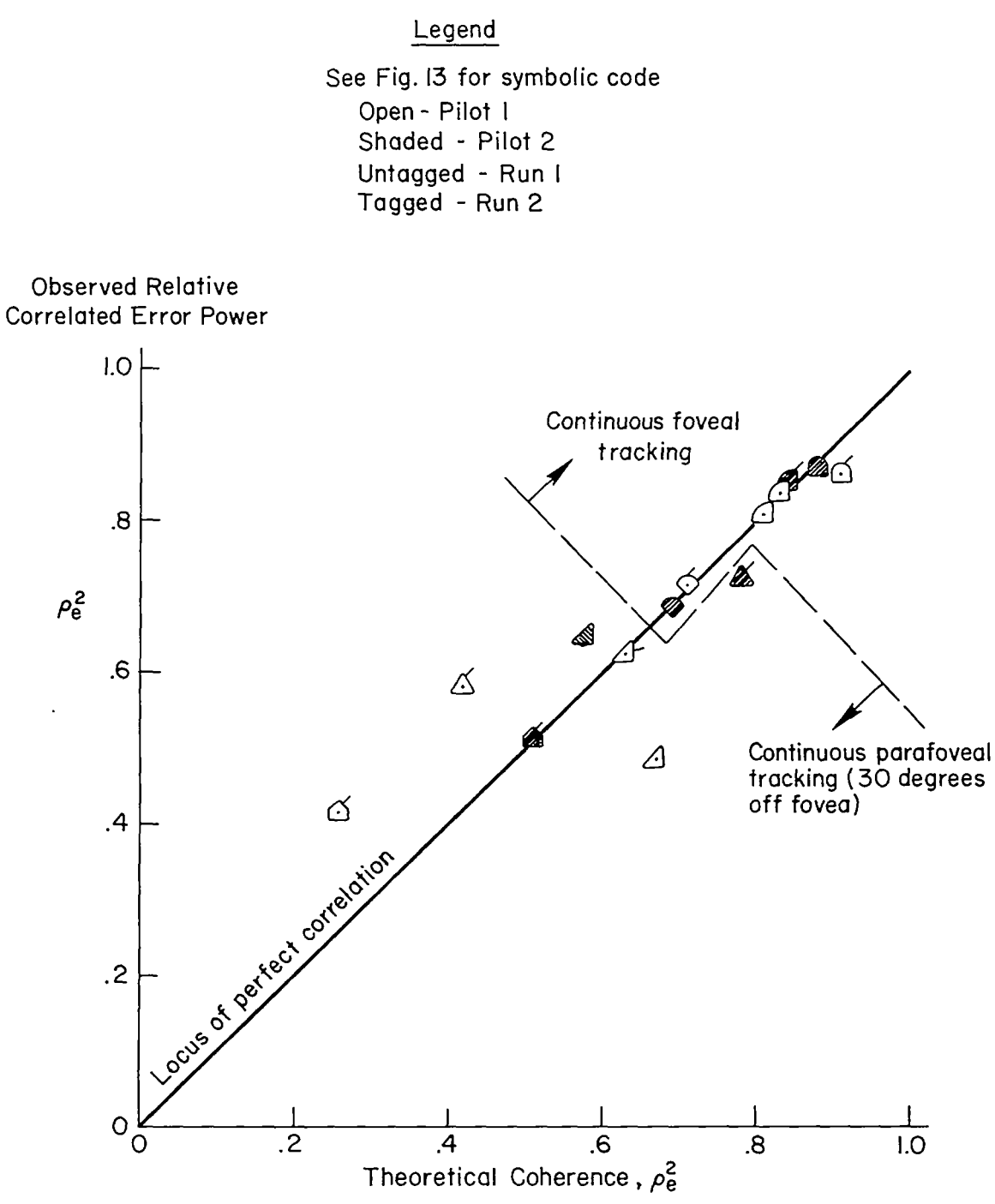

Figure 42. Comparison of Experimental Error Coherence with Theoretical Values Under Continuous Foveal and Continuous Parafoveal Tracking Conditions

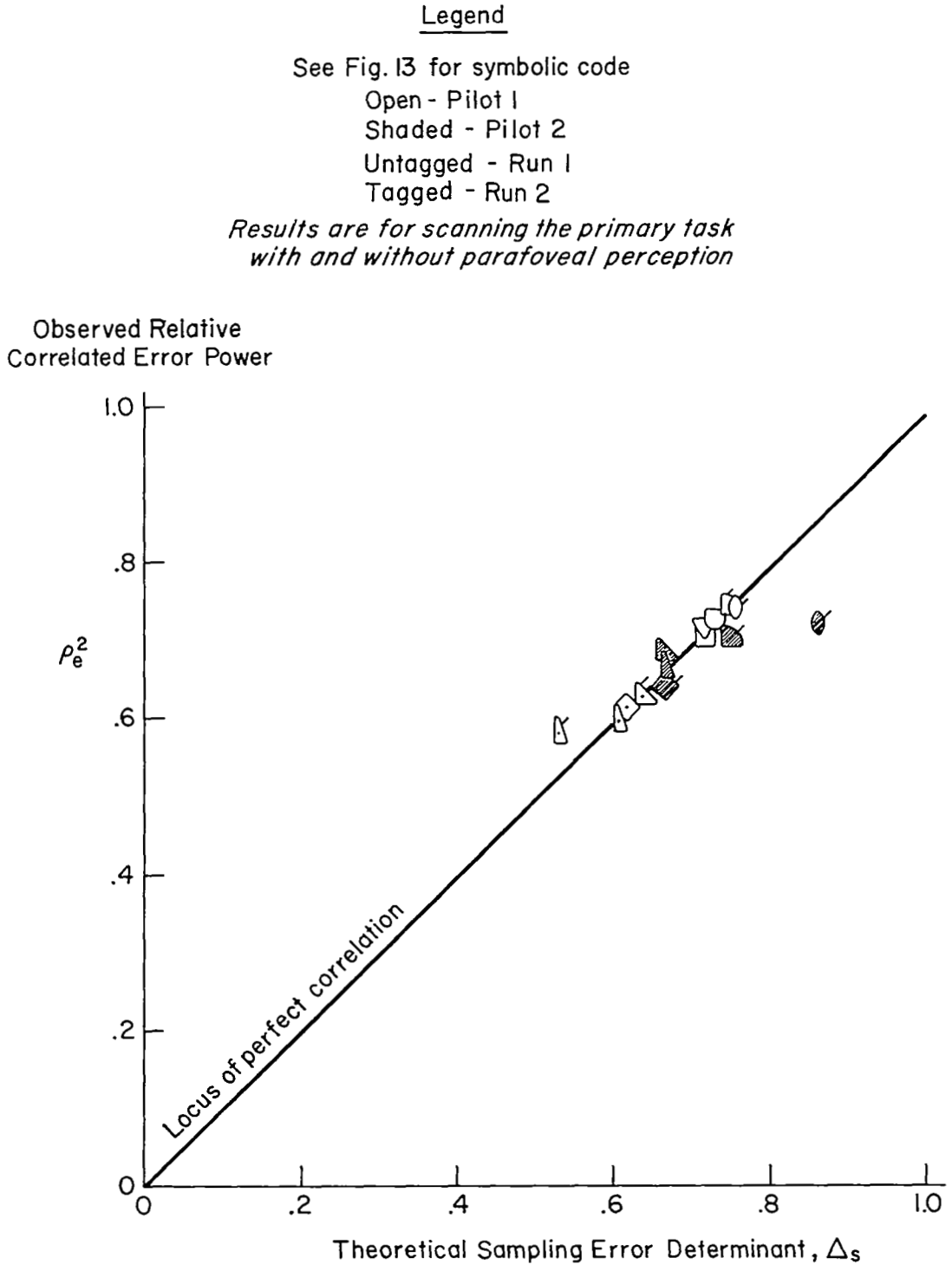

Figure 43. Comparison of Experimental Error Coherence with Theoretical Values for Sampling Remnant Determinant

2. Mean-Squared Error

Experimental measurements of **input-correlated error** on the main task, $\overline{e_i^2}/\sigma_i^2$, are compared with theoretical predictions of the same in Fig. 44. Theoretical values are based on the crossover model computations in Ref. 60 with a sharply cut off input of uniform power spectral density. Since the experimental input spectrum (Fig. 11) contained power above its enveloping half-power frequency, measured correlated relative error might be expected to exceed theoretical error. Figure 44 shows that the observed correlated error did consistently exceed the theoretical estimates, in all but one of the scanning conditions (⊙). Theoretical estimates are poor with the most difficult side task instability (⊡) and with truncated blanked scanning (◺). However, the observed relative errors for the continuous foveal tracking conditions agree very well with the theoretical computations of Ref. 60 (Fig. 11 therein).

Observations of **total normalized mean-squared error** on the main task, $\overline{e^2}/\sigma_i^2$, are compared with theoretical predictions of the same in Fig. 45. To correct for the previously noted bias in e_i^2/σ_i^2, a systematic deviation of 30 percent of the theoretical input-correlated relative error has been added to the theoretical correlated values (with scanning), before dividing each by Δ_s, to estimate total relative error. Since observed coherence correlated quite well with Δ_s, most of the scatter which remains in Fig. 45 is attributable to the bias in the input-correlated values.

3. Crossover Frequency (Open-Loop Gain)

Since the pilots were instructed to minimize average tracking error to the best of their ability on the primary display, it is also of interest to compare their adopted crossover frequencies with theoretical crossover frequencies for minima in normalized mean-squared error. This comparison is made in Fig. 46, using the normalized crossover frequency, $\tau_e\omega_c$, for convenience in comparison with the theoretical values of Ref. 60. The remnant levels for the foveal cases are based on data in Ref. 59. This comparison shows that in most cases the pilots adopted normalized crossover frequencies slightly below the theoretical values for corresponding minima.

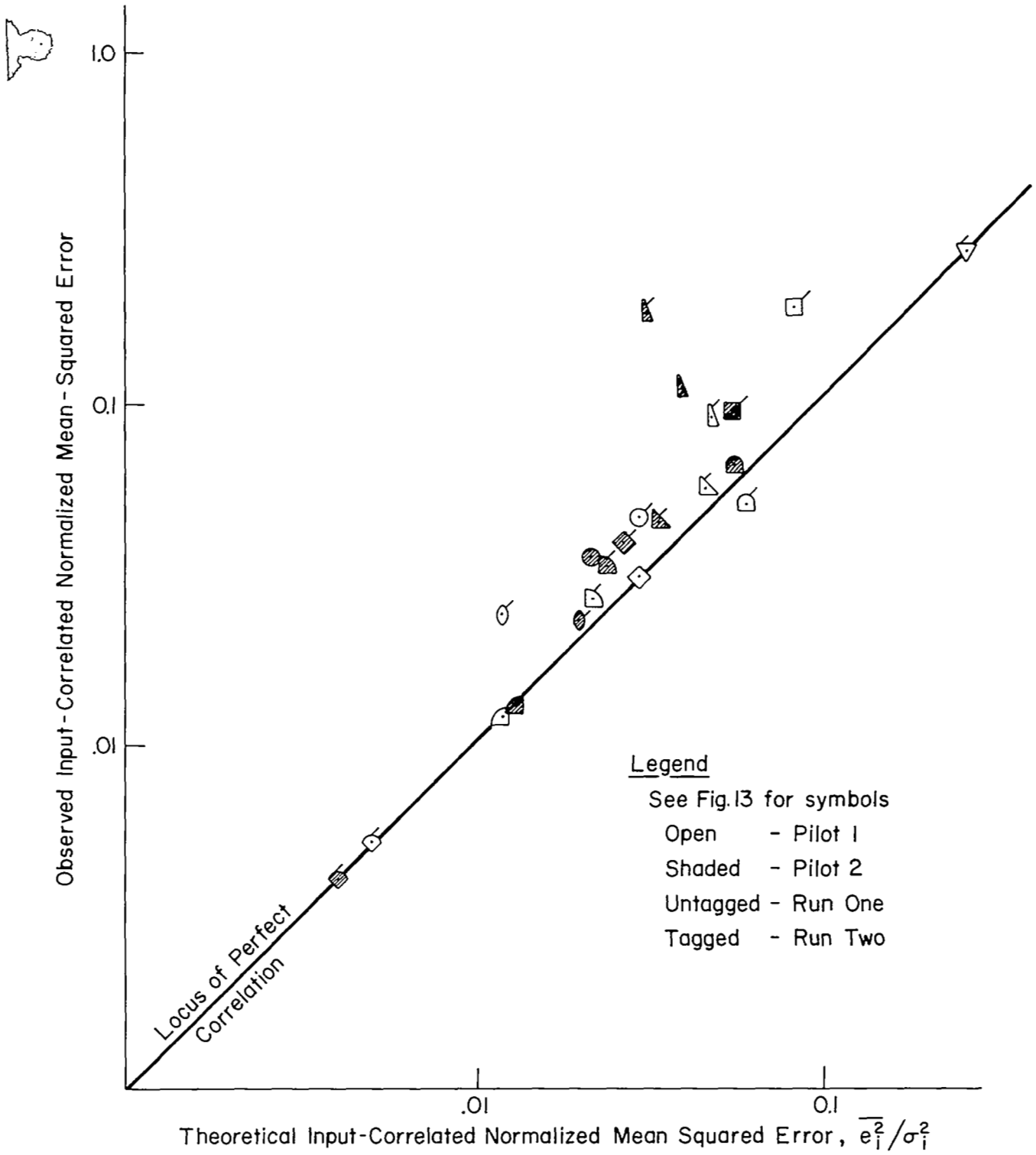

Figure 44. Comparison of Experimental Correlated Error with Theoretical Predictions (Ref. 52)

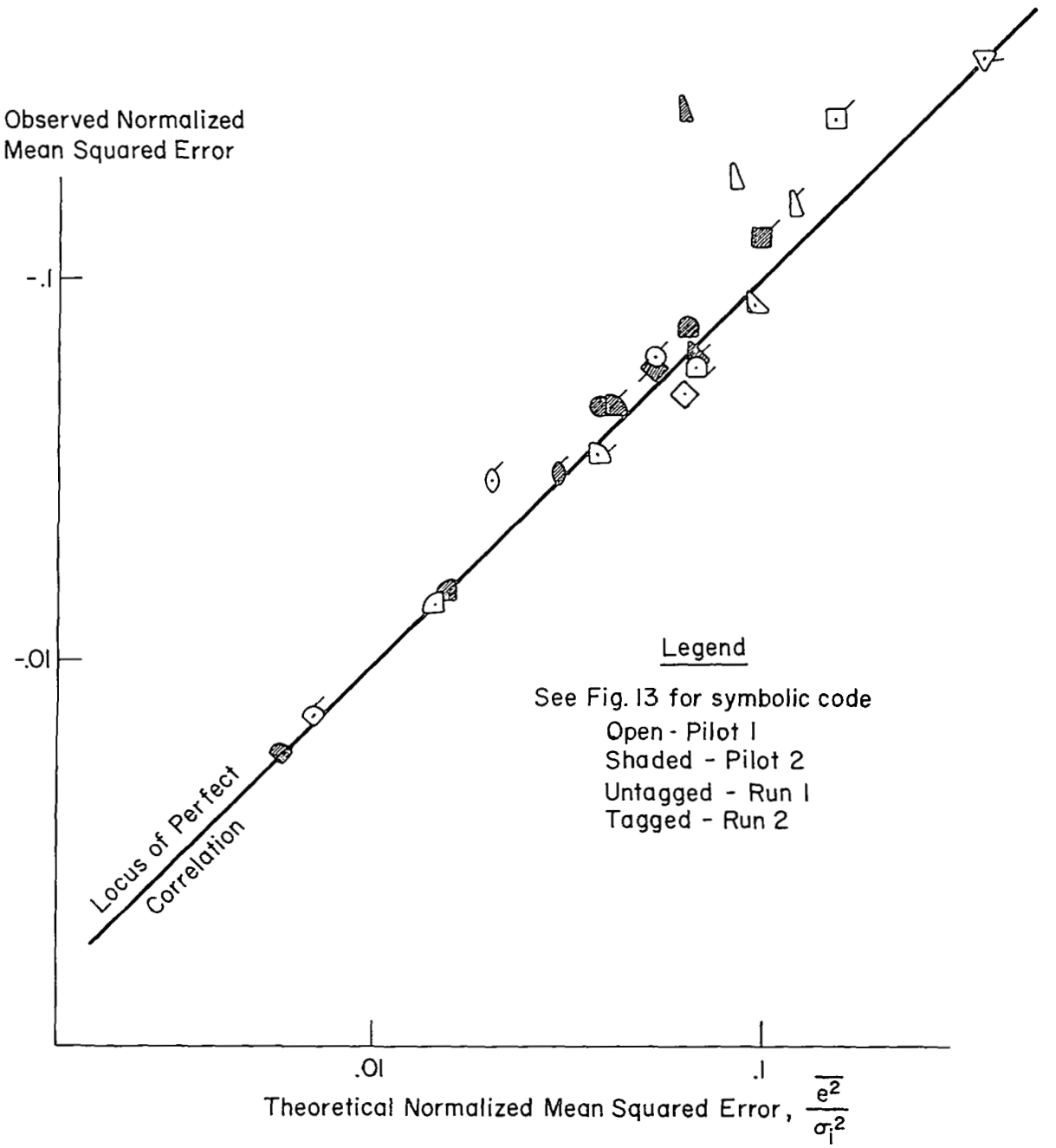

Figure 45. Comparison of Experimental Total Error with Theoretical Predictions

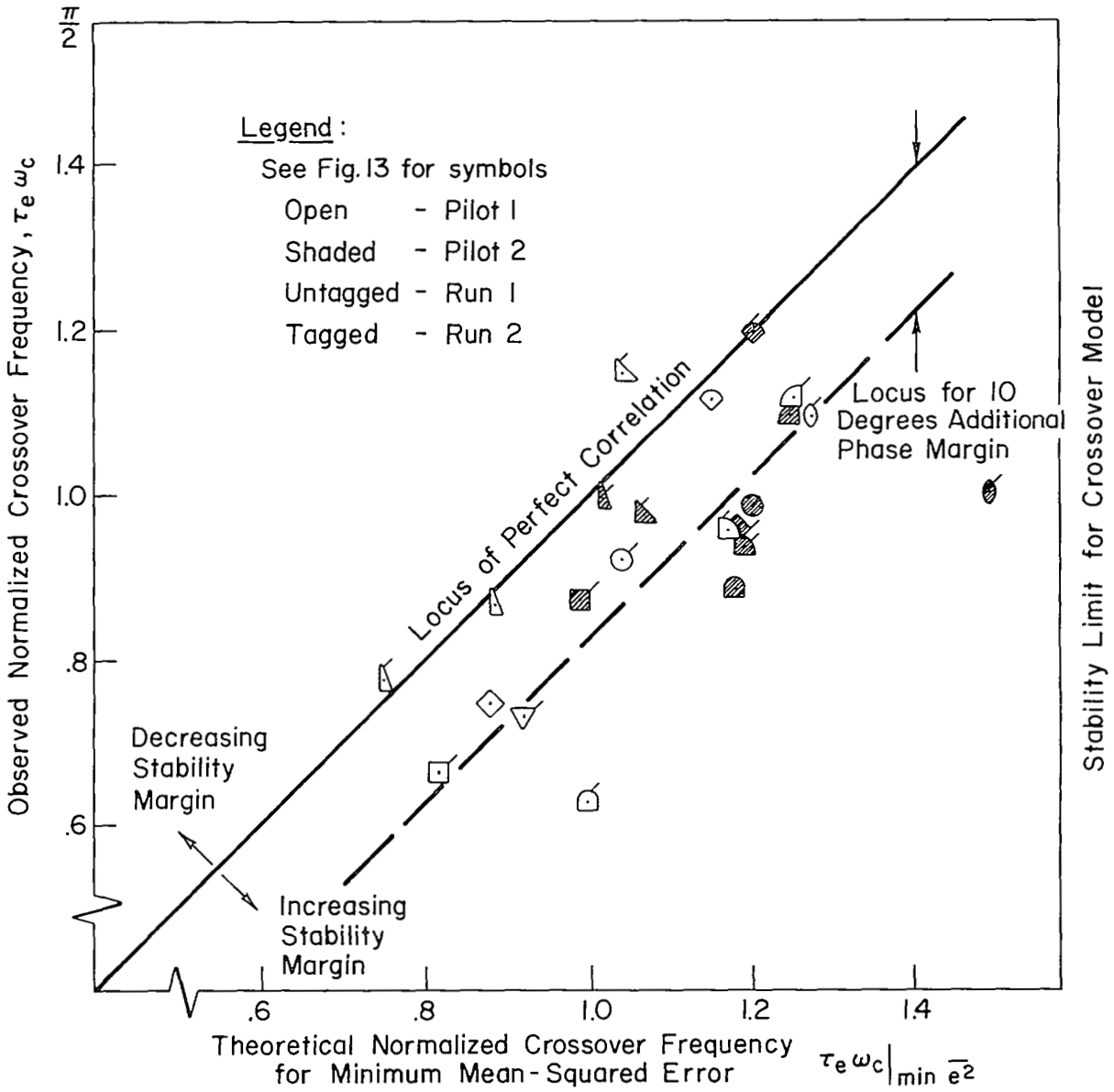

Figure 46. Comparison of Adopted Crossover Frequency with Theoretical Value for Minimum Mean-Squared Error

The observed values of normalized crossover frequency for nearly all of the scanning conditions with display blanking are within 10 deg phase margin* of the theoretical values for minimum mean-squared error. The adopted values for continuous foveal tracking with 0.5 and 1.0 rad/sec input bandwidth are also within 10 deg phase margin of theoretical values for corresponding minima. However, the pilot-subjects apparently adopted phase margins between 10 and 20 deg greater than theoretical values for minimum mean-squared error in most of the scanning conditions with parafoveal perception and in continuous foveal tracking with 2 rad/sec input bandwidth. Apparently the pilots succeeded well in following the instructions to minimize error on the main task as the side task difficulty increased.

In summary at this juncture, the Pearson random finite-dwell sampling remnant model appears to be capable of predicting adopted crossover frequency, mean-squared error and relative correlated error power for most of the scanning and sampling conditions tested with display blanking. Although the model tends to slightly overestimate adopted gain (crossover frequency) for the scanning conditions tested with parafoveal perception, its predictions are still quite good for making relative estimates of performance.

*The phase margin (PM) of stability for the crossover model is related to the normalized crossover frequency (or gain) by the relation $PM = \pi/2 - \omega_c \tau_e$ (units of radians).

SECTION VI

CONCLUSIONS

This report has presented some new developments in modeling the effects of random scanning and sampling on tracking performance, and a detailed description of experiments designed to test the basic assumptions and alternative signal reconstruction modes implied by the theory. The major conclusions drawn from this work are as follows:

1. Section II describes the properties of two main types of model for the mental signal reconstruction which can be employed by the human operator following foveal scans:

    a. Switched Gain Model — the operator alternates between a foveal dwell with gain of unity, and a parafoveal view with a reduced effective gain. The theory shows that this model implies negligible time delays, reduced crossover frequency, and a large wideband remnant.

    b. Reconstruction-Hold Model — the operator reconstructs an almost continuous signal between dwells by weighting the average position and rate in some appropriate manner. Analysis of this mode shows that it will yield appreciable time-delay increments, little attenuation, and generally lower remnant than the switched-gain case.

    The theory shows that in either case the sampling-induced remnant power scales as the square of the perceived error signal (Eq. 3). The experimental results generally favored the simpler switched-gain model for a tracking task requiring no operator equalization. However, there was some evidence for a reconstruction mode in a secondary task involving stabilization only.

2. The "subcritical tracking task" can be used successfully as a secondary loading task to regulate an operator's natural scanning and sampling behavior on a primary tracking task. If instructions are to minimize primary task error, while maintaining secondary error below a generous threshold, there is no tendency for the subcritical secondary task to become the primary task.

3. Parafoveal perception is beneficial while scanning between two tracking tasks, such as studied here. It can be excluded by blanking the nonfixated display in order to study the natural foveal sampling behavior of the human operator under controlled conditions. Parafoveal perception of the nonfixated display produced a small reduction in scanning frequency, little change in the relative scanning remnant, and a substantial increase in the average gain, resulting in appreciably better performance.

4. The operator's sampling remnant power appears to be the single outstanding property which affects his adopted crossover frequency. To minimize tracking error he reduces his open-loop gain and increases his stability margins.

5. The data conclusively show that a pilot's average behavior and performance during scanning can be accurately modeled by a random-input describing function plus a wide-band remnant. The simple analytical expression of Eq. 3 fits our scanning remnant data very well. This is equivalent to injection of first-order filtered "observation noise."

6. A Pearson random sampling remnant model, which includes effects of sampling interval, finite-dwell interval, and variance of sampling frequency about its mean value, predicts quite accurately, in conjunction with the crossover model, at least four aspects of observed scanning performance when parafoveal perception is excluded:

    a. Shape and level of the remnant spectrum.

    b. Adopted crossover frequency to minimize tracking error.

    c. Relative error power correlated with the input forcing function.

    d. Total mean-squared tracking error.

7. These models and data may be used to predict human operator performance and scanning statistics in other multidisplay situations, when two displays dominate the scanning activity.

These results may also be used to extend the models to cases where pilot equalization is required (e.g., $Y_c = K/s^2$, which requires lead; and $Y_c = K$, which requires lag), and to investigate scanning statistics, describing functions, and remnant for a very realistic, multidisplay multi-axis task (as close as possible to full instrument flight). This would verify that the models developed here can be applied to such complex situations. Parallel theoretical improvements are also needed to cover "almost-periodic" sampling and to evolve the scanning adaptation laws for complex multidisplay systems.

REFERENCES

1. McRuer, D. T., and H. R. Jex, "A Systems Analysis Theory of Manual Control Displays," Third Annual NASA-University Conference on Manual Control, NASA SP-144, 1967, pp. 9-28.

2. McRuer, Duane, Henry R. Jex, Warren F. Clement, and Dunstan Graham, Development of a Systems Analysis Theory of Manual Control Displays, Systems Technology, Inc., Tech. Rept. 163-1, Oct. 1967.

3. Allen, R. W., and H. R. Jex, An Experimental Investigation of Compensatory and Pursuit Tracking Displays with Rate and Acceleration Control Dynamics and a Disturbance Input, NASA CR-1082, June 1968.

4. McRuer, D. T., and H. R. Jex, "A Review of Quasi-Linear Pilot Models," IEEE Trans., Vol. HFE-8, No. 3, Sept. 1967, pp. 231-249.

5. Clement, Warren F., Dunstan Graham, and John J. Best, A Reexamination of Eye Movement Data, Systems Technology, Inc., Tech. Memo 163-A, 30 Nov. 1966 (rev. 28 Feb. 1967). (AD 667 768)

6. Clement, Warren F., "Cardinal Reconstruction Theory — A Tool for Estimating Effects of Display Scanning," Fourth Annual NASA-Univ. Conf. on Manual Control, Univ. of Michigan, Ann Arbor, Mich., 21-23 Mar. 1968.

7. Levison, W. H., and J. I. Elkind, Studies of Multivariable Manual Control Systems; Two-Axis Compensatory Systems with Separated Displays and Controls, NACA CR-875, Oct. 1967.

8. Stapleford, R. L., D. T. McRuer, and R. E. Magdaleno, "Pilot Describing Function Measurements in a Multiloop Task," IEEE Trans., Vol. HFE-8, No. 2, June 1967, pp. 113-124.

9. Stapleford, Robert L., and Samuel J. Craig, Measurement of Pilot Describing Functions in Single-Controller Multiloop Tasks, Systems Technology, Inc., Tech. Rept. 167-1, Aug. 1967 (forthcoming NASA CR-).

10. McRuer, D. T., L. G. Hofmann, H. R. Jex, et al, New Approaches to Human-Pilot/Vehicle Dynamic Analysis, AFFDL-TR-67-150, June 1967.

11. McRuer, D. T., R. E. Magdaleno, and G. P. Moore, "A Neuromuscular Actuation System Model," Third Annual NASA-University Conference on Manual Control, NASA SP-144, 1967, pp. 281-304.

12. Craik, J., "Theory of the Human Operator in Control Systems; I, The Operator as an Engineering System; II, Man as an Element in a Control System;" Brit. J. Psychol., Dec. 1947 and Mar. 1948.

13. North, J. D., The Human Transfer Function in Servo Systems, Directorate of Weapons Research, (British) Ministry of Defense, Rept. No. WRD/6/50, 1950. (Reprinted in Automatic and Manual Control, ed. by A. Tustin, Butterworths, London, 1958, pp. 473-502.)

26. Cole, E. L., J. L. Milton, and B. B. McIntosh, Routine Maneuvers under Day and Night Conditions, Using an Experimental Panel Arrangement, WADC-TR-53-220, Mar. 1954.

27. Senders, J. W., "Man's Capacity to Use Information from Complex Displays," Information Theory in Psychology, H. Quastler, ed., The Free Press, Glencoe, Ill., 1955.

28. Watts, A. F. A., and H. C. Wiltshire, Investigation of Eye Movements of an Aircraft Pilot under Blind Approach Conditions, The College of Aeronautics, Note No. 26, May 1955.

29. Lennox, D., Airline Pilots' Eye Movements during Take-Off and Landing in Visual Meteorological Conditions, Aeronautical Research Labs. Human Engineering Note 15, Aug. 1963.

30. Winblade, R. L., Current Research on Advanced Cockpit Display Systems, AGARD Rept. No. 491, Oct. 1964.

31. Senders, J. W., Tracking with Intermittently Illuminated Displays, WADC TR 55-378, Oct. 1955.

32. Senders, J. W., "The Human Operator as a Monitor and Controller of Multidegree of Freedom Systems," IEEE Trans., Vol. HFE-5, Sept. 1964, pp. 2-5.

33. Senders, J. W., J. I. Elkind, M. C. Grignetti, and R. D. Smallwood, An Investigation of the Visual Sampling Behavior of Human Observers, NASA CR-434, Apr. 1966.

34. Senders, John W., Jaime R. Carbonell, and Jane L. Ward, Human Visual Sampling Processes: A Simulation Validation Study, NASA CR-1258, Jan. 1969.

35. Battig, W. F., J. F. Voss, and W. J. Brogden, "Effect of Frequency of Target Intermittence upon Tracking," J. Exp. Psychol., Vol. 49, Apr. 1955, pp. 244-284.

36. Katz, M. S., and S. D. S. Spragg, "Tracking Performance as a Function of Frequency of Course Illumination," J. Psychol., Vol. 40, 1955, pp. 181-191.

37. Platzer, H. L., and E. S. Krendel, A Non-Linear Approach to Human Traching, Franklin Institute Interim Tech. Rept. No. I-2490-1, 21 Dec. 1955.

38. Bennett, C. A., "Sampled-Data Tracking: Sampling of the Operator's Output," J. Exp. Psychol., Vol. 51, 1956, pp. 429-438.

39. Vossius, G., "Die Vorhersageeingenshaften des Systems der Willkurbewegung," Neuere Ergebuisse der Kybernetik, R. Oldenbourg, Munich, 1964; The Prediction Capabilities of the System of Tracking Motions, Systems Technology, Inc., Tech. Translation No. 2, July 1965.

14. Hayes, The Intermittent Nature of the Response of a Human Operator, Royal Military College of Science, Electrical Engineering Branch, Rept. 1/54, 1954.

15. Ward, J. R., The Dynamics of a Human Operator in a Control System; A Study Based on the Hypothesis of Intermittency, University of Sydney, Dept. of Aeronautics, Ph.D. Thesis, May 1958.

16. Lemay, L. P., and J. H. Wescott, The Simulation of Human Operator Tracking Using an Intermittent Model, paper presented to the IRE International Congress on Human Factors in Electronics, Long Beach, Calif., 3-4 May 1962.

17. Bekey, G. A., "The Human Operator as a Sampled-Data System," IRE Trans., Vol. HFE-3, No. 2, Sept. 1962, pp. 43-51.

18. Biddle, J., A. Jacobsen, and G. A. Bekey, "The Effect of Random Sampling Intervals on Sampled Data Models of the Human Operator," Third Annual NASA-University Conference on Manual Control, NASA SP-144, 1967, pp. 247-258.

19. Jones, R. E., J. L. Milton, and P. M. Fitts, Eye Fixations of Aircraft Pilots; I. A Review of Prior Eye Movements Studies and a Description of a Technique for Recording the Frequency, Duration, and Sequences of Eye Fixations during Instrument Flight, Air Material Command AF TR-5837, Sept. 1949 (includes summary of McGehee's studies circa 1944).

20. Milton, J. L., R. E. Jones, and P. M. Fitts, Eye Fixations of Aircraft Pilots; II. Frequency, Duration, and Sequence of Fixations when Flying the USAF Instrument Low Approach System (ILAS), Air Materiel Command AF TR-5839, Oct. 1949.

21. Fitts, P. M., R. E. Jones, and J. L. Milton, Eye Fixations of Aircraft Pilots; III. Frequency, Duration, and Sequence of Fixations when Flying Air Force Ground Controlled Approach System (GCA), Air Materiel Command AF TR-5967, Feb. 1950.

22. Jones, R. E., J. L. Milton, and P. M. Fitts, Eye Fixations of Aircraft Pilots; IV. Frequency, Duration, and Sequence of Fixations during Routine Instrument Flight, Air Materiel Command AF TR-5975, Dec. 1949.

23. Fitts, P. M., R. E. Jones, and J. L. Milton, "Eye Movements of Aircraft Pilots during Instrument-Landing Approaches," Aero. Eng. Rev., Vol. 9, No. 2, Feb. 1950, pp. 24-29.

24. Milton, J. L., B. B. McIntosh, and E. L. Cole, Eye Fixations of Aircraft Pilots; VI. Fixations during Day and Night ILAS Approaches using an Experimental Instrument Panel Arrangement, Air Materiel Command AF TR-6570, Oct. 1951.

25. Milton, J. L., and F. J. Wolfe, Fixations during Zero-Reader Approaches in a Jet Aircraft, WADC-TR-52-17, Feb. 1952.

40. Wezel, F., "Untersuchunger Uber die Willkurbewegung der Menschlichen Hand Mit Getastet Dargebotenen Reizmustern," Thesis, J. W. Goethe University, Frankfurt am Main, 1962; Investigations of Tracking Movements of Human Hand with Sampled Stimuli, Systems Technology, Inc., Tech. Translation No. 3, July 1965.

41. Nyquist, H., "Certain Topics in Telegraph Transmission Theory," Trans. of the AIEE, Vol. 47, Apr. 1928, p. 617.

42. Shannon, C. E., "Communication in the Presence of Noise," Proc. of the IRE, Vol. 37, No. 1, Jan. 1949, pp. 10-21.

43. Linden, D. A., and N. M. Abramson, "A Generalization of the Sampling Theorem," Information and Control, Vol. 3, No. 1, 1960, pp. 26-31.

44. Poulton, E. C., "The Basis of Perceptual Anticipation in Tracking," Brit. J. Psychol., Vol. 43, 1952, pp. 295-302.

45. Fitts, P. M., and C. W. Simon, "Effect of Horizontal versus Vertical Stimulus Separation on Performance in a Dual Pursuit Task," Amer. Psychologist, Vol. 4, 1949, pp. 304-305.

46. Wierwille, W. W. and G. A. Gagne, "Nonlinear and Time-Varying Dynamical Models of Human Operators in Manual Control Systems", Human Factors, Vol. 8, No. 2, April 1966, pp. 97-120.

47. Jury, E. I., Sampled-Data Control Systems, John Wiley and Sons, New York, 1958.

48. Ragazzini, J. R., and G. F. Franklin, Sampled Data Control Systems, McGraw-Hill, New York, 1958.

49. Clement, W. F., Cardinal Reconstruction Theory—A Tool for Estimating Effects of Display Scanning, STI TM-163-B, 1 March 1967.

50. Farmanfarma, G., Analysis of Sampled-Data Systems with Finite Pulse Width, Ph.D. Thesis, Dept. of Electrical Engineering, Univ. of California at Berkeley, 1957.

51. Bergen, A. R., "On the Statistical Design of Linear Random Sampling Schemes," Proc. IFAC, Vol. 1, Butterworth, London, 1961, pp. 430-436.

52. Clement, W. F., Random Sampling Remnant Theory Applied to Manual Control, STI TM-183-A.

53. Jex, H. R., "Two Applications of the Critical Instability Task to Secondary Work Load Research", IEEE Trans., Vol. HFE-8, No. 4, December 1967. pp. 279-282.

54. Bullard, E. C., F. E. Oglebay, W. H. Munk, and G. R. Miller, A User's Guide to BOMM—A System of Programs for the Analysis of Time Series, Inst. of Geophysics and Planetary Physics, Univ. of California at La Jolla, January 1966.

55. Coonan, Thomas J. and Edmund T. Klemer, Reading Linear Scales: The Contribution of Eye Movements to Accuracy, AFCRC-TN-56-8, October 1956.

56. King-Smith, E. A., "Predictive Compensation in Time Delayed Manual Control Systems," Fourth Annual NASA-University Conference on Manual Control, Univ. of Michigan, Ann Arbor, Michigan, 21-23 Mar. 1968.

57. McColgin, Franklin H., "Movement Thresholds in Peripheral Vision", J. Opt. Soc. Amer., Vol. 50, August 1960, pp. 774-779.

58. Zelen, Marvin and Norman C. Severo, "Probability Functions", Handbook of Mathematical Functions with Formulas, Graphs, and Mathematical Tables, National Bureau of Standards Applied Mathematics Series No. 55, November 1964, p. 930.

59. Levison, William H., David L. Kleinman, and Sheldon Baron, A Model for Human Controller Remnant, Bolt, Beranek and Newman Inc. Report No. 1731, 15 October 1968.

60. McRuer, Duane, Dunstan Graham, Ezra Krendel, and William Reisener, Jr., Human Pilot Dynamics in Compensatory Systems — Theory, Models, and Experiments with Controlled Element and Forcing Function Variations, AFFDL-TR-65-15, July 1965.

"The aeronautical and space activities of the United States shall be conducted so as to contribute . . . to the expansion of human knowledge of phenomena in the atmosphere and space. The Administration shall provide for the widest practicable and appropriate dissemination of information concerning its activities and the results thereof."

—NATIONAL AERONAUTICS AND SPACE ACT OF 1958

NASA SCIENTIFIC AND TECHNICAL PUBLICATIONS

TECHNICAL REPORTS: Scientific and technical information considered important, complete, and a lasting contribution to existing knowledge.

TECHNICAL NOTES: Information less broad in scope but nevertheless of importance as a contribution to existing knowledge.

TECHNICAL MEMORANDUMS: Information receiving limited distribution because of preliminary data, security classification, or other reasons.

CONTRACTOR REPORTS: Scientific and technical information generated under a NASA contract or grant and considered an important contribution to existing knowledge.

TECHNICAL TRANSLATIONS: Information published in a foreign language considered to merit NASA distribution in English.

SPECIAL PUBLICATIONS: Information derived from or of value to NASA activities. Publications include conference proceedings, monographs, data compilations, handbooks, sourcebooks, and special bibliographies.

TECHNOLOGY UTILIZATION PUBLICATIONS: Information on technology used by NASA that may be of particular interest in commercial and other non-aerospace applications. Publications include Tech Briefs, Technology Utilization Reports and Technology Surveys.

Details on the availability of these publications may be obtained from:

SCIENTIFIC AND TECHNICAL INFORMATION DIVISION

NATIONAL AERONAUTICS AND SPACE ADMINISTRATION

Washington, D.C. 20546